

12-2015

Model Development and Validation for Wind Generation Transmission Systems

Mahmood Shihadeh Saadeh
University of Arkansas, Fayetteville

Follow this and additional works at: <https://scholarworks.uark.edu/etd>



Part of the [Electrical and Electronics Commons](#), and the [Power and Energy Commons](#)

Citation

Saadeh, M. S. (2015). Model Development and Validation for Wind Generation Transmission Systems. *Graduate Theses and Dissertations* Retrieved from <https://scholarworks.uark.edu/etd/1333>

This Dissertation is brought to you for free and open access by ScholarWorks@UARK. It has been accepted for inclusion in Graduate Theses and Dissertations by an authorized administrator of ScholarWorks@UARK. For more information, please contact scholar@uark.edu.

Model Development and Validation
for Wind Generation Transmission Systems

A dissertation submitted in partial fulfillment
of the requirements for the degree of
Doctorate of Philosophy in Electrical Engineering

by

Mahmood Shihadeh Saadeh
Jordan University of Science & Technology
Bachelor of Science in Electrical Engineering, 2009
University of Arkansas
Masters of Science in Electrical Engineering, 2011

December 2015
University of Arkansas

This thesis is approved for recommendation to the Graduate Council.

Dr. Roy McCann
Dissertation Director

Dr. Juan Balda
Committee Member

Dr. Simon Ang
Committee Member

Dr. Dale Thompson
Committee Member

Dr. Terry Martin
Committee Member

Abstract

In this research a new benchmark system is proposed for wind energy transmission systems. New model development, validation, and calibration methods for power transmission systems are proposed and implemented as well. First, a model reduction criteria is chosen based on electrical interconnection and geographical information. Model development is then done using reduction techniques on an operation model provided by a transmission operator based on the chosen criteria. Then model validation is performed using actual PMU synchrophasor measurements provided by a utility company. The model development and validation process ensures the accuracy of the developed model and makes for a realistic benchmark system for wind generation transmission systems. The new proposed model development and validation methods are generic and can be used to model any power transmission system for various simulation needs. Nevertheless, the accuracy of the benchmark model is constrained by the accuracy of the initial operational model. In this research, a new parameter estimation technique for determining the bus admittance matrix (Y_{bus}) is also proposed to further calibrate power system models. Y_{bus} estimation is done using recorded PMU synchrophasor measurements. The approach proposed in this research is based on recognizing that bus injection currents I_{bus} can be viewed as signals produced by a random process. In this manner, the corresponding bus voltages V_{bus} are also stochastic signals that are related through a cross-covariance matrix to the vector I_{bus} . Using estimation techniques developed for statistical signal processing, the cross-covariance matrix is shown to be Z_{bus} .

©2015 by Mahmood Shihadeh Saadeh
All Rights Reserved

Acknowledgments

This research was funded in part by the National Science Foundation Industry/University Cooperative Research Center on Grid-connected Advanced Power Electronics Systems (GRAPES.uark.edu) under grant number 0934390, which provided access to the synchrophasor data used in conducting this research.

Dedication

This dissertation is dedicated to my parents, Dr. Shihadeh Saadeh and Omaila Sakhnini. I would like to express my appreciation to my advisor Dr. Roy McCann for his continued support and guidance throughout my PhD study. I would also like to thank the rest of my thesis committee for their support. Special thanks to my friends for their continued support and encouragement especially through the final steps in preparing this dissertation. I also would like to thank my parents and siblings for being there for me and for all they have done for me throughout the years. Special thanks to my older brother Dr. Osama Saadeh for his help, support, and encouragement throughout my graduate study.

Table of Contents

I.	Introduction.....	1
A.	The need for a wind energy benchmark system.....	1
B.	The need for new model development and validation methods	3
C.	Synchrophasors	4
D.	Model parameter extraction	6
II.	Power System Modeling	9
A.	Steady State System Model	10
B.	Dynamic System Model.....	11
a.	Synchronous Generators	11
b.	Excitation	14
c.	Power System Stabilizers	16
d.	Wind Energy Plants.....	16
III.	Synchrophasors	19
IV.	Model Development Method	22
A.	Power System Reduction	22
B.	Model Development Process.	25
V.	Model Validation Method.....	28
A.	Qualitative model validation.....	28
B.	Quantitative model validation.....	36
VI.	Wind Energy Benchmark System.....	39
A.	Wind Energy Transmission Model Development.....	39
B.	Wind Energy Transmission Model Validation	50
a.	Qualitative model validation	50
b.	Quantitative model validation	52
VII.	Ybus Estimation.....	60
A.	Ibus Formulation from Synchrophasor Measurements	62
B.	Statistical Properties of Synchrophasors.....	66
C.	Finding the Functional Relationship through Correlation	69
D.	Implementation	71
a.	Randomly Generated Ybus systems.....	72
b.	Validation using the 68-bus benchmark system.....	78

c. Implementation requirements.....	92
VIII. Conclusions & Future Work	94
IX. References.....	96
X. Appendix.....	100
A. Representative Matlab m-file script.....	100
B. Randomly generated Ybus systems M-files	104
a. Ybus estimation error calculation	104
b. Ybus error estimation.	110
C. IEEE 68-bus benchmark system M- files	114
a. Ybus estimation error calculation	115
b. Ybus error estimation.	118
D. Benchmark system Ybus estimation.....	123

List of Figures

Fig. 1. IEEE DC1A PowerWorld implementation.	15
Fig. 2. IEEE exciter ST1 A PowerWorld implementation.	15
Fig. 3. PowerWorld implementation of the PSS.	16
Fig. 4. WT2E exciter model.	18
Fig. 5. WT2P stabilizer model.	18
Fig. 6. Synchrophasor viewing platform.	21
Fig. 7. Ward reduction method subsystems.	24
Fig. 8. Model development process.	27
Fig. 9. Illustration of power system simulation voltage angles.	29
Fig. 10. Illustration of synchrophasor voltage angles.	30
Fig. 11. Plot of power transfer dependence on power angle.	31
Fig. 12. Synchrophasor voltage angles across the 345 kV line.	33
Fig. 13. System frequency from synchrophasor measurements.	34
Fig. 14. Raw synchrophasor calculated power angle.	35
Fig. 15. Corrected synchrophasor power angle.	35
Fig. 16. Geographical representation of the proposed benchmark model.	40
Fig. 17. Measured power angle of transmission line 2.	50
Fig. 18. Measured power angle of transmission line 3.	51
Fig. 19. Measured power angle of transmission line 4.	51
Fig. 20. Measured power angle of transmission line 6.	52
Fig. 21. IEEE 68-bus benchmark system.	63
Fig. 22. Example substation design.	65
Fig. 23. Simplified substation layout.	66
Fig. 24. Cumulative probability function for voltage magnitude data.	67
Fig. 25. Cumulative probability function for voltage angle data.	68
Fig. 26. Cumulative probability function for current magnitude data.	68
Fig. 27. Cumulative probability function for current angle data.	69
Fig. 28. Y_{bus} estimation process.	72
Fig. 29. Y_{bus} estimation error calculation flow chart.	74
Fig. 30. Max error vs. number of samples for randomly generated systems.	75
Fig. 31. Accuracy range for multiple cases for randomly generated systems.	76
Fig. 32. Accuracy vs. number of samples for randomly generated systems.	77
Fig. 33. Effect of a missing measurement.	78
Fig. 34. Max error vs. number of samples for the IEEE 68-bus benchmark system.	79
Fig. 35. Accuracy range for multiple cases for the IEEE 68-bus benchmark system.	80
Fig. 36. Accuracy vs. number of samples for the IEEE 68-bus benchmark system.	81
Fig. 37. Power spectral density of white noise.	82
Fig. 38. Centered power spectral density of actual synchrophasors.	83
Fig. 39. Power spectral density of actual synchrophasors.	83
Fig. 40. White noise filtration.	84
Fig. 41. Centered power spectral density of filter output.	85

Fig. 42. Power spectral density of filter output	85
Fig. 43. Y_{bus} estimation process using filtered white noise.	86
Fig. 44. Max error vs. number of samples for the IEEE 68-bus benchmark system using Gaussian filtered white noise.....	87
Fig. 45. Accuracy vs. number of samples for the IEEE 68-bus benchmark system using Gaussian filtered white noise.....	88
Fig. 46. Accuracy vs. number of samples for the IEEE 68-bus benchmark system using Gaussian filtered white noise.....	89
Fig. 47. Max error vs. number of samples for the IEEE 68-bus benchmark system using Gaussian filtered white noise.....	89
Fig. 48. Max error vs. number of samples for the IEEE 68-bus benchmark system using Gaussian filtered white noise.....	90
Fig. 49. Accuracy vs. number of samples for the IEEE 68-bus benchmark system using Gaussian filtered white noise.....	91

List of Tables

Table 1. Synchrophasor data reporting format.....	19
Table 2. Proposed benchmark generator data.	41
Table 3. Proposed benchmark bus data.	41
Table 4. Proposed benchmark load data.	45
Table 5. Proposed benchmark line information.	46
Table 6. Measured vs. simulated power angles ($^{\circ}$).	52
Table 7. Quantitative validation results for first event.	54
Table 8. Quantitative validation results for second event.	55
Table 9. Quantitative validation results for third event.	56
Table 10. Quantitative validation for power flows of the first event.	58
Table 11. Quantitative validation for reactive power flows of the first event.	59
Table 12. Terminal IDs corresponding to current injections.	92

I. Introduction

In this chapter an introduction to the dissertation is given. It mainly discusses the need and motivation for the research performed. First it discusses the need for a benchmark model for wind energy systems. Then it discusses the motivation for new model development and validation methods. Then it introduces Synchrophasors and their potential impact on power systems. Finally an introduction about the Y_{bus} parameter extraction method is presented.

A. The need for a wind energy benchmark system

The US department of energy estimates that wind energy could constitute 20% of total US electricity consumption by 2030 [1]. As wind turbine installations increase to achieve this vision, new technologies will need to be adopted in order to accommodate the increasing amounts of wind energy in the power system. This integration of large amounts of wind energy into the existing transmission grid should be done while maintaining reliability, power quality, and economical operation. Presently there is 30 GW of wind generation capacity installed in the Great Plains region of the United States [2]. Due to being located in low population areas, most of this wind generated electricity is transmitted eastward to major load centers. The main concern for system planners is that wind energy capacity might be brought online faster than the supporting infrastructure can be upgraded in order to maintain system reliability in accordance with relevant NERC requirements such as TPL-001-4 [3]. From an operational point of view, it would be beneficial for wind generation to not have transmission constraints such that it could be transmitted to distant major load centers. These limitations include transmission capacity and transient stability concerns. Solutions to such limitations might require upgrading the existing transmission configuration. This upgrade includes grid expansion and fully utilizing existing

lines and wind farms. Under consideration would be siting of new lines and adoption of new flexible ac transmission technologies (FACTS). Alternatively, HVDC transmission systems have been proposed as a solution to avoid congestion in adjacent EHV ac transmission networks. As an example, HVDC projects proposed by Clean Line Energy Partners are presently under review [4] that would provide a path of connecting wind generation in the central states directly to major load centers in the eastern US.

A large portion of existing and proposed wind generation sites are located in sparsely populated areas with low population densities. In particular, in the central US, this region extends from northern Texas and eastern New Mexico northward through Minnesota. The transmission system includes a limited amount of 345 kV lines and was not historically intended to carry large amounts of electrical power. Until recently that has not been a concern due to this region having relatively few major load centers and the wind farm installations did not exceed the capabilities of the transmission system when accounting for 138/230 kV lines in addition to the 345 kV infrastructure. As the capacity for wind power increases, so does the concern over the limitation of the regional transmission system. In general, this presents a need to perform stability analysis of weakly-connected remotely located wind sources under a variety of contingencies. For example, power systems are prone to low frequency oscillation when weak ties or heavily loaded transmission lines are compensated with series capacitors [5].

It would be beneficial to have a wind energy benchmark system that captures such characteristics. The use of a realistic wind energy benchmark system increases the credibility of studies and technologies that are meant to accelerate and enable the increase of wind energy utilization. Industry professionals and policy makers can be more informed that the analytical

results are relevant and realistic when an appropriate benchmark system is used. A proposed wind power transmission benchmark system has been developed as part of this research.

The proposed benchmark system is based on the transmission and generation grid in western Oklahoma. This region presently includes about 2955 MW of wind generation capacity. The proposed benchmark includes a reduced model of the surrounding region that includes southern Kansas, western Arkansas and dc-ties to ERCOT passing through southern Oklahoma. The proposed benchmark model is based on an operation model provided by a transmission operator. The model was provided in a PSS/E .raw file format. It was translated to the PowerWorld_{TM} Simulator [6], then reduced. The approximate geographical layout of the reduced benchmark system is shown in Fig. 16. The model includes the major generating stations in the region and all 138 kV and above transmission lines. Parameters for transient stability analysis were also adapted from the MDWG PSS/E configuration.

B. The need for new model development and validation methods

Power system models are the foundation of power system simulations. Having an accurate power system model is very important as power system studies can only be reliable if accurate models are used. One of the uses for power system simulations is to perform planning studies. One of the needs for such study is to set power flow limits. Inaccurate models will lead to unrealistic results and therefore setting inappropriate limits. A good example of this scenario is the major disturbance that occurred in the western interconnection on July 2nd, 1996. When engineers tried to simulate the event using existing models at the time, they failed to reproduce the results. The models used were the same models used to set the operating power transfer limits. This led to a pessimistically conservative view of the power system model and simulation

results. The consequence of that was the derating of power transfer limits. Some transmission lines power flow limits were derated down to 65% of the original power flow limit [7]. The use of inaccurate models can lead to financially inefficient operation and/or insecure stability operation.

Even though more frequent model validation would be beneficial, it is not currently practiced. The reasons for that is the lack of methods and tools to perform rapid model validation [8]. NERC recommends utilities to validate operation and planning models using synchrophasor data. To do this effectively power flow model development and validation needs to be improved, standardized and incorporate the use of synchrophasor data. The goal of the work done in this research is standardized model development and validation methods.

C. Synchrophasors

A phasor measurement unit (PMU) is “a device that produces synchronized phasor, frequency, and rate of change of frequency (ROCOF) estimates from analog voltage and/or current signals and a time synchronizing signal” [9]. A synchrophasor is a phasor calculated from data samples using a GPS time signal as the reference for the measurement. By employing synchrophasors, the calculation of phasors is done with respect to absolute time provided by a GPS time signal. Synchrophasors allow for system wide synchronized measurements, which has not been historically possible. Each set of data produced by the PMU containing a set of synchrophasor, frequency, and ROCOF is called a frame. As per IEEE standard C37.118.1 a PMU reports Frames at sub-multiples of the nominal power-line frequency. That is 60, 30, 20, 15, 12, and 10 frames per second (FPS).

Real-time voltage and current measurements are taken using current transformers (CTs) and potential transformers (PTs). Those measurements are then sent to a PMU for processing and synchrophasors are produced. The reference for synchrophasors is an internally generated 60.000 Hz cosine wave in each PMU. This internal reference is generated with its peak precisely aligned to the second based on the GPS time signal [10]. This is done with a precision on the order of the microsecond.

PMUs come as standalone units or relays with built-in PMU functionality. PMU functionality has been provided by manufacturers as a standard feature since 2002 [10]. Therefore in a given substation, it is more likely than not that enough PMUs are already installed for protection purposes. Due to the mass availability of PMU technologies, accuracy and high resolution of synchrophasor measurements, they are ideal for power system model validation. Actual synchrophasors obtained from a utility company were used to validate the proposed benchmark model.

Electric power systems are continuously subjected to random disturbances. For example, during fault conditions such as a shorted line-to-ground fault, these disturbances can be very large. However, there are small fluctuations in load currents during normal operation due to the natural variability of operating electrical equipment throughout a large-scale electric power system. The net effect of all of these small load disturbances propagate throughout a transmission network and cause corresponding small variations in voltages in accordance with standard nodal analysis from electric circuit theory. If the load fluctuations are sufficiently large, then there will be automatic compensation to regulate voltages within acceptable ranges. However, the action of compensators such as tap-changing transformers and voltage regulators are relatively slow acting compared to the electrical behavior relating instantaneous bus voltages

and currents. The recent development and deployment of synchrophasors has enabled the measurement of small electrical variations throughout a large electric power system. This is in contrast to what was previously available with supervisory control and data acquisition technology (SCADA).

There are many differences between PMU technology and SCADA technology. SCADA systems have low resolution of 1 sample every 2-4 seconds. It only measures the magnitude of the quantity being measured, and measurements are not synchronized. The focus of SCADA systems is local monitoring and control. In contrast, synchrophasors have high resolution of 10-60 samples per second. It measures both the magnitude and the phase of the measured quantity. And synchrophasor measurements as mentioned above are GPS time synchronized. The focus of synchrophasor measurements are for wide area monitoring and control.

Synchrophasor technology has allowed for advancements in power systems operation, control, and modeling. More specifically, synchrophasors are used for modeling, generator performance monitoring, disturbance analysis, situational awareness for dispatchers and reliability coordinators, and real-time wide area controls design [11].

D. Model parameter extraction

This research proposes a new parameter estimation technique for determining the bus admittance matrix Y_{bus} of power transmission systems from recorded synchrophasor measurements. The Y_{bus} (and the corresponding impedance matrix Z_{bus}) is used in power-flow studies for system planning and expansion studies. The impedance matrix Z_{bus} is also used for other purposes such as determining settings in protective relays. The approach described in this research is based on recognizing that bus injection currents I_{bus} can be viewed as signals

produced by a random process. In this manner, the corresponding bus voltages V_{bus} are also stochastic signals that are related through a cross-covariance matrix to the vector I_{bus} . Using estimation techniques developed for statistical signal processing, the cross-covariance matrix is shown to be Z_{bus} . The increasing use of synchrophasors has enabled large-scale data collection of time synchronized bus injection currents and voltages. The new Z_{bus} estimation method is applied to the IEEE 68 bus benchmark system to demonstrate the validity of the approach. The accuracy and convergence rate of the method is evaluated under conditions corresponding to wide-area synchrophasor data collection. The results indicate that the method is broadly applicable in determining Y_{bus} and Z_{bus} for electric power transmission systems equipped with synchrophasors data collection technology.

Models of transmission networks are needed for a variety of purposes in designing and operating electric power systems. For steady-state analysis, power or load-flow analysis is performed to properly size and specify electric power system components such as transformers, capacitor banks, circuit switchers, and conductor sizing. The validity of load-flow analysis is predicated upon having accurate admittance and impedance values of the system under study. Likewise, for transient behavior during fault conditions is important to understand system admittances and impedances in order to properly determine protective relay settings. In each of these cases, there is a need for having accurate parameter values for the bus admittance Y_{bus} and impedance Z_{bus} matrices.

The organization of the rest of this paper is as follows. The second chapter discusses power system modeling. The third chapter discusses synchrophasors in more detail. The fourth chapter discusses the model development method, including model reduction and the development method. The fifth chapter discusses the model validation method developed,

including a quantitative validation and a qualitative validation. The sixth chapter discusses the proposed benchmark model developed using the methods previously discussed. The seventh chapter discusses the proposed statistical parameter extraction method and the theoretical basis of the method. It also discusses the properties of synchrophasors and how they are used to perform the discussed statistical parameter extraction method.

II. Power System Modeling

Power systems are large complex nonlinear systems that are composed of electrical and electro-mechanical components. Different studies are done regularly on power systems. These studies include load flow, transient stability, short circuit, optimal generation dispatch, and optimal power flow studies. Due to the complexity and nonlinearity of power systems, the main method to perform power system analysis is through simulations [12].

A power system model is composed of the network model and the power system operating conditions. The power system network model consists of a steady state power flow model and a transient stability model. Operating conditions mainly refer to generation levels. There are two main types of models currently in use by industry. Planning models and operation models. Operation models are used on a daily basis. They are used for analyzing the real-time state of systems such as real-time power flows and transfer limits. Planning models are used for planning and expansion studies set for the distant future. Historically, these models are developed separately by different groups within a utility company.

Operational models do change from day to day and possibly from minute to minute. As breaker, disconnect switches, tap changers, etc., affects the network model. Operations models are mainly interested with power flow and steady state results. As operational models represent the actual state of the system at specific times, they can be validated versus synchrophasor data. This possible because synchrophasor data represent actual measurements taken for the system.

Planning models do not change as often as operation models do as they are intended for long term planning and they do not represent actual system operation. Planning models cannot be validated against synchrophasor data as they do not represent actual system operation at specific

times. Nevertheless, ideally the network model in planning models should be accurate and representative of the system to the furthest extent possible. Below is a description of steady state models and transient stability models.

A. Steady State System Model

A vector of bus current injections is referred to as I_{bus} . A vector of bus voltages is referred to as V_{bus} . V_{bus} and I_{bus} are related via (1) or alternatively by (2).

$$I_{bus} = Y_{bus} V_{bus} \quad (1)$$

$$V_{bus} = Z_{bus} I_{bus} \quad (2)$$

Y_{bus} is referred to as the admittance matrix. Y_{bus} is a mathematical representation of the network power flow model. If I_{bus} and V_{bus} are known, Y_{bus} can be solved analytically [13]. To solve for Y_{bus} analytically, bus interconnection information is needed. The size of the Y_{bus} matrix or actual power systems is on the order of thousands of buses.

Due to the complexity of such systems, it is a common practice to use reduced power system models. Using reduced models, reduces the computation and time resources needed for power system analysis. As in most cases, analysis and studies are more interested in a particular area of interest rather than in the full system, justifying the use of reduced network models. For a reduced model a new Y_{bus} will be developed.

B. Dynamic System Model

The dynamic model of a power system consists of each subsystem and components along with the interconnection between these subsystems. The principle subsystems are generating stations and power sources. The interconnection is the transmission network connecting the power sources. The dynamic model for each subsystem consists of the models for each component [14]. Those power system components in each subsystem are the generators, the excitation system, and the power system stabilizers. The dynamic model of each of these components is a system of differential and algebraic equations (DAE) for vector valued functions of time. The following models in (3) - (12) used for each component and associated subsystems are derived in [14]. The PowerWorld implementation of the component models are shown in the block diagrams in Fig. 1 through Fig. 5.

a. *Synchronous Generators*

Generator models are well established in the literature [15]. A two axis machine model from [14] is used. Saturation is ignored and governor dynamics are neglected. The resulting set of DAE is as follows:

$$\frac{d\delta_i}{dt} = \omega_B(\omega_i - \omega_S) = \omega_B S_{mi} \quad (3)$$

$$2H_i \frac{dS_{mi}}{dt} = (T_{mi} - T_{ei}) - D_i S_{mi} \quad (4)$$

where,

$$\begin{aligned}
T_{ei} = & E'_{di} I_{di} \frac{(X'''_{qi} - X_{lsi})}{(X'_{qi} - X_{lsi})} + E'_{qi} I_{qi} \frac{(X''_{di} - X_{lsi})}{(X'_{di} - X_{lsi})} - I_{di} I_{qi} (X''_{di} - X''_{qi}) \\
& + \psi_{1di} I_{qi} \frac{(X'_{di} - X''_{di})}{(X'_{di} - X_{lsi})} - \psi_{2di} I_{di} \frac{(X'_{qi} - X''_{qi})}{(X'_{qi} - X_{lsi})},
\end{aligned}$$

and,

$$\begin{aligned}
I_{qi} + jI_{di} = & 1/(R_{ai} + jX''_{di}) \left\{ E'_{qi} \frac{(X''_{di} - X_{lsi})}{(X'_{di} - X_{lsi})} + \psi_{1di} \frac{(X'_{di} - X''_{di})}{(X'_{di} - X_{lsi})} - V_{qi} \right. \\
& \left. + j \left[E'_{di} I_{di} \frac{(X'_{qi} - X_{lsi})}{(X'_{qi} - X_{lsi})} - \psi_{2di} \frac{(X'_{qi} - X''_{qi})}{(X'_{qi} - X_{lsi})} - V_{di} + E'_{dci} \right] \right\},
\end{aligned}$$

and,

$$T_{ci} \frac{dE'_{dci}}{dt} = I_{qi} (X''_{di} - X''_{qi}) - E'_{dci}$$

$$T'_{qoi} \frac{dE'_{di}}{dt} = -E'_{di} + \quad (5)$$

$$(X_{qi} - X'_{qi}) \left\{ -I_{qi} + \frac{(X'_{qi} - X''_{qi})}{(X'_{qi} - X_{lsi})^2} \left((X'_{qi} - X_{lsi}) I_{qi} - E'_{di} - \psi_{2qi} \right) \right\}$$

$$T'_{doi} \frac{dE'_{qi}}{dt} = -E'_{fdi} - E'_{qi} + \quad (6)$$

$$(X_{di} - X'_{di}) \left\{ -I_{qi} + \frac{(X'_{di} - X''_{di})}{(X'_{di} - X_{lsi})^2} (\psi_{1di} - (X'_{di} - X_{lsi}) I_{di} - E'_{qi}) \right\}$$

$$T''_{doi} \frac{d\psi_{1qi}}{dt} = E'_{qi} ((X'_{di} - X_{lsi}) I_{di} - \psi_{1di}) \quad (7)$$

$$T''_{qoi} \frac{d\psi_{2qi}}{dt} = -E'_{di} \left((X'_{qi} - X_{lsi}) I_{qi} - \psi_{2qi} \right). \quad (8)$$

If subtransient reactances are neglected, then from the dynamic models for each component the following dynamic state-space model for each subsystem is derived.

$$\begin{aligned}
\begin{bmatrix} \Delta \dot{\delta}_i \\ \Delta \dot{\omega}_i \\ \Delta \dot{E}'_{qi} \\ \Delta \dot{E}'_{di} \\ \Delta \dot{E}'_{fdi} \\ \Delta \dot{V}_{Ri} \\ \Delta \dot{R}_{Fi} \end{bmatrix} &= \begin{bmatrix} 0 & 1 & 0 & 0 & 0 & 0 & 0 \\ 0 & \frac{-D_i}{M_i} & \frac{-I_{qio}}{M_i} & \frac{-I_{dio}}{M_i} & 0 & 0 & 0 \\ 0 & 0 & \frac{-1}{T'_{doi}} & 0 & \frac{1}{T'_{doi}} & 0 & 0 \\ 0 & 0 & 0 & \frac{-1}{T'_{qoi}} & 0 & 0 & 0 \\ 0 & 0 & 0 & 0 & f_{si}(E_{fdio}) & \frac{1}{T_{Ei}} & 0 \\ 0 & 0 & 0 & 0 & \frac{K_{Ai}K_{Fi}}{T_{Ai}T_{Fi}} & \frac{-1}{T_{Ai}} & \frac{K_{Ai}}{T_{Ai}} \\ 0 & 0 & 0 & 0 & \frac{K_{Fi}}{(T_{Fi})^2} & 0 & \frac{-1}{T_{Fi}} \end{bmatrix} \begin{bmatrix} \Delta \delta_i \\ \Delta \omega_i \\ \Delta E'_{qi} \\ \Delta E'_{di} \\ \Delta E'_{fdi} \\ \Delta V_{Ri} \\ \Delta R_{Fi} \end{bmatrix} \\
+ \begin{bmatrix} 0 & 0 \\ \frac{I_{qio}(X'_{di} - X'_{qi}) - E'_{dio}}{M_i} & \frac{I_{dio}(X'_{di} - X'_{qi}) - E'_{qio}}{M_i} \\ -\left(\frac{X_{di} - X'_{di}}{T'_{doi}}\right) & 0 \\ 0 & \frac{X_{qi} - X'_{qi}}{T'_{qoi}} \\ 0 & 0 \\ 0 & 0 \\ 0 & 0 \end{bmatrix} \begin{bmatrix} \Delta I_{di} \\ \Delta I_{qi} \end{bmatrix} \\
+ \begin{bmatrix} 0 & 0 \\ 0 & 0 \\ 0 & 0 \\ 0 & 0 \\ 0 & 0 \\ 0 & \frac{-K_{Ai}}{T_{Ai}} \\ 0 & 0 \end{bmatrix} \begin{bmatrix} \Delta \theta_i \\ \Delta V_i \end{bmatrix} + \begin{bmatrix} 0 & 0 \\ \frac{1}{M_i} & 0 \\ 0 & 0 \\ 0 & 0 \\ 0 & 0 \\ 0 & \frac{K_{Ai}}{T_{Ai}} \\ 0 & 0 \end{bmatrix} \begin{bmatrix} \Delta T_{Mi} \\ \Delta V_{refi} \end{bmatrix}. \tag{9}
\end{aligned}$$

b. Excitation

IEEE standard exciter models DC1A and ST1A are used. Both models are supported by PowerWorld. The differential equations describing those exciters are given by (10) and (11) respectively.

$$T_E \frac{dE_{fd}}{dt} = V_r - (K_E E_{fd} + E_{fd} A_{ex} e^{B_{ex} E_{fd}}) \quad (10)$$

where,

$$T_r \frac{dV_r}{dt} = V_t - V_r, T_f \frac{dV_f}{dt} = E_{fd} - V_f,$$

and,

$$T_A \frac{dV_A}{dt} = K_A \left(V_{ref} + V_s - V_r - \frac{K_F}{T_F} [E_{fd} - V_f] \right) - V_A$$

$$E_{fd} = K_A (V_{ref} + V_s - V_r), T_r \frac{dV_r}{dt} = V_t - V_r. \quad (11)$$

The block diagram of the PowerWorld implementation of the IEEE DC1A exciter is given in Fig. 1 below. The block diagram of the PowerWorld implementation of the IEEE ST1A exciter is shown in Fig. 2 below.

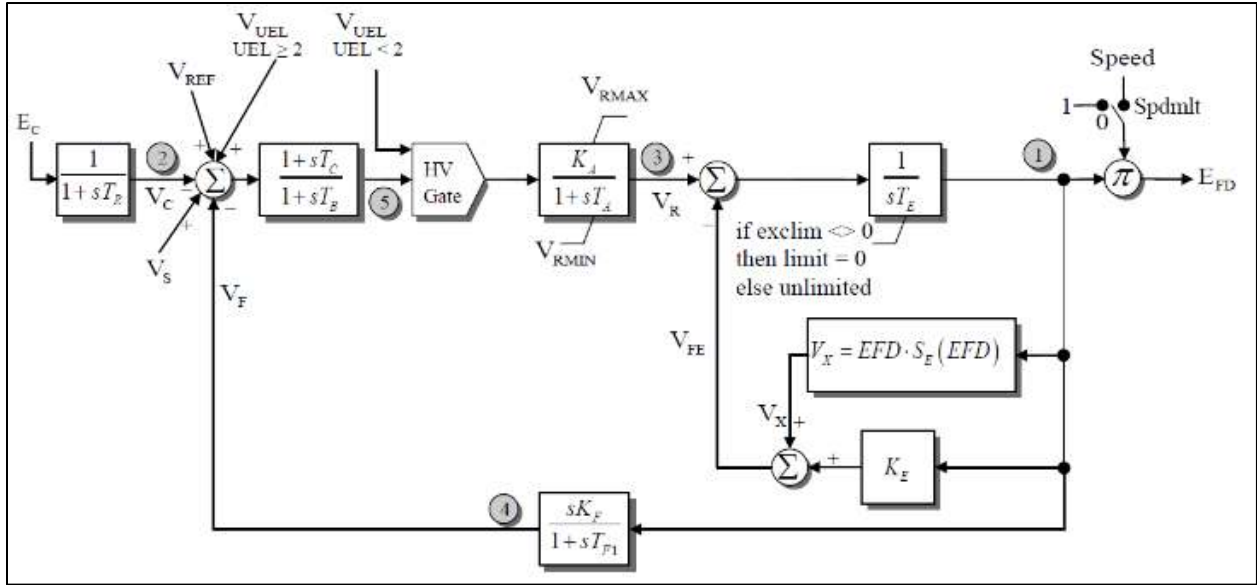


Fig. 1. IEEE DC1A PowerWorld implementation.

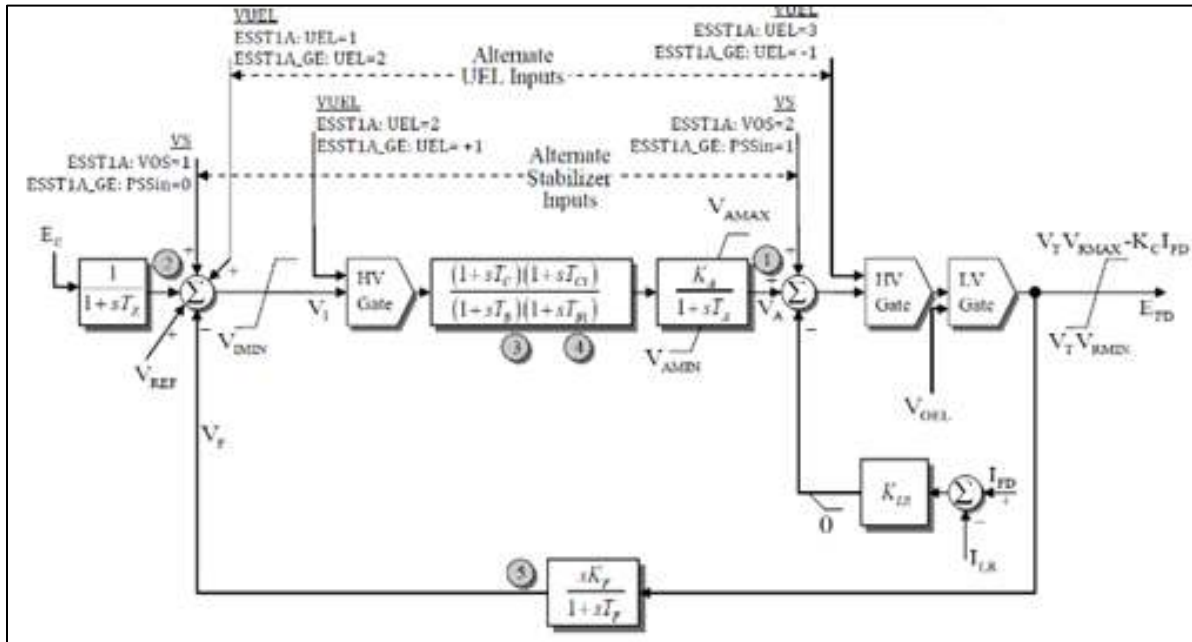


Fig. 2. IEEE exciter ST1A PowerWorld implementation.

c. Power System Stabilizers

Power System Stabilizers are often used for improving the stability of electrical generators. A speed-sensitive stabilizing model STAB1 is used. The speed in per unit is used as the feedback signal to the PSS. The resulting dynamic equation is given in (12).

$$V_s = K_{pss} \frac{ST_w (1+ST_{11}) (1+ST_{21})}{(1+ST_w) (1+ST_{12}) (1+ST_{22})} S_m. \quad (12)$$

Fig. 3 below shows the block diagram of the PowerWorld implementation of the power system stabilizer.

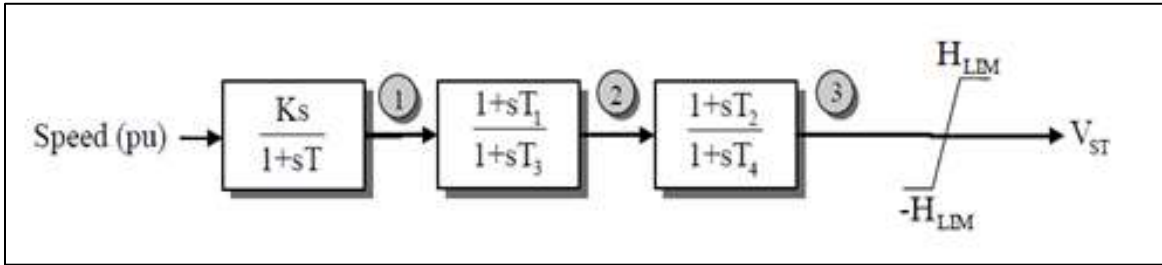


Fig. 3. PowerWorld implementation of the PSS.

d. Wind Energy Plants

Wind turbine modeling is somewhat different than synchronous machine models. For a synchronous machine power plant, the subsystem model includes the models for the machine, exciter, governor and stabilizer. For a wind energy power plant, the subsystem model includes the wind induction machine model, electrical model, mechanical model, pitch control model, and aerodynamic model.

For the machine dynamic model of wind energy plants in this benchmark, a second generation (type-2) wind turbine WT2G models is used for simplicity. The WT2G model is based on a standard induction machine model, and accounts for the rotor flux dynamics. This model along with supporting dynamic models mentioned above was developed through the

Western Electricity Coordinating Council (WECC) Modeling and Validation Work Group (MVWG) [16]. These WECC models were designed specifically for large transmission network planning studies including large numbers of generators, loads, and dynamic components [16]. They are designed to evaluate the transient performance of such systems, for example transmission level faults and transients, which make them suitable for a wind energy transmission benchmark system.

In power system simulators, an analogy is made between wind machine models and synchronous machine models, between wind electrical models and exciter models, between wind pitch control models and stabilizer models, and also between wind aerodynamic models and stabilizers as well.

The models developed by the WECC MVWG were developed as sets of compatible models. The WT2G wind machine model is compatible with WT2E Exciter model, the WT2T governor model, and the WT2P stabilizer model. Fig. 4 shows the block diagram for the WT2E exciter model used. Fig. 5 below show the block diagram for the stabilizer models used.

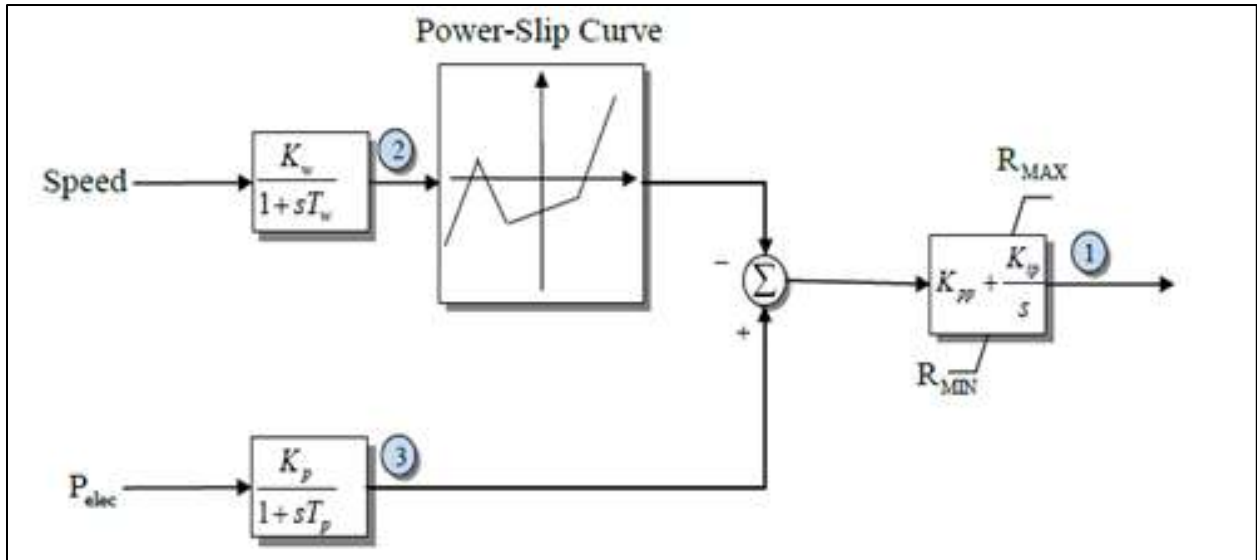


Fig. 4. WT2E exciter model.

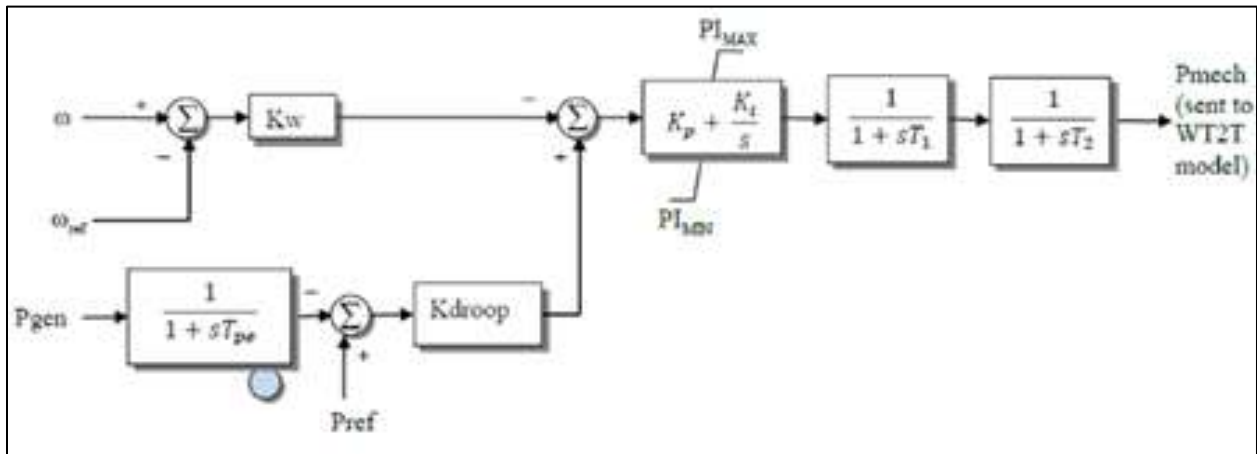


Fig. 5. WT2P stabilizer model.

III. Synchrophasors

Actual synchrophasor data were provided by a utility company. Synchrophasors were provided for multiple events. An event represents recorded synchrophasor measurements for a particular duration at a particular time and particular date. Synchrophasor data was provided in a “.phasor” file format for each event. Those were provided with a “MakeCSV” utility that created a comma separated values file (.CSV file) for each event. Each event CSV file contained data frames for 268 terminal IDs at a sampling rate of 30 frames per second. Each frame is composed of the time stamp, terminal ID number, current magnitude, current angle, voltage magnitude, voltage angle, frequency, rate of change of frequency (ROCOF).

The sizes of the resulting CSV files varied by the duration of the event. For some events, the resulting CSV file was about 3 million lines long. It was a challenge visualizing and processing synchrophasor data of such size. Frames were reported by for all terminal IDs before a time step occurs. Table 1 below illustrates the formatting of the CSV files.

Table 1. Synchrophasor data reporting format

Time stamp (mm/dd/yyyy hh:mm:ss.000)	Term ID	I Mag (A)	I Angle (Degrees)	V Mag (V)	V Angle (Degrees)	F (Hz)	DFDT (Hz/s)
t1	1	***	***	***	***	***	***
t1	2	***	***	***	***	***	***
⋮	⋮	***	***	***	***	***	***
t1	Term ID _n	***	***	***	***	***	***
t2	1	***	***	***	***	***	***
t2	2	***	***	***	***	***	***
⋮	⋮	***	***	***	***	***	***
t2	Term ID _n	***	***	***	***	***	***
⋮	⋮	***	***	***	***	***	***
t_n	Term ID _n	***	***	***	***	***	***

To process this synchrophasor data, a python script was written to extract specific synchrophasor measurements (i.e. voltage) for specific terminal ID's (i.e. Term ID X). The results were column vectors for specific synchrophasor measurements at specific terminal IDs. Each element corresponds to a time step. These column vectors were then processed in both Matlab and Excel, as will be discussed in the subsequent chapters for model validation and parameter extraction purposes.

Another tool that was used to visualize and process the available synchrophasor data was "Power BI". It is a business intelligence data analytics tool provided by Microsoft. Power BI was meant for big data analysis, where multiple tables are to be analyzed with existing relationships between tables. First CSV files were formatted as Excel tables, then those tables were imported to Power BI. The relationships between tables were defined, and a viewing platform was developed to visualize those synchrophasors. Fig. 6 below shows a snap shot for one for the viewing platforms of one of the events provided by a transmission operator.

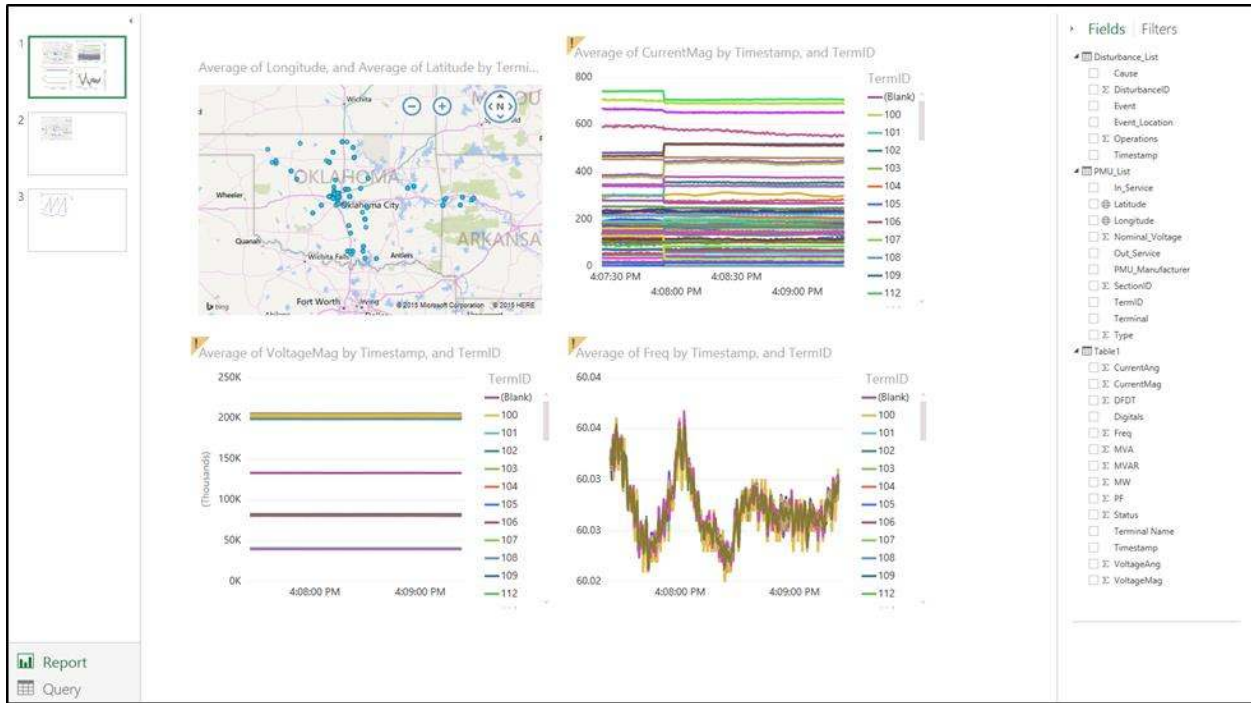


Fig. 6. Synchrophasor viewing platform.

Fig. 6 shows the location, current magnitude, voltage magnitude, and frequency for a particular event for all terminal IDs. Top left is the location, top right is the current magnitude, lower left is for the voltage magnitude, and lower left for the frequency. The platform is interactive, clicking on a particular term ID location will filter all other plots to only show that particular term ID measurements.

More description about synchrophasor theory in general, and particular information about PMU terminals and synchrophasor data made available will be presented and discussed later where relevant in the validation and the Y_{bus} estimation chapters.

IV. Model Development Method

This chapter discusses the model development process. This includes the reduction technique used, and how this technique was used to develop the benchmark model. The model development process is intended to be generic. It can be applied using various criteria to different systems to develop various models for specific simulation needs.

A. Power System Reduction

As power transmission networks are large and complex so are power system transmission models. It is common practice in the power system field to use reduced power system models, which accurately captures the main features and details of the original system. Using reduced models reduces the computation and time resources needed for power system analysis. As in most cases, analysis and studies are more interested in a particular area of interest rather in the full system. Therefore the power system to be simplified or reduced is normally divided to two areas, an area of interest and an external area. There are many reduction methods that are well established in the literature.

Power system reduction techniques can be classified in two major categories. Static power system reduction methods and dynamic power system reduction methods. Static methods are suitable for static analysis including power flow studies, system operation studies and planning studies. Dynamic methods are suitable for dynamic studies such as inter-area oscillations.

The two most used dynamic reduction methods are the Balanced Truncation (BT), and Modal Truncation (MT) methods [17]. In modal truncation, certain dominant modes including

electromechanical modes are identified to be retained in the external system based on the time constants of the decaying transients. One of the shortcomings of this method is that it does not retain steady state values. This method is suitable for controller design and stability studies. In balanced truncation methods modes that are less controllable or observable are eliminated. Balanced truncation methods do not retain the external system modes accurately but provide a better frequency response approximation than modal truncation methods.

The main static reduction methods include Dima's method, Kron reduction, Ward reduction, and Zhukov's method. One way to check the validity of such methods is to compare the results of the full system and the reduced system. Many comparison studies have been performed on these methods [18]. One way of comparing those methods is to compare how closely the results of the reduced system follows the original system for each method. The Kron method is less accurate than other methods. The Ward method is the most accurate. Both, the Kron and the Ward methods are less complex than the other two methods. Zhukov's method is accurate for small systems, but is not accurate for large systems. Dima's method is accurate for small load variations, but loses accuracy as load changes increase. The Ward reduction method has been selected for the purposes of this research due to its accuracy and compatibility with power system simulation software.

The Ward reduction method was proposed in [19]. It is the most commonly used power system reduction technique. It is based on dividing the system into internal and external subsystems. The internal subsystem remains explicitly detailed. The external subsystem is equivalenced via Gaussian elimination. This is illustrated in Fig. 7 below. This method was proposed for power flow studies. It is not suitable for transient stability and contingency analysis as it does not model external area reactive power support.

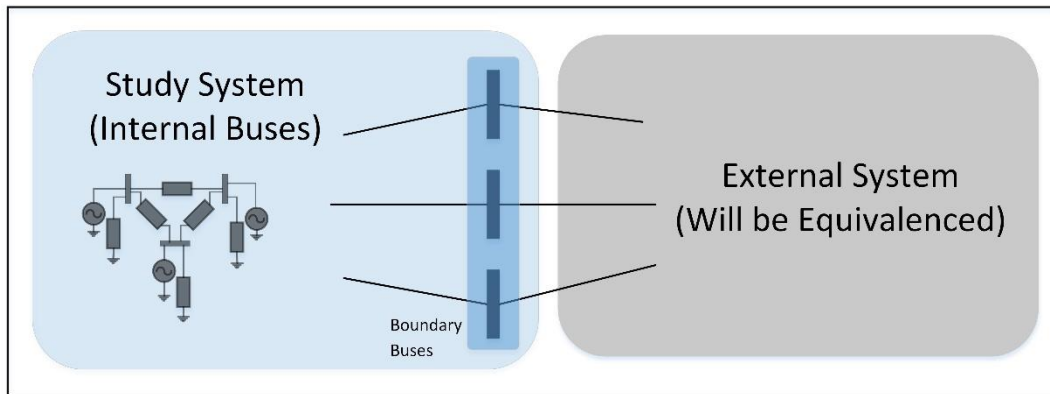


Fig. 7. Ward reduction method subsystems.

Even though a static reduction method is used, the reduced equivalent model is also suitable for transient stability studies. The goal of this task was to produce a benchmark model for wind energy systems. Therefore, the area of interest was selected to be the wind generation dense area of north-western Oklahoma. The further away we get from the area of interest the less detailed modeling is needed. The area of interest as defined in Chapter 6 is maintained fully detailed and is described explicitly. The rest of the network is considered an external network and is reduced. Since the wind energy area of interest is fully detailed including the transient stability models, it is a fair claim that this benchmark is suitable for realistic transient stability studies for wind energy systems. This benchmark model will not be suitable for transient stability studies for the actual transmission system as the Ward reduction method is only suitable for static analysis. To summarize, the resulting benchmark system is suitable for generic realistic wind energy transient stability studies. It is also suitable for static studies and planning purposes for the actual system.

B. Model Development Process.

This section outlines the model reduction process used to develop the benchmark model. This process assumes a more detailed full system model is available and it is desired to reduce the system to obtain a simpler model for specific purposes.

It is recommended to perform system reduction in three steps. Those are geographical reduction, substation reduction, and transmission system reduction sequentially as illustrated in Fig. 8 below. First, a geographical area of interest is selected based on the purpose of the benchmark model. The system is divided into internal buses and external buses based on the geographical selection. All buses within the area of interest and some of the surrounding area are to be considered the internal buses or “study system” buses. All other buses are considered external buses. After the study system bus selection is done, the Ward reduction method is implemented based on the “Study”/“external” system selection. The result is the first reduced version of the model. The resulting model contains all internal buses, and an equivalent of the external system. For a transmission level analysis a substation appears a single bus with interconnected elements. The second step is to reduce all substations left in the first reduced model. To do this, only the transmission level bus and the generator bus of each substation are considered the study system. Everything else within each substation is equivalenced. This results in the second reduced version of the model. Finally the system is reduced based on the transmission voltage level of interest based on the purpose of the model. All buses that meet the voltage level criteria are considered “study” buses, and all other buses are reduced. After the last reduction step is completed an inspection of the system is to be performed to ensure that the model includes all the intended details and none of the unintended details. It is also recommended to generate a one-line diagram of the system to visually inspect the system. Depending on the

results of the last reduction step, another iteration of reduction might be necessary to refine the model.

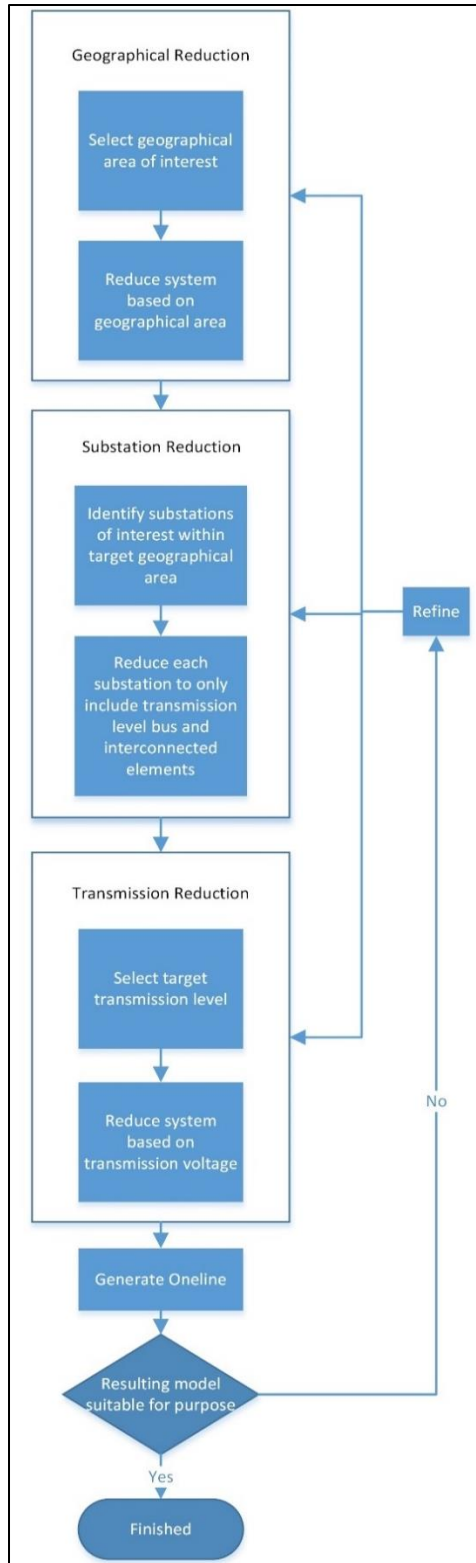


Fig. 8. Model development process.

V. Model Validation Method

Now that the model development process has been established it will be used to develop the proposed wind energy benchmark model. The model then needs to be validated. Synchrophasors are to be used for model validation. The model needs to be validated both qualitatively and quantitatively. Exact matches for flows should not be expected. As per NERC Model Validation Working Group recommendation modeled power flow should be within +/- 10% of measured values [8]. NERC recommends the comparison of bus voltage angles wherever available [8]. Model validation has been done using actual PMU synchrophasor measurements provided by a utility company.

A. Qualitative model validation

Traditional phasor analysis in the frequency domain treats phasors as stationary vectors. The magnitude of those vectors is the magnitude of the sinusoidal signals under investigation. The angle of those vectors are the angles of the sinusoidal signals under investigation with respect to the angle of a reference signal. This reference signal in traditional power system analysis is chosen to be the voltage of the slack bus. Fig. 9 below illustrates the phasor angles of three arbitrary waveforms. If those phasors were to be in real-time, they would be rotating vectors. The rotation speed is the frequency of the signal under investigation. In most cases this frequency would be slightly variable and slightly off nominal frequency. Therefore the rotation of the voltage phasor is not at nominal frequency and not constant.

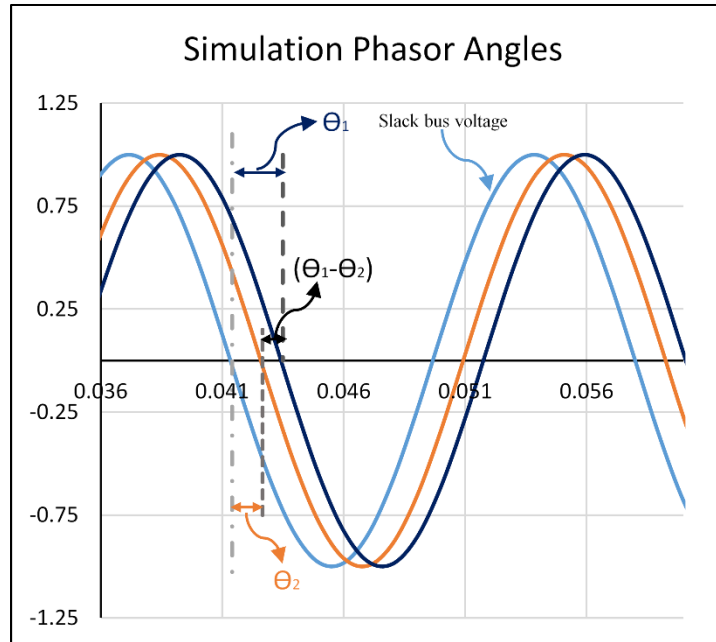


Fig. 9. Illustration of power system simulation voltage angles.

Current and voltage synchrophasors are synchronized phasors. They are synchronized via a GPS signal. The reference for synchrophasors is an internally generated 60.000 Hz cosine wave in each PMU. This internal reference is generated with its peak precisely aligned to the second based on a GPS time signal. This is done with a precision on the order of the microsecond. Fig. 10 illustrates synchrophasor angle processing.

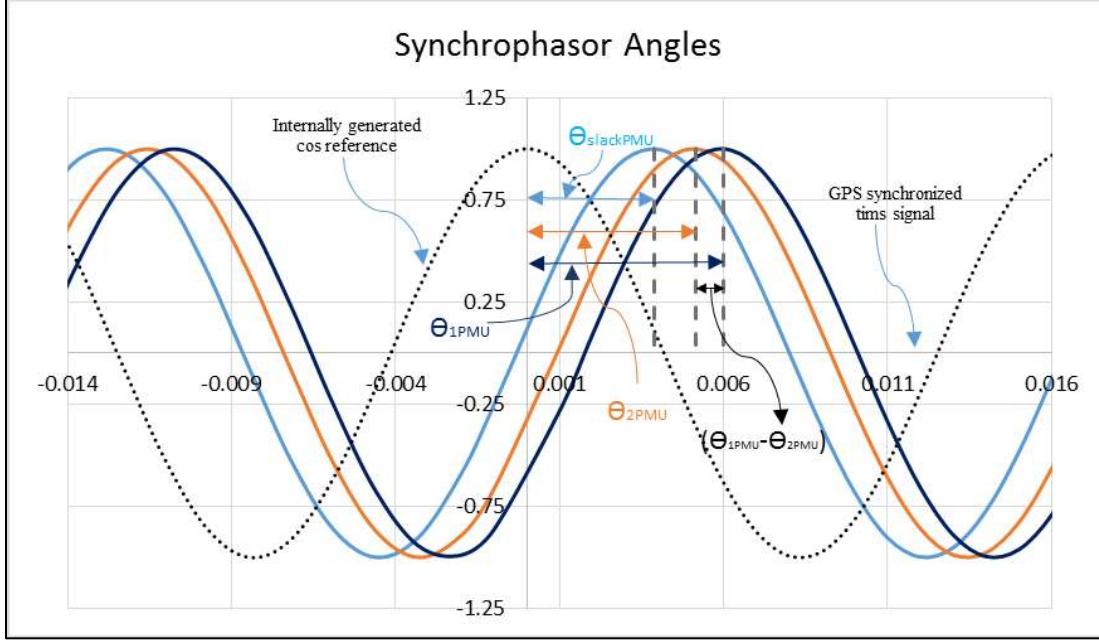


Fig. 10. Illustration of synchrophasor voltage angles.

One effective method to validate the proposed benchmark model is to compare model simulation results to the actual power system synchrophasor measurements. One important quantity to compare is the voltage angle. Direct comparison of voltage angles between PMU voltage synchrophasor angles and simulation voltage angles is not valid as those angles have different references. The solution is to compare angle differences. This solves the issue of reference difference, and provides insight into power transfer. If the two buses, bus₁ and bus₂ are connected through a transmission line then the power transfer between bus one and two follows the relationship in (13). The angle difference ($\theta_1 - \theta_2$) is referred to as the power angle, with maximum power transfer occurring at a 90° difference as can be seen in Fig. 11. Comparing the angle difference ($\theta_1 - \theta_2$) from Fig. 9 to the angle difference ($\theta_{1PMU} - \theta_{2PMU}$) from Fig. 10 illustrates the validity of the approach.

$$P = \frac{|V_1||V_2|}{X} \sin (\theta_1 - \theta_2) \quad (13)$$

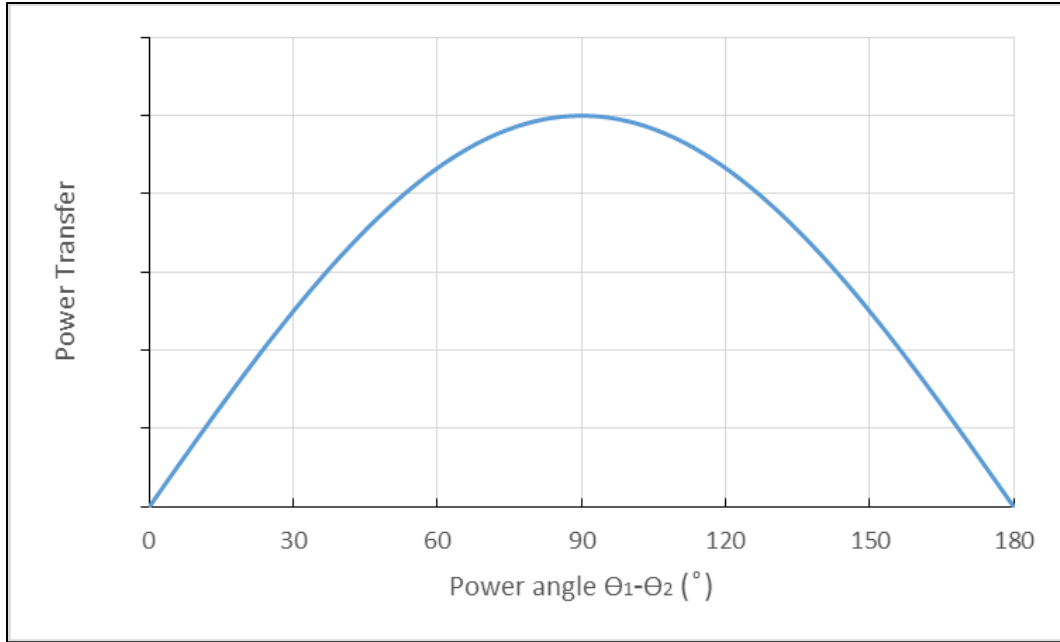


Fig. 11. Plot of power transfer dependence on power angle.

Actual synchrophasor data provided by a utility company were used for system validation. Synchrophasors were provided in a “.phasor” file format for each event. Those were provided with a “MakeCSV” utility that created a comma separated values file (.CSV file) for each event. Each event CSV file contained data frames for 268 terminal IDs at a sampling rate of 30 frames per second. Each frame is composed of the time stamp, terminal ID number, current magnitude, current angle, voltage magnitude, voltage angle, frequency, rate of change of frequency (ROCOF).

Each terminal ID corresponds to a specific PMU. PMUs were named based on the type of synchrophasor it measures as follows:

❖ **For lines:**

The terminal name is in the format of “from substation” – “to substation”. The current synchrophasor is the current through the line, while voltage synchrophasor is the voltage at the “from-bus”.

❖ **For generators:**

The terminal name is in the format of “substation”-“generation unit number”.

❖ **For transformers:**

The terminal name is in the format of “substation”-“transformer number”. Parenthesis show where the measurement is coming from (kV-kV).

As discussed above, the power angle is ideal for validation purposes. For that reason, transmission line PMUs were used for validation. Therefore, voltage angles needed to be extracted for validation. To process these synchrophasor data, a python script was written to extract voltage angles for specific terminal ID's (i.e. Term ID X). The results were column vectors for voltage angles at specific system buses. Each element in the vector corresponding to a time step. These column vectors were then processed and plotted. To demonstrate, an example plot of voltage angle column vectors for the two buses across a 345 kV transmission line is shown in Fig. 12 below.

Fig. 13 below illustrates an example of system frequency throughout the entire system as measured by the PMUs provided by a utility company. It can be observed that the system oscillates at an off-nominal frequency of an average of about 60.04 Hz. This causes the voltage synchrophasors to rotate at the same off-nominal frequency. The internally generated reference signal rotates at the nominal frequency of 60 Hz. The difference of frequency between the

reference signal and the actual voltage synchrophasors lead to a continuous increase in the phase angle. This effect can be observed in Fig. 12. The difference of frequency also leads to a wrapping effect where the voltage synchrophasors do an additional rotation every ~25 seconds (~1/0.04 s). This effect can be visually observed in Fig. 12 as well. It manifests in the jump from 180° to -180° every ~25 seconds.

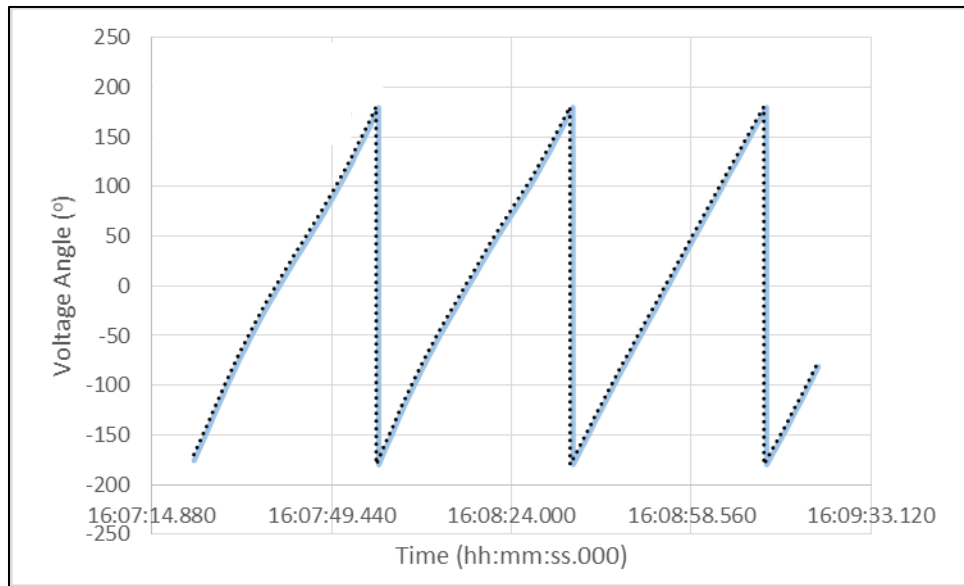


Fig. 12. Synchrophasor voltage angles across the 345 kV line.

$(\Theta_{1PMU} - \Theta_{2PMU})$ or in other word, the power angle of the 345 kV transmission line is plotted in Fig. 14 below. Some off-shoots of about 350° can be observed. Those off-shoots are due to the difference in phase angle. This causes the “wrapping effect” to occur at different times corresponding the phase angle difference. When eliminating the few off-shoot data points, a more meaningful plot is produced. A corrected plot of the power angle of the 345 kV transmission line is presented in Fig. 15 below. Another way to eliminate those shoot-offs is to use the identities in (14) and (15). If those identities are applied for those shoot-off data points,

that would yield a corrected graph. In other words $\cos(350^\circ) = \cos(-350^\circ) = \cos(360^\circ - 350^\circ) = \cos(10^\circ)$.

$$\cos(x) = \cos(-x) \quad (14)$$

$$\cos(x) = \cos(x + 360^\circ) \quad (15)$$

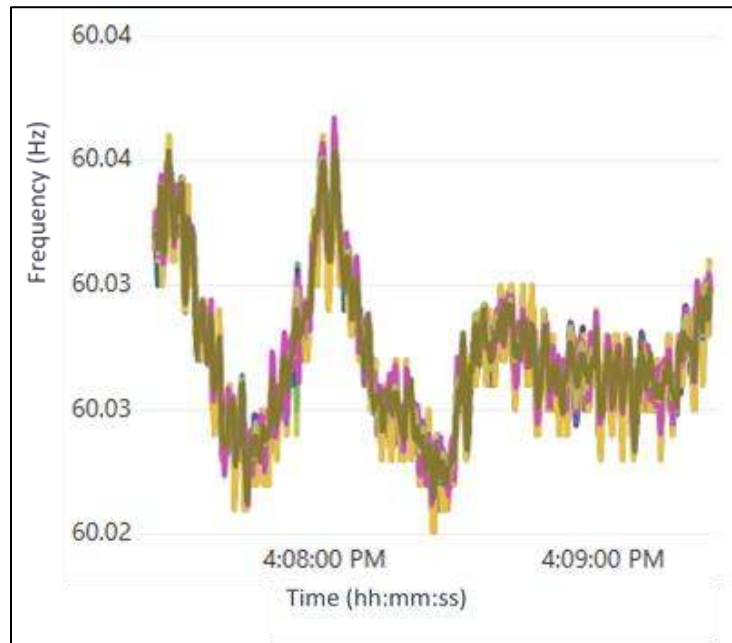


Fig. 13. System frequency from synchrophasor measurements.

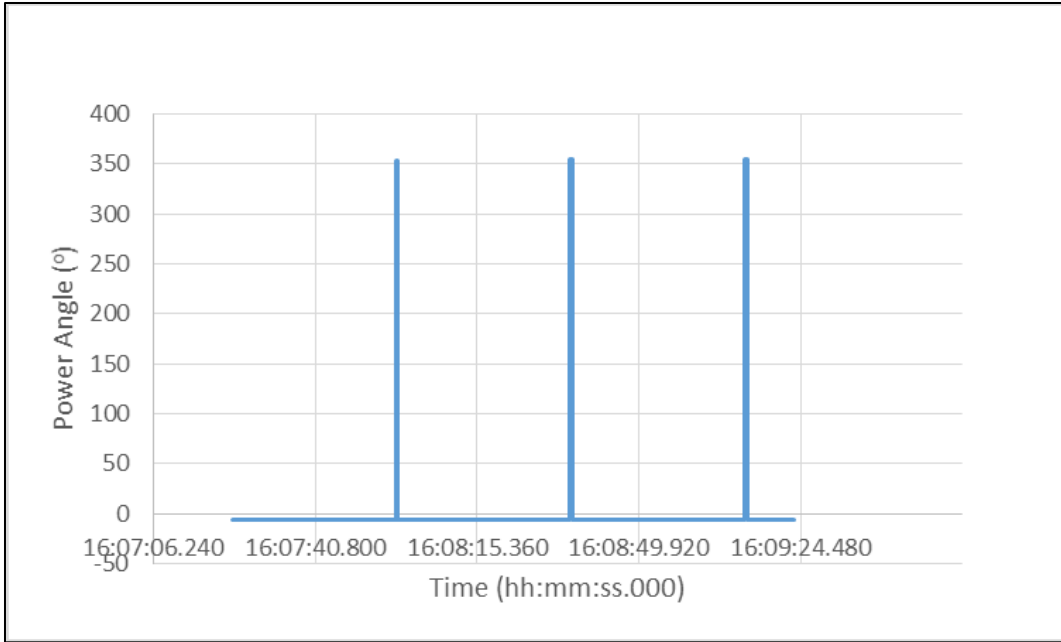


Fig. 14. Raw synchrophasor calculated power angle.

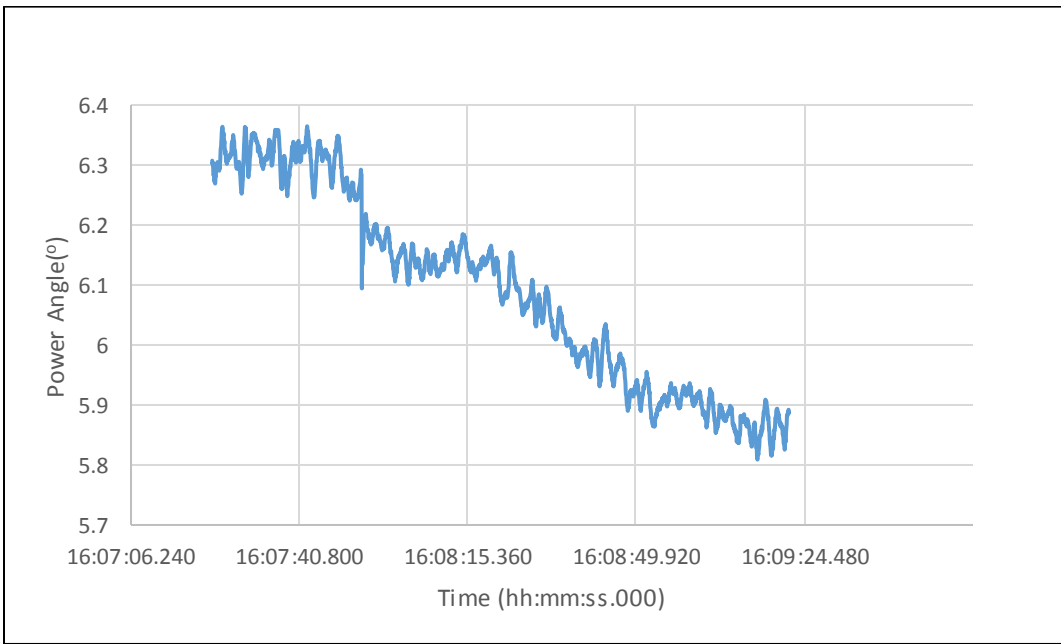


Fig. 15. Corrected synchrophasor power angle.

The power angle result from Fig. 10 will then be compared to the simulated power angle from the reduced benchmark model as described in Fig. 4 for a qualitative validation.

B. Quantitative model validation

Now that the model has been validated qualitatively, validation needs to be done quantitatively as well. An error function was derived to serve as a comparison metric between the simulated results and the measured results. The simulated results are the results of the benchmark model. The measured results are the PMU synchrophasor data. The main result of interest is the real power flow in the transmission line. Power flow from bus j to bus k through transmission line l is governed by (16).

$$P_{jk} = -P_{kj} = \frac{|V_j||V_k|}{|Z|} \cos(\theta - \delta) - \frac{|V_k|^2}{|Z|} \cos(\theta). \quad (16)$$

Where,

$$\bar{Z} = |Z| \angle \theta \quad (17)$$

is the impedance of transmission line l .

$$\delta_{jk} = \delta_j - \delta_k. \quad (18)$$

where, δ_j , and δ_k are the voltage angles at buses k and i respectively. Typically the resistance of the transmission line is much smaller than the reactance of the transmission line, thus the assumption can be made that

$$|Z| \approx X_{jk} \quad (19)$$

and,

$$\theta \approx 90^\circ. \quad (20)$$

Under these approximations, (16) reduces to

$$P_{jk} = \frac{|V_j||V_k|}{X} \sin(\delta_{jk}). \quad (21)$$

For a small power angle δ_{jk} , (21) can be approximated as

$$P_{jk} = \frac{|V_j||V_k|}{X_{jk}} \delta_{jk}. \quad (22)$$

If voltage magnitudes are assumed to be constant at 1.0 per unit, real power flow can be simplified to follow (23), where P_{jk} is the real power flow between bus j and bus k , δ_j and δ_k are the voltage angles at buses j and k respectively, and X_{jk} is the reactance of transmission line l connecting buses j and k . From (23) and (18) power angles are directly proportional to real power flow, therefore they were used to estimate the error.

$$P_{jk} = \frac{\delta_j - \delta_k}{X_{jk}} \quad (23)$$

Simulated power angles and measured power angles were used to calculate the power angle error for each of the n transmission lines. Power angle errors were weighted according the participation factor in (24) and (25). The participation factor P_h represents the real power flow in transmission line h . Weighted power angles were then used to derive a normalized relative error for the entire system as in (26). It is worth noting that this is done for all transmission lines where a PMU synchrophasor measurement is available at both ends of the transmission line.

$$W_h = \frac{P_h}{\sum_{h=1}^n P_h} \quad (24)$$

$$W_h = \frac{abs(\delta_{jk})}{\sum_{h=1}^n abs(\delta_{jk})} \quad (25)$$

$$\varepsilon = \frac{\left[\frac{1}{n} \sum_{h=1}^n (\delta_{h \text{ pmu}} - \delta_{h \text{ benchmak}})^2 w_h \right]^{\frac{1}{2}}}{\left[\frac{1}{n} \sum_{h=1}^n \delta_{h \text{ pmu}}^2 \right]^{\frac{1}{2}}} \quad (26)$$

This relative error was then used to derive a measure of confidence σ as in (27).

$$\sigma = 100\%(1 - \varepsilon) \quad (27)$$

NERC recommends that the error in power flows be within +/- 10%. Therefore it is desired that the maximum error be within the 10% range. For that reason, a more representative error norm corresponding to NERC recommendations is the ∞ -norm as described in (28).

$$\|Error\|_{\infty} = \max_{h=1}^n |Error_h| \quad (28)$$

VI. Wind Energy Benchmark System

A. Wind Energy Transmission Model Development

The initial model from which the benchmark model was derived is a transmission operator operation model. The model is made up of 15814 buses. It includes 17204 transmission lines, and 2796 generators. The benchmark model is a reduced version of the aforementioned model. It is based on the transmission network of Oklahoma including the wind generation concentration in the surrounding region. Most of the conventional power plants are connected to transmission lines operating at 345 kV and above. Most wind generation plants are connected to the 138 kV and above transmission network. As this is intended to be a wind energy transmission benchmark model, it focuses on the wind generation concentrated in western Oklahoma. Most of this capacity is transmitted eastwards toward the major load centers.

The initial model was provided by a transmission operator in a PSSE “.raw” format. This model was imported into the PowerWorld simulator, and then reduced via the Ward reduction method discussed above in the PowerWorld simulator to arrive at the benchmark model. Then the model was verified and validated using PMU synchrophasor measurements with help from Oklahoma Gas and Electric.

As discussed above, the reduction is done in three steps. Those are geographical reduction, then substation reduction, then transmission system reduction. In each one of those steps, first the study system buses were selected based on the chosen criteria. Then the Ward reduction method was employed.

The criteria for bus selection was based on the purpose of the benchmark model. As discussed above, the area of interest is western Oklahoma due to the purpose of the benchmark to serve as a wind energy benchmark model. This area was allocated as a “zone” code in the operational model used. The first reduction step was to reduce all buses external to the identified zone. Then, each substation in the system was reduced to a transmission level bus with connected generators, loads, and compensation. Then entire system was reduced again to maintain only transmission level voltage of interest of 138 kV and above. The transmission level voltage selection was based on the realization that wind generation in the Oklahoma operating region is connected to the 138 kV and above transmission network. The resulting system contained 96 buses, 180 transmission lines, and 11 generators. A geographical representation of the transmission network is presented in Fig. 16 below.

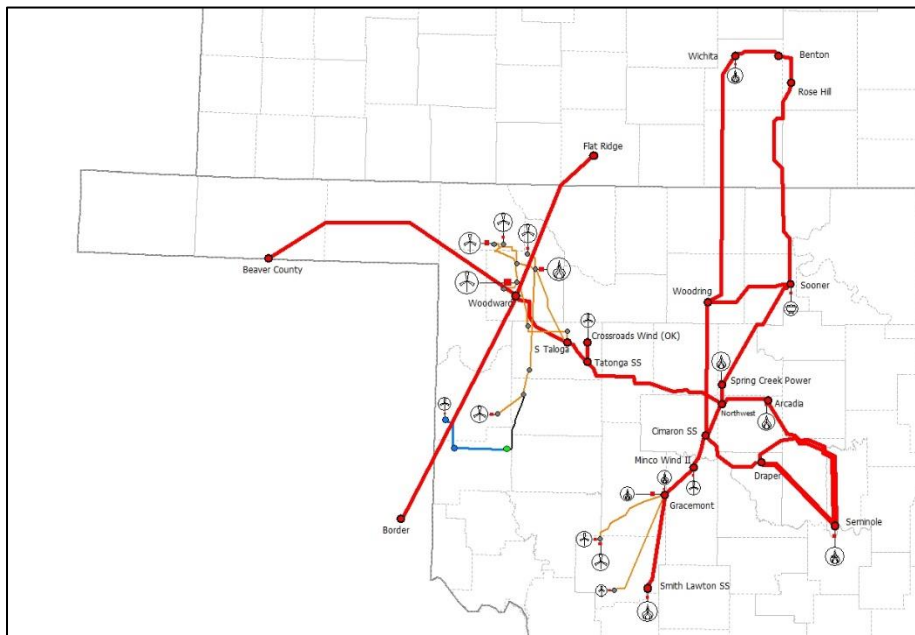


Fig. 16. Geographical representation of the proposed benchmark model.

Generator information for the reduced model are tabulated in Table 2 below. Load flow results are tabulated in Table 3. Load information are tabulated in Table 4. Line information are

tabulated in Table 5. Full simulation files of the benchmark model are available for download to the public at “grapes.uark.edu” in a “.raw” format. Next, load flow results are validated using PMU Synchrophasor measurements.

Table 2. Proposed benchmark generator data.

Bus Number	Generation (MW)	Generation (MVR)
44	412	32.13
45	393	-61.87
48	4	1.31
55	10	3.29
57	14	4.6
59	9	2.93
67	42	11.82
71	11	3.62
72	47	6.87
73	18	8.44
96	7	2.3

Table 3. Proposed benchmark bus data.

Bus number	Nominal Voltage (kV)	Voltage (kV)	Angle (°)
1	138	140.361	-20.11
2	138	140.004	-20.9
3	138	140.884	-19.48
4	138	141.879	-14.14
5	138	141.181	-16.04
6	138	141.226	-15.87
7	138	141.035	-18.27
8	138	141.075	-19.37
9	138	141.05	-20.35

10	138	140.938	-19.98
11	138	139.884	-21
12	138	141.025	-16.84
13	138	141.153	-19.25
14	345	350.965	-16.36
15	138	140.68	-20.41
16	138	141.327	-19.25
17	138	140.353	-21.08
18	138	141.872	-14.14
19	138	141.035	-18.13
20	138	140.361	-18.4
21	138	140.397	-18.39
22	138	139.092	-19.56
23	138	140.527	-18.34
24	138	138.591	-20.71
25	138	139.147	-19.86
26	138	140.727	-18.07
27	138	139.069	-19.97
28	138	140.153	-21.18
29	138	141.623	-18.66
30	138	141.24	-20.9
31	138	140.255	-21.87
32	138	140.036	-19.37
33	138	140.898	-21
34	138	140.593	-21.56
35	138	140.383	-21.41
36	138	140.454	-20.99
37	138	139.401	-23.67
38	138	140.107	-19.99

39	138	141.905	-14.2
40	138	141.875	-14.22
41	138	142.14	-13.46
42	345	348.45	-13.29
43	138	138.084	-21.58
44	22	22.222	-40.72
45	20	19.99	-39.67
46	345	348.974	-13.66
47	138	140.781	-19.16
48	34.5	35.247	-18.93
49	138	141.422	-18.71
50	345	351.852	-18.19
51	138	139.725	-18.96
52	138	138.435	-20.97
53	138	140.004	-20.9
54	138	140	-20.95
55	34.5	35.5	-20.07
56	138	141.522	-20.63
57	34.5	35.146	-18.03
58	138	140.016	-18.7
59	34.5	35.091	-18.31
60	138	139.918	-18.82
61	138	141.291	-15.7
62	138	140.666	-19.7
63	345	355.05	-17.49
64	138	141.358	-15.66
65	138	141.36	-19.44
66	345	355.35	-17.39
67	34.5	35.93	-15.11

68	345	349.419	-22.25
69	345	351.61	-16.3
70	345	351.61	-16.3
71	34.5	35.289	-15.68
72	34.5	35.749	-12.43
73	34.5	35.365	-15.31
74	138	141.164	-19.16
75	138	141.167	-19.16
76	345	351.717	-16.39
77	138	140.375	-18.73
78	138	139.87	-19.17
79	138	140.26	-21.9
80	345	354.432	-17.91
81	138	140.256	-21.87
82	138	140.187	-18.89
83	345	349.099	-13.56
84	138	139.39	-19.4
85	345	355.688	-17.5
86	345	355.077	-17.49
87	345	354.515	-17.92
88	345	351.928	-18.19
89	345	350.917	-18.1
90	345	348.974	-13.66
91	345	354.553	-17.92
92	138	140.383	-20.07
93	138	139.915	-21.01
94	138	140.841	-21.03
95	138	141.131	-20.85
96	34.5	35.409	-20.33

Table 4. Proposed benchmark load data.

Bus number	Load (MW)	Load (MVR)	Load (MVA)
1	4.61	0.6	4.65
3	14.76	8.76	17.16
7	20.6	1.8	20.68
8	7.25	1.13	7.34
10	4.21	0	4.21
12	21.42	7.93	22.84
16	8.61	1.49	8.74
18	7.92	1.04	7.99
19	2.68	0.35	2.7
20	59.35	27.04	65.22
21	12.54	5.89	13.85
23	20.37	11.81	23.55
26	2.39	0	2.39
28	7.17	0	7.17
30	4.86	0.28	4.87
33	3.27	0	3.27
34	0.65	0.09	0.66
34	2.7	0.49	2.74
35	2.65	0.49	2.69
36	4.08	0.53	4.11
38	7.19	5.02	8.77
40	2.06	1.07	2.32
44	0	0	0
45	0	0	0
48	0	0	0
49	9.81	1.33	9.9
52	2.49	0.17	2.5

55	0	0	0
57	0	0	0
59	0	0	0
61	3.93	1.54	4.22
62	0	0	0
67	0	0	0
71	0	0	0
72	0	0	0
73	0	0	0
74	0.91	0.4	0.99
78	10.49	5.33	11.77
79	3.52	0.5	3.56
93	10.7	4.23	11.51
96	0	0	0

Table 5. Proposed benchmark line information.

Line Number	R	X	B
1	0.03036	0.08257	0.01964
2	0.00125	0.0034	0.00081
3	0.00085	0.00899	0.00273
4	0.01063	0.02892	0.00687
5	0.00002	0.00004	0.00001
6	0.00134	0.01419	0.00431
7	0.0001	0.0005	0
8	0.00144	0.0051	0.00139
9	0.0009	0.00963	0.00287
10	0.00205	0.02199	0.00656
11	0.00054	0.0062	0.00159

12	0.00483	0.0289	0.00756
13	0.00684	0.06426	0.02664
14	0.00985	0.05878	0.0155
15	0.00812	0.04827	0.01291
16	0.00045	0.00256	0.00075
17	0.00442	0.02624	0.00709
18	0.0045	0.02535	0.00755
19	0.00797	0.04503	0.01333
20	0.00243	0.01407	0.00451
21	0.00229	0.01186	0.00608
22	0.01003	0.05962	0.01603
23	0.00233	0.02185	0.36537
24	0.0011	0.01031	0.17229
25	0.00304	0.01799	0.00487
26	0.00544	0.03062	0.00908
27	0.00199	0.01124	0.00333
28	0.00161	0.00911	0.0027
29	0.00354	0.01317	0.00328
30	0.0064	0.01741	0.00414
31	0.00492	0.0527	0.01572
32	0.00026	0.00148	0.00044
34	0.00243	0.01374	0.00407
35	0.00065	0.00368	0.00109
36	0.00842	0.0313	0.00782
37	0.00409	0.02332	0.00666
38	0.00434	0.01616	0.00403
39	0.00163	0.00605	0.00151
40	0.01251	0.04655	0.01161
41	0.00065	0.00241	0.0006

42	0.00338	0.03561	0.01099
43	0.00399	0.02331	0.00649
44	0.00899	0.02436	0.00583
45	0.05152	0.11279	0.02577
46	0.00004	0.00024	0.00007
47	0.03712	0.12614	0.03751
48	0.00151	0.01078	0.00775
49	0.00302	0.02417	0.014
50	0.02392	0.05206	0.01202
51	0.02169	0.08073	0.02013
52	0.01372	0.07524	0.02347
53	0.00775	0.04597	0.01244
54	0.01006	0.05959	0.01617
55	0.0114	0.06525	0.01879
56	0.00452	0.01622	0.00433
57	0.00092	0.00989	0.00295
58	0.00088	0.01495	0.26665
59	0.00389	0.01447	0.00361
60	0	0.00004	0.00066
61	0.00145	0.0251	0.4252
62	0.00279	0.04603	0.8323
63	0.00294	0.04657	0.91318
64	0.00294	0.04657	0.91318
65	0.00054	0.0049	0.08712
66	0.0034	0.0338	0.0115
67	0.00527	0.02888	0.009
68	0.00053	0.00296	0.00091
69	0.00185	0.01045	0.00309
70	0.00587	0.02087	0.00567

71	0.0101	0.02737	0.00655
72	0.00862	0.02335	0.00559
73	0.00054	0.00454	0.09258
74	0.00156	0.01419	0.2527
75	0.00032	0.00294	0.05227
76	0	0.00002	0.00032
77	0.0011	0.01035	0.1731
78	0.00067	0.00399	0.00108
79	0.00761	0.04358	0.01242
80	0.00211	0.01214	0.00345
81	0.00223	0.01228	0.00387
82	0.00023	0.00222	0.0482
83	0.01282	0.07313	0.02092
84	0.00034	0.00581	0.10355
85	0.00025	0.00247	0.0836
86	0.00893	0.05049	0.01497

B. Wind Energy Transmission Model Validation

a. Qualitative model validation

Qualitative validation was performed on the developed wind energy system as described in chapter 5. The power angle results as demonstrated in Fig. 15 is compared to the simulated power angle from the reduced benchmark model as described in Fig. 9. For a more rigorous validation, the same validation process was done for various transmission lines in the system for various events. Each event representing different operating conditions for the model. Table 6 below tabulates the simulated power angles and the measured synchrophasor processed power angles for transmission lines in the wind generation region of benchmark model. Fig. 17 through Fig. 20 shows the processed power angle of four different lines in the wind generation region.

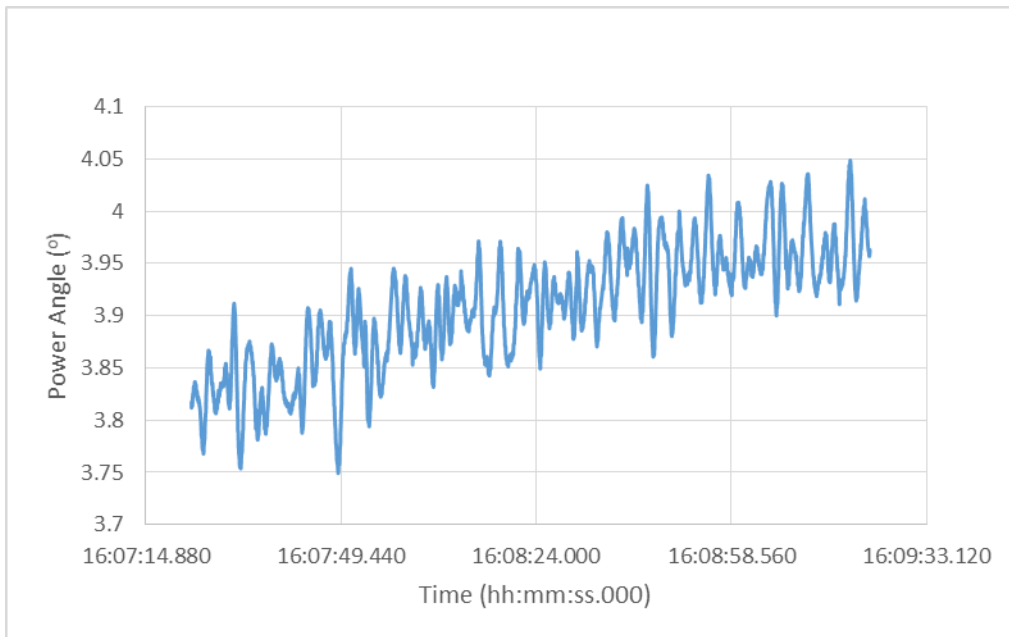


Fig. 17. Measured power angle of transmission line 2.

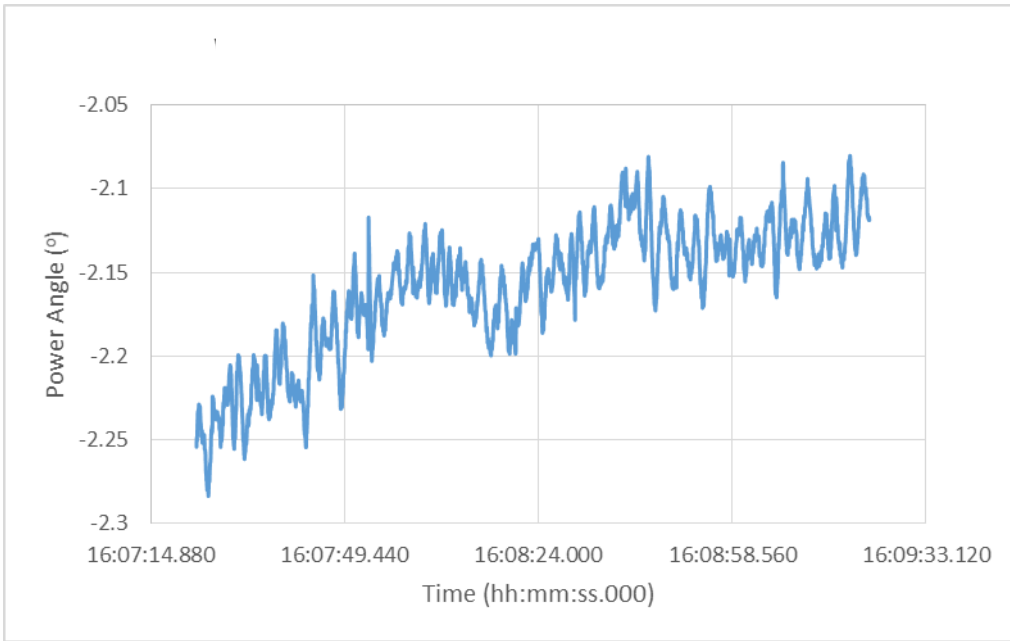


Fig. 18. Measured power angle of transmission line 3.

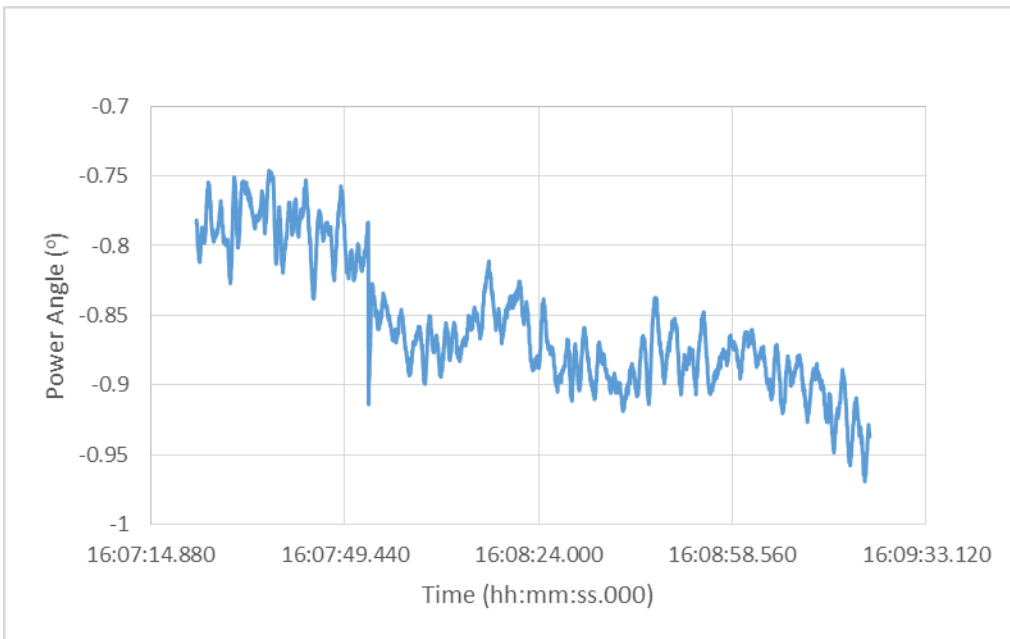


Fig. 19. Measured power angle of transmission line 4.

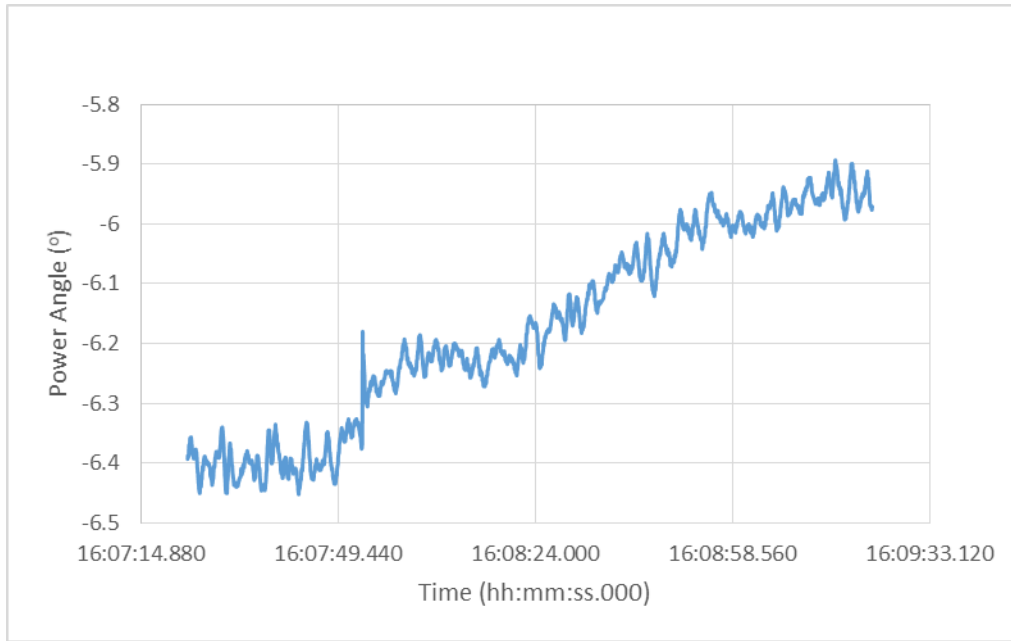


Fig. 20. Measured power angle of transmission line 6.

Table 6. Measured vs. simulated power angles (°).

Line number	Model			PMU
	From bus	To bus	Power angle	Power angle
2	-12.16	-16.08	3.92	3.836
3	-12.16	-9.79	-2.37	-2.216
4	-12.16	-11.29	-0.87	-0.785
6	-18.48	-11.29	-7.19	-6.398

b. Quantitative model validation

Now that the model has been developed and validated qualitatively, quantitative validation needs to be done as well. The quantitative model validation method discussed in chapter 5 is used for that purpose. For a rigorous validation, validation was done using various transmission lines and under various operating conditions. All transmission lines of 138 kV and above where a synchrophasor measurement is available were used in the validation process. Various events were used for validation. The use of various operating conditions (events) in the

validation process ensures the validity of the model under different conditions. The results discussed in (23) through (28) are tabulated in Table 7 through Table 9 for the various events used. For the first event, the normalized error ϵ was 1.97%, well within NERC recommendation [8]. The confidence measure σ was 98%. The error values of the other events can be viewed in Table 7 through Table 9.

Table 7 Quantitative validation results for first event.

h	$\delta_{h \text{ benchmak}}(^{\circ})$	$\delta_{h \text{ pmu}}(^{\circ})$	Error	Error²	w_h	Error²*w_h	$\delta_{h \text{ pmu}}^2$
2	4.50	4.60	0.10	0.01	0.09	0.00	21.17
3	-5.54	-5.64	-0.10	0.01	0.11	0.00	31.84
4	1.87	2.39	0.52	0.27	0.05	0.01	5.69
6	-16.41	-15.86	0.55	0.30	0.32	0.10	251.63
7	0.63	0.25	-0.38	0.14	0.01	0.00	0.06
8	2.01	1.61	-0.40	0.16	0.03	0.01	2.59
9	-0.03	-0.23	-0.20	0.04	0.00	0.00	0.05
10	0.31	0.87	0.56	0.32	0.02	0.01	0.76
12	-1.32	-0.74	0.58	0.34	0.01	0.01	0.54
13	2.20	2.30	0.10	0.01	0.05	0.00	5.28
14	-2.29	-2.09	0.20	0.04	0.04	0.00	4.37
15	-0.78	-0.58	0.20	0.04	0.01	0.00	0.33
16	4.52	4.78	0.26	0.07	0.10	0.01	22.84
17	-0.63	-0.25	0.38	0.14	0.01	0.00	0.06
18	4.35	4.59	0.24	0.06	0.09	0.01	21.06
19	-1.21	-1.17	0.04	0.00	0.02	0.00	1.37
24	1.16	0.91	-0.25	0.06	0.02	0.00	0.82
28	0.79	0.87	0.08	0.01	0.02	0.00	0.75
Σ						0.14	371.20
Σ/n						0.01	20.62
$\sqrt{\Sigma/n}$						0.09	4.54
ϵ						1.97%	
σ						98.03%	

Table 8. Quantitative validation results for second event.

h	$\delta_{h \text{ benchmak}}(^{\circ})$	$\delta_{h \text{ pmu}}(^{\circ})$	Error	Error²	w_h	Error²*w_h	$\delta_{h \text{ pmu}}^2$
2	3.920	3.836	-0.084	0.007	0.005	0.000	14.718
3	-2.370	-2.216	0.154	0.024	0.016	0.000	4.911
4	-0.870	-0.785	0.085	0.007	0.005	0.000	0.617
6	-7.190	-6.398	0.792	0.627	0.430	0.270	40.940
7	1.010	1.310	0.300	0.090	0.062	0.006	1.716
8	-0.780	-0.823	-0.043	0.002	0.001	0.000	0.677
9	-0.370	-0.178	0.192	0.037	0.025	0.001	0.032
10	3.060	2.623	-0.437	0.191	0.131	0.025	6.881
12	2.270	1.794	-0.476	0.227	0.156	0.035	3.217
13	0.450	0.301	-0.149	0.022	0.015	0.000	0.091
14	-2.170	-2.317	-0.147	0.022	0.015	0.000	5.370
15	0.310	0.430	0.120	0.014	0.010	0.000	0.185
16	2.450	2.435	-0.015	0.000	0.000	0.000	5.928
17	-1.010	-1.310	-0.300	0.090	0.062	0.006	1.716
18	4.250	4.366	0.116	0.013	0.009	0.000	19.061
19	-0.010	0.202	0.212	0.045	0.031	0.001	0.041
24	-0.100	-0.270	-0.170	0.029	0.020	0.001	0.073
28	1.230	1.134	-0.096	0.009	0.006	0.000	1.285
Σ						0.346	107.457
Σ/n						0.019	5.970
$\sqrt{\Sigma/n}$						0.139	2.443
ϵ						5.67%	
σ						94.33%	

Table 9. Quantitative validation results for third event.

h	$\delta_{h \text{ benchmak}}(^{\circ})$	$\delta_{h \text{ pmu}}(^{\circ})$	Error	Error²	w_h	Error²*w_h	$\delta_{h \text{ pmu}}^2$
2	5.97	6.12	-0.15	0.02	0.11	0.0024	35.68
3	-3.60	-3.68	0.08	0.01	0.07	0.0004	12.97
4	0.03	0.1	-0.07	0.01	0.00	0.0000	0.00
6	-9.43	-8.81	-0.62	0.38	0.18	0.0673	88.83
7	1.59	1.61	-0.02	0.00	0.03	0.0000	2.52
8	-4.02	-3.85	-0.17	0.03	0.08	0.0022	16.15
9	-0.57	-0.7	0.13	0.02	0.01	0.0002	0.33
10	5.49	5.76	-0.27	0.07	0.10	0.0073	30.19
12	3.03	3.26	-0.23	0.05	0.06	0.0030	9.18
13	0.89	-0.15	1.04	1.09	0.02	0.0183	0.80
14	-4.62	-4.81	0.19	0.03	0.09	0.0030	21.38
15	3.04	2.62	0.42	0.18	0.06	0.0103	9.26
16	0.06	-1.84	1.90	3.62	0.00	0.0044	0.00
17	-1.59	-1.61	0.02	0.00	0.03	0.0000	2.52
18	3.72	3.62	0.10	0.01	0.07	0.0007	13.84
19	1.95	0	1.95	3.81	0.04	0.1402	3.81
24	0.85	1.09	-0.24	0.06	0.02	0.0009	0.72
28	2.50	2.49	0.01	0.00	0.05	0.0000	6.24
		Σ				0.26	254.44
		Σ/n				0.01	14.14
		$\sqrt{\Sigma/n}$				0.12	3.76
		ϵ				3.20%	
		σ				96.80%	

For more rigorousness, the model was also validated for actual real and reactive power flow through the lines. The metrics discussed in (23) through (28) are tabulated in Table 10 and Table 11 below for real and reactive power respectively. The normalized error \mathcal{E} was 1.5%, well within NERC recommendation. The confidence measure σ was 98.5%. For reactive power the normalized error \mathcal{E} was 21%. This large error is due to the poor performance of the Ward reduction method in modeling external area reactive power support.

Table 10. Quantitative validation for power flows of the first event.

h	PMU (MW)	Benchmark (MW)	Error	Error²	w_h	Error²*w_h	PMU (MW)²
2	172.51	176.09	-3.58	12.82	0.06	0.77	29759.67
3	228.81	209.30	19.51	380.57	0.08	30.17	52353.14
4	168.00	134.17	33.83	1144.46	0.06	66.61	28223.93
6	836.87	797.01	39.86	1588.47	0.22	357.03	700344.01
7	149.61	140.66	8.95	80.05	0.05	4.15	22382.32
8	266.26	269.24	-2.98	8.85	0.09	0.82	70896.97
9	24.39	19.29	5.10	26.05	0.01	0.22	595.08
10	23.12	18.04	5.08	25.81	0.01	0.21	534.56
12	103.44	108.16	-4.72	22.31	0.04	0.80	10699.06
13	387.71	387.68	0.03	0.00	0.13	0.00	150316.16
14	145.84	143.00	2.84	8.07	0.05	0.41	21269.48
15	134.63	138.73	-4.10	16.78	0.05	0.78	18126.33
16	451.32	457.56	-6.24	38.95	0.16	6.09	203688.66
18	229.04	225.48	3.56	12.68	0.08	1.01	52460.02
19	93.30	56.25	37.05	1372.67	0.03	44.37	8704.81
24	158.08	163.61	-5.53	30.54	0.05	1.67	24990.48
28	150.38	142.83	7.55	57.05	0.05	2.97	22615.05
		Σ				481.87	1417959.74
		Σ/n				28.35	83409.40
		$\sqrt{\Sigma/n}$				5.32	288.81
		ϵ					1.84%
		σ					98.16%

Table 11. Quantitative validation for reactive power flows of the first event.

h	PMU (MVAR)	Benchmark (MVAR)	Error	Error²	w_h	Error²*w_h	PMU (MVAR)²
2	-39.21	-24.59	-14.62	213.68	0.05	10.75	1537.24
3	46.40	-34.84	81.24	6599.19	0.06	392.73	2152.53
4	-21.12	-23.84	2.72	7.38	0.03	0.20	446.18
6	39.12	42.04	-2.92	8.51	0.05	0.43	1530.55
7	-37.65	-115.20	77.55	6013.58	0.05	290.44	1417.73
8	-34.29	-37.58	3.29	10.85	0.04	0.48	1175.53
9	62.12	36.94	25.18	634.15	0.08	50.53	3859.17
10	8.03	-28.59	36.62	1341.15	0.01	13.82	64.51
12	-59.26	-29.40	-29.86	891.64	0.08	67.78	3511.79
13	-44.93	-52.64	7.71	59.42	0.06	3.42	2018.82
14	-19.14	-58.61	39.47	1558.08	0.02	38.25	366.24
15	29.73	24.51	5.22	27.27	0.04	1.04	884.00
16	-45.56	16.17	-61.73	3810.03	0.06	222.64	2075.29
18	-84.88	-55.88	-29.00	841.15	0.11	91.58	7205.05
19	-90.03	-61.83	-28.20	795.07	0.12	91.81	8104.86
24	-58.73	-80.19	21.46	460.68	0.08	34.70	3448.80
28	-59.40	28.43	-87.83	7714.51	0.08	587.82	3528.63
Σ						1898.42	43326.93
Σ/n						111.67	2548.64
$\sqrt{\Sigma/n}$						10.57	50.48
ϵ						20.93%	
σ						79.07%	

VII. *Ybus Estimation*

Even though the proposed model development and validation methods are generic and can be used on any power system to create benchmark models for various simulation needs, the resulting benchmark model is only as accurate as the original operations model used. In this research a new parameter estimation technique is proposed to determine the bus admittance matrix.

A vector of bus current injections is referred to as I_{bus} . A vector of bus voltages is referred to as V_{bus} . V_{bus} and I_{bus} are related via (29).

$$I_{bus} = Y_{bus}V_{bus} \quad (29)$$

Y_{bus} is referred to as the admittance matrix. If I_{bus} and V_{bus} are known, Y_{bus} can be solved for analytically. To solve for Y_{bus} analytically, bus interconnection information is needed.

In this research the I_{bus} and V_{bus} are formulated from synchrophasors, and then are used to estimate Y_{bus} statistically. For this proposed statistical estimation technique, no Y_{bus} interconnection information is needed. Instead, interconnection information is inherently extracted with the Y_{bus} algorithm.

The proposed parameter estimation technique determines the bus admittance matrix Y_{bus} for power transmission systems from recorded synchrophasor measurements. The approach described in this research is based on recognizing that measurements of bus injection currents I_{bus} could be viewed as signals produced by a random process. In this manner, the corresponding bus voltages V_{bus} are also stochastic signals that are related through a cross-covariance matrix to the vector I_{bus} . Using estimation techniques developed for statistical signal processing, the cross-

covariance matrix is shown to be Z_{bus} . The increasing use of synchrophasors has enabled large-scale data collection of time synchronized bus injection currents and voltages. The new Z_{bus} estimation method is applied to the IEEE 68-bus benchmark system to demonstrate the validity of the approach. The accuracy and convergence rate of the method is evaluated under conditions corresponding to wide-area synchrophasor data collection. The results indicate that the method is broadly applicable to determining Y_{bus} and Z_{bus} for electric power transmission and systems equipped with synchrophasors data collection technology. After demonstrating the validity of the approach, it is used on the proposed benchmark model using available synchrophasor data.

Research done previously in this area requires the prior knowledge of the electrical interconnection as well as full availability of PMU measurements. This method does not depend on prior knowledge of the electrical interconnection between the buses. It extracts the electrical interconnection and the parameters of the network model in the form of Y_{bus} . It also does not require full availability of PMU measurements at each bus in the system. It estimates the partial Y_{bus} based on the available PMUs.

In this chapter the formulation of bus current injection from synchrophasor measurements is discussed first. Then, the statistical properties of synchrophasors are investigated. After that, a discussion of the proposed statistical method and the theoretical basis of the method is presented. This chapter also discusses finding the functional relationship through finding the cross-covariance matrix. It also discusses applying said theory to power transmission systems and extracting the Y_{bus} . Then, it discusses the Matlab implementation of the method, validation and its accuracy. Then a test case is performed using the IEEE 68-bus benchmark system.

A. *I_{bus} Formulation from Synchrophasor Measurements*

For the purposes of the Y_{bus} estimation method proposed, both V_{bus} and I_{bus} are needed. V_{bus} is a column matrix of the voltage phasor at each bus in the system. I_{bus} is another column matrix for the current injection at each bus in the system. Power system buses are classified as PQ buses or PV buses. PQ buses represent load buses, while PV buses represent generator buses. It is standard practice in power system analysis to treat loads as negative power generation. When loads are treated as negative generations, they can be lumped with any generators at a local bus. This new equivalent lumped generator injects a current I_i into the bus. Current injections are combined to formulate the current injection column matrix I_{bus} . Therefore current injections can be computed by adding all currents of all loads and generators taking into consideration their respective polarity. Another approach is to add all branch currents connected to a bus excluding load and generator currents.

Current is a through quantity, meaning it is defined through a branch. Current injections are quantities defined at a bus. Current synchrophasors represent branch currents [20]. If enough PMUs are installed, they can be used to compute the current injection from synchrophasor measurements depending on their placement within a substation. PMUs come as standalone units or relays with built-in PMU functionality. PMU functionality has been provided by manufacturers as a standard feature since 2002. Therefore in a given substation, it is more likely than not that enough PMUs are already installed for protection purposes.

For a transmission network study, a substation is reduced to a bus with connected components via equivalencing methods. For both PV and PQ buses alike, adding synchrophasors

for all generators and loads or adding all line synchrophasors will produce the current injection at that bus.

To demonstrate, the IEEE 68-bus benchmark system with flows superimposed is shown in Fig. 21 below [21]. Bus 17 is a PV bus, adding the current flows of generator 13 and that of the local load will yield the current injection. Similarly adding the current flow through the two transmission lines connecting bus 17 to buses 43 and 36 will also yield the current injection. For a PQ bus such as bus 46, a similar approach can be used. The current of the local load represents the current injection, or alternatively adding the current through each of the lines connecting bus 46 to buses 49 and 38 will also yield the current injection. Both approaches are valid. The reason for outlining both is that the selection of which one to use will depend on the availability of PMUs and synchrophasor measurements.

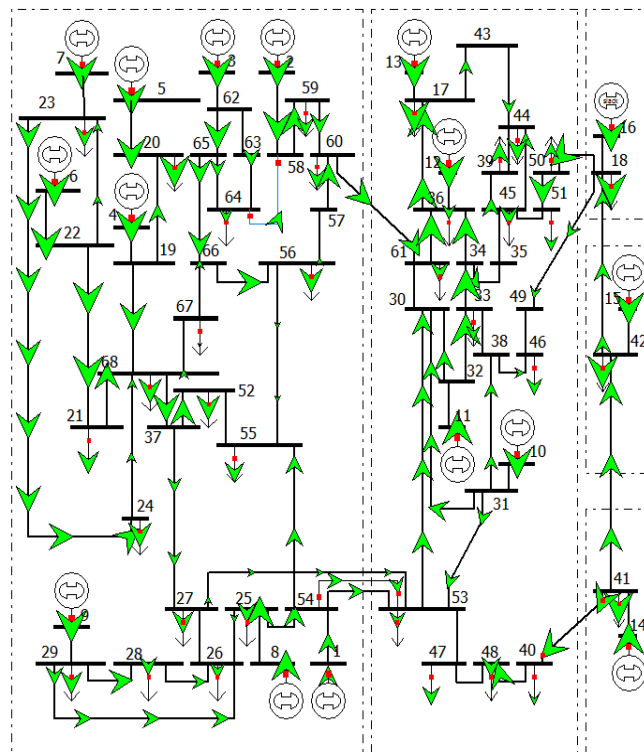


Fig. 21. IEEE 68-bus benchmark system.

A typical substation contain many relays for protection purposes. An actual substation design of a 69 kV gas turbine generation substation provided by an electric utility is presented in Fig. 22. It is a simple two bus generation substation. It contains three generation units at 13.8 kV, a 13.8/69 kV step up delta-wye transformer, and two outgoing lines. It also contains many instrumentation transformers, relays, and various protective equipment. A simplified bus diagram of this substation is shown in Fig. 23 below. This simplified bus diagram was obtained through the removal of all unused instrumentation transformers, disconnect switches, and communication capacitive transformers. The Schweitzer PMU-capable relays are represented with the blue blocks on the diagram. Those are SEL-587, SEL-351, and SEL 321. By looking at the placement of the current transformers connected to those relays, we can see that branch currents can be measured for all three generators, the load and the outgoing transmission lines. The injected current can be computed by adding the three generator currents and the load current or by adding the outgoing line currents. It is mainly a matter of activating the PMU feature of these relays and setting up the data and communication infrastructure to handle synchrophasor processing and storage. It is worth noting that for a transmission level system study, this entire substation represented by Fig. 22 is reduced to single bus with three generators, a load, and two transmission lines connected to it. This entire substation is one PV bus.

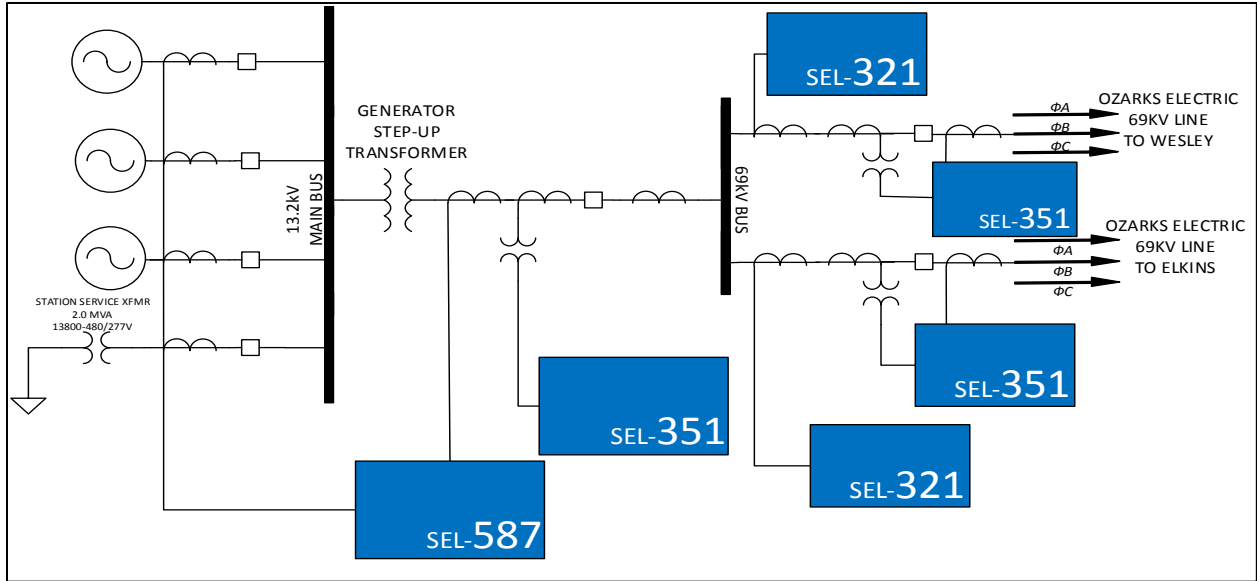


Fig. 23. Simplified substation layout.

B. Statistical Properties of Synchrophasors

This is a statistical Y_{bus} estimation approach based on random signal processing methods using current and voltage synchrophasors. Therefore it is necessary to understand the statistical properties and probability distribution of actual synchrophasor data.

Actual synchrophasor data provided by a utility company were analyzed. Synchrophasor's ".phasor" files were converted to ".CSV" files. Those ".CSV" files were then process using a python script that was written to extract specific synchrophasor measurements (i.e. voltage) for specific terminal ID's (i.e. Term ID X). The results were column vectors for specific synchrophasor measurements at specific terminal IDs. Each element corresponding to a time step.

These resulting column vectors were then processed in Matlab. They were analyzed as random signals to gain a better understanding of them, to later use in simulations. Fig. 24 through Fig. 27 below illustrates the cumulative probability function of the current magnitude,

current angle, voltage magnitude, and voltage angle of the analyzed synchrophasors. It can be observed that under steady state conditions, synchrophasor measurements follow a normal probability distribution.

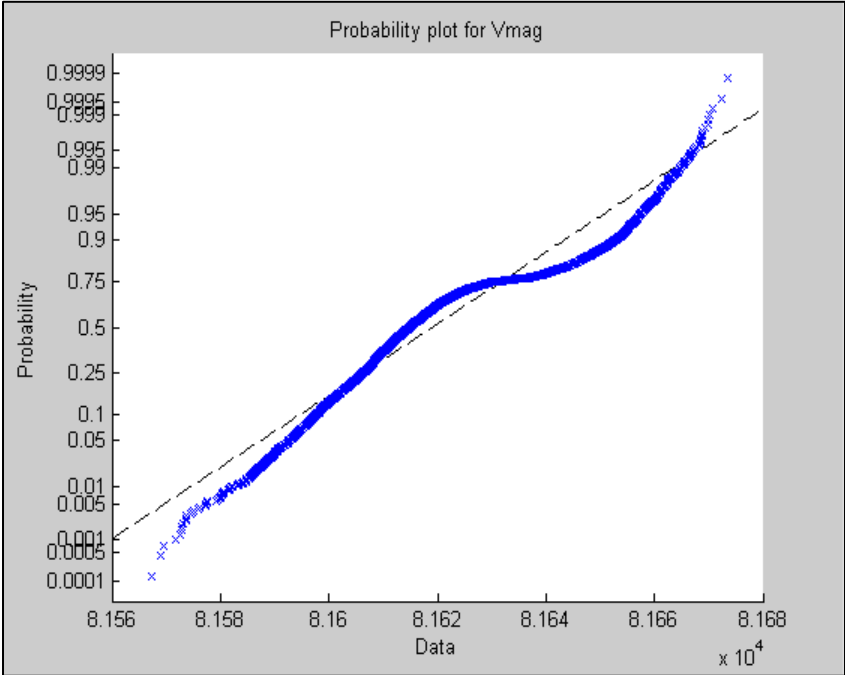


Fig. 24. Cumulative probability function for voltage magnitude data.

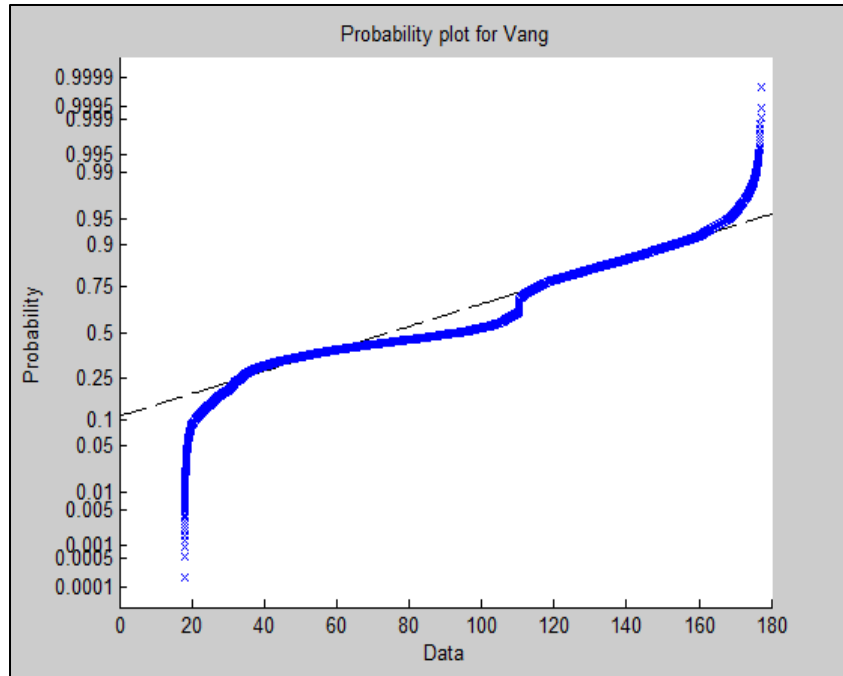


Fig. 25. Cumulative probability function for voltage angle data.

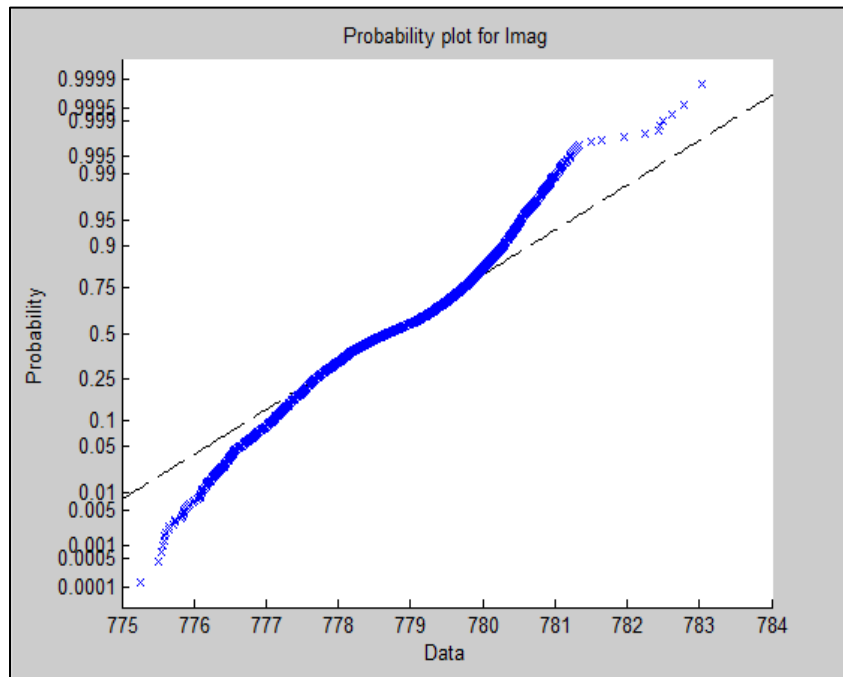


Fig. 26. Cumulative probability function for current magnitude data.

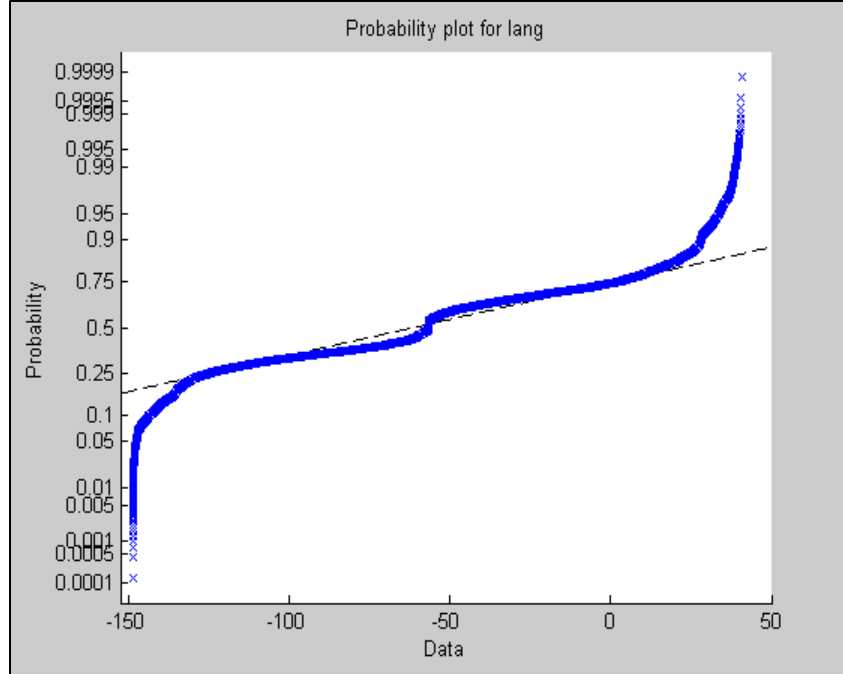


Fig. 27. Cumulative probability function for current angle data.

C. Finding the Functional Relationship through Correlation

The proposed method of estimating the Z_{bus} matrix is based on estimating the cross-correlation between the I_{bus} and V_{bus} values when interpreted as random vectors. For purposes of this research, it is assumed that time synchronized phasor measurements at time tk of the column vectors $I_{bus}(tk)$ and $V_{bus}(tk)$ are available from synchrophasor measurements and are made available for post-processing. The columns of I_{bus} and V_{bus} are of dimension N, where N is the number of buses or nodes for the system under consideration. In a typical application, N could be on the order of hundreds to thousands of elements. Based on the results presented in the previous section, the statistics of the elements of I_{bus} and V_{bus} are normally distributed. That is, the statistical characteristics of I_{bus} and V_{bus} are adequately described by their first and second moments and do not change over short time intervals (i.e. a stationary process). It is assumed that

Z_{bus} is a symmetric positive definite matrix. Data matrices are defined by concatenating a sequence of M bus measurements,

$$I_{data} = [I_{bus}(t_1) \quad \dots \quad I_{bus}(t_M)], \quad (30)$$

$$V_{data} = [V_{bus}(t_1) \quad \dots \quad V_{bus}(t_M)] \quad (31)$$

The dimensions of the data matrices are N -rows by M -columns. The data value at time t_k is the k th column of the respective data matrix and is denoted by $I_{bus}^{(k)}$ and $V_{bus}^{(k)}$. The estimated mean value of the data matrices are computed as

$$\bar{I}_{bus} = \frac{1}{M} \sum_{k=1}^M I_{data}^{(k)} \quad (32)$$

$$\bar{V}_{bus} = \frac{1}{M} \sum_{k=1}^M V_{data}^{(k)} \quad (33)$$

In order to estimate the cross-covariance between the injection currents and bus voltages, the mean values are subtracted from the respective data matrices:

$$I_{\sigma}^{(k)} = I_{data}^{(k)} - \bar{I}_{bus} \quad (34)$$

$$V_{\sigma}^{(k)} = V_{data}^{(k)} - \bar{V}_{bus} \quad (35)$$

where bus injection current and bus voltage column data elements are each normalized in order to scale to units of ohms needed for the impedance matrix Z_{bus} . The following variances are defined:

$$\sigma_I = \frac{1}{N} \sum_{k=1}^M \left(I_{data}^{(k)} - \bar{I}_{bus} \right)^2 \quad (36)$$

$$\sigma_V = \frac{1}{N} \sum_{k=1}^M \left(V_{data}^{(k)} - \bar{V}_{bus} \right)^2 \quad (37)$$

with variance normalized data values for the i th bus defined with respect to the variance estimated at each bus:

$$\bar{I}_{\sigma(i)}^{(k)} = \frac{1}{\sigma_{I(i)}} I_{\sigma(i)}^{(k)}. \quad (38)$$

$$\bar{V}_{\sigma(i)}^{(k)} = \frac{1}{\sigma_{V(i)}} V_{\sigma(i)}^{(k)}. \quad (39)$$

The impedance matrix is then estimated from the variance-normalized zero-mean data as

$$\hat{Z}_{bus} = \frac{1}{M} \sum_{k=1}^M \bar{V}_{\sigma}^{(k)} \bar{I}_{\sigma}^{(k)*T} \quad (40)$$

and the estimated admittance matrix is found by inverting the impedance matrix,

$$\hat{Y}_{bus} = \hat{Z}_{bus}^{-1} \quad (41)$$

A representative Matlab m-file script is provided in the Appendix as an example of estimating an impedance matrix from normally distributed random current injection and bus voltage measurements.

D. Implementation

The Y_{bus} estimation method was further evaluated under various system conditions. The evaluation was primarily applied to the IEEE 68-bus benchmark system that was developed for analyzing power system stability [21]. But it was prudent to show that this method works for a variety of systems. Therefore this method was also applied to randomly generated systems to ensure its validity for a wide range of systems.

a. Randomly Generated Ybus systems

A flow chart describing the process which was followed in the Y_{bus} estimation is presented in Fig. 28.

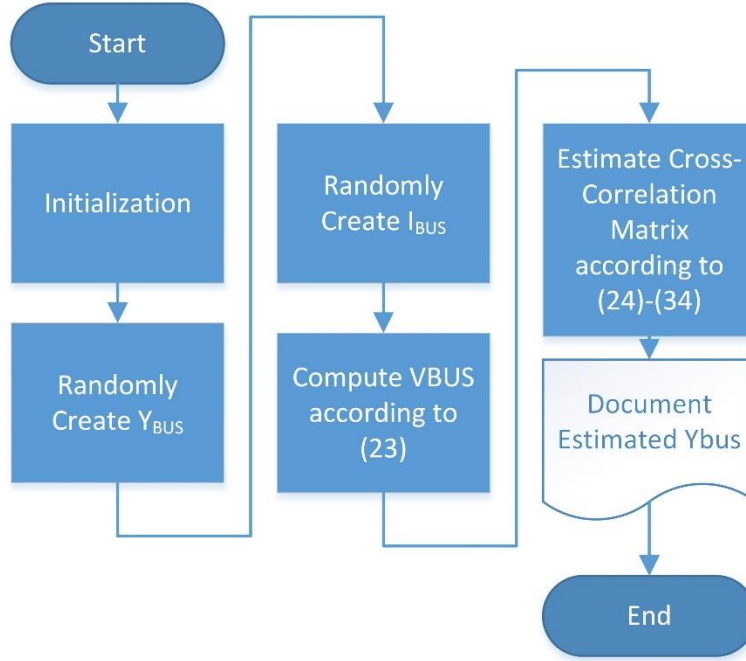


Fig. 28. Y_{bus} estimation process.

If the number of samples is sufficiently large enough, then the Y_{bus} estimation method is expected to yield accurate results. Since this method in estimating the Y_{bus} is based on a statistical cross-correlation matrix estimation, a similar approach is used for accuracy calculations. A statistical method was used to determine how large of a sample is needed to yield a sufficiently accurate result. In this approach, multiple cases were simulated using the Y_{bus} estimation method. The accuracy of the estimated Y_{bus} was assessed by comparing it to the known Y_{bus} that was used in generating the injection currents and bus voltage data. Each case corresponds to an estimation of the Y_{bus} using a certain number of I_{bus} and V_{bus} samples. For each case the number of samples was changed to compute the dependence of the accuracy of this method on the number of

samples used. Each case was repeated one hundred times to statistically compute the expected accuracy of using this method. The error index used here is defined as the norm of the estimated Z_{bus} minus the actual Z_{bus} divided by the norm of the actual Z_{bus} as described by (42).

$$\delta_Z = \frac{\|Z_{bus} - \hat{Z}_{bus}\|}{\|Z_{bus}\|} \quad (42)$$

The closer the error index is to zero, the more accurate the estimated Z_{bus} is. An accuracy norm was also used. The accuracy used follows (36). A detailed flow chart is presented in Fig. 29 to show the process that was followed.

$$\text{accuracy} = \frac{\|\hat{Z}_{bus}\|}{\|Z_{bus}\|} \quad (37)$$

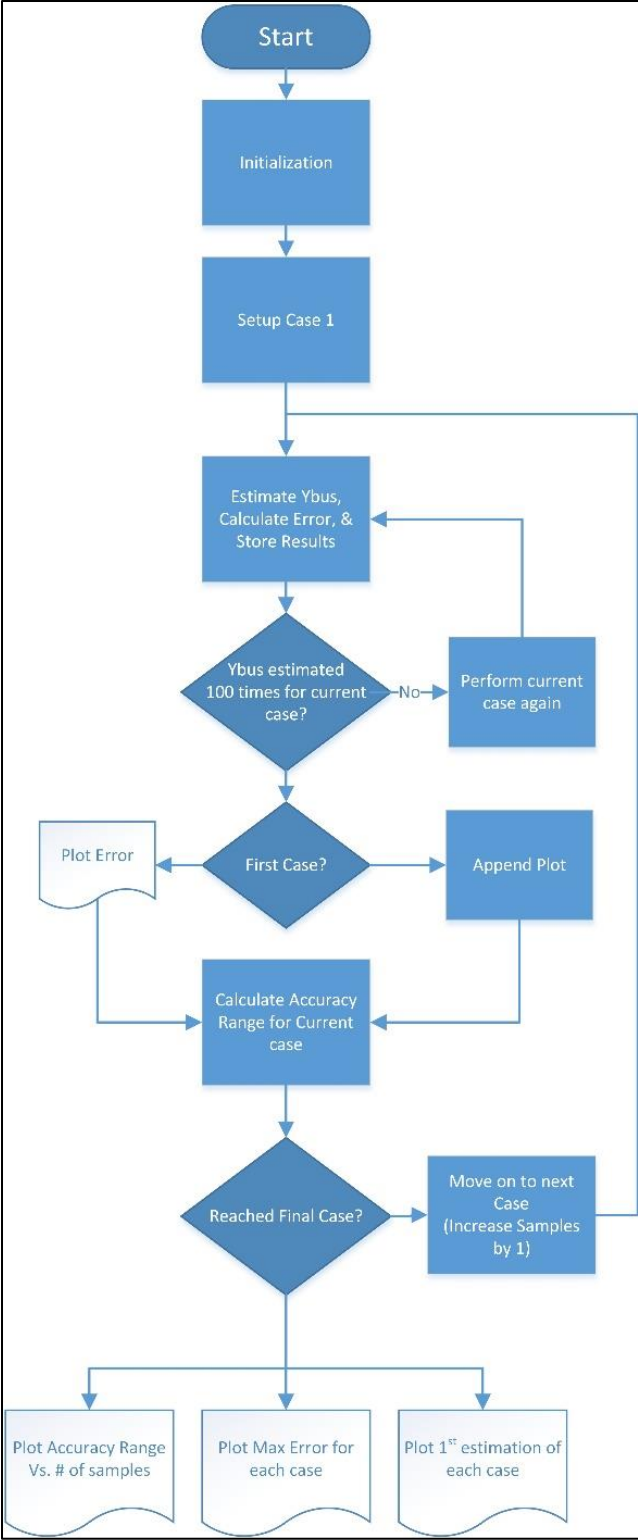


Fig. 29. Y_{bus} estimation error calculation flow chart.

Fig. 30 shows the accuracy of the method for each case. Each case corresponds to a number of samples used. The number of samples is on the x-axis, while the accuracy of the estimate is on the y-axis. As can be seen, the accuracy of the method increased as the number of samples increased. It is concluded that the Y_{bus} estimation method produced sufficiently accurate results to within one percent of the true value when 500 samples or more were used. From the previous synchrophasor discussion, I_{bus} and V_{bus} samples are produced for each frame. Therefore using 500 samples corresponds to using 500 synchrophasor frames. Given that data frames are produced at a rate of 30 frames per second per the IEEE C37.118 synchrophasor standard, then using 500 samples corresponds to an acquisition duration of 16.67 seconds of recorded synchrophasor data.

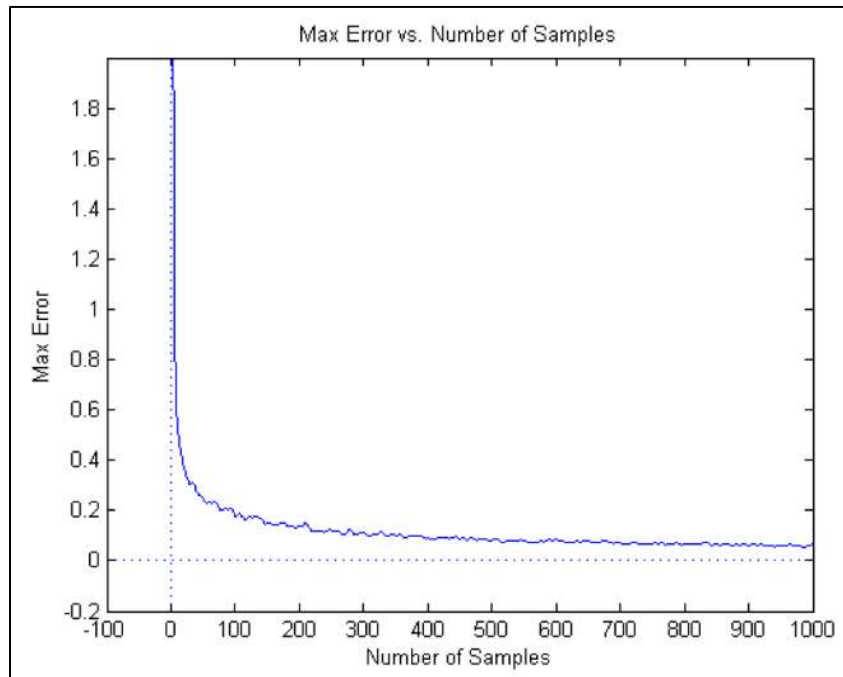


Fig. 30. Max error vs. number of samples for randomly generated systems.

Each case was evaluated 100 times. The accuracy was plotted once for each time the case was repeated. Over repeated cases this yields a vertical line corresponding to the range over

multiple values per case. The plot in Fig. 31 shows the accuracy range for each case. This plot indicates a series of parallel lines perpendicular to the x-axis that shows the range of accuracy values over the 100 sample evaluations. As the case number increases, the number of used samples increases. It can be seen that as the number of used samples increase, the accuracy index range narrows down to unity (i.e., it converges to the true value).

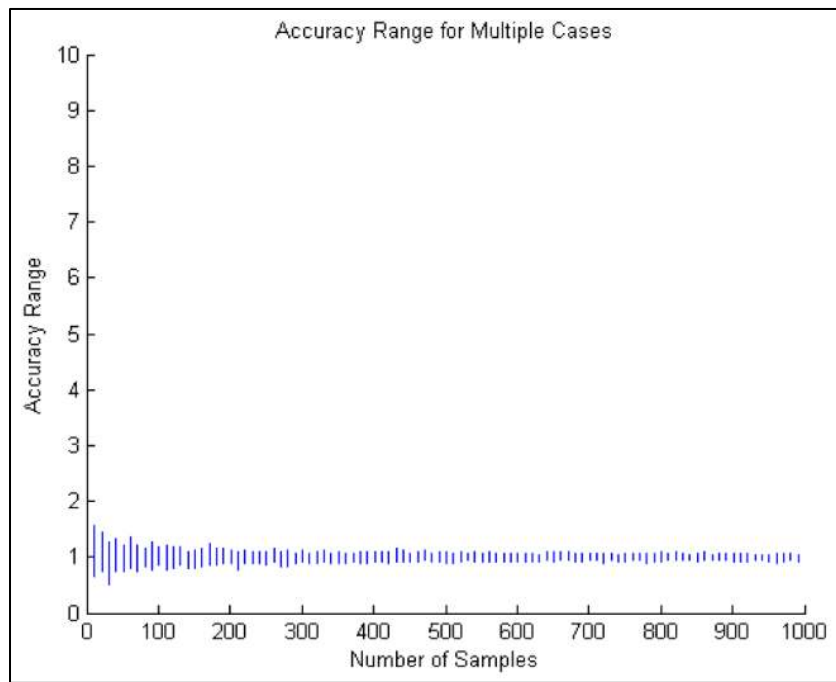


Fig. 31. Accuracy range for multiple cases for randomly generated systems.

The plot in Fig. 32 shows the worst case error that might be encountered. This is determined as the average of the maximum accuracy minus the minimum. It can be seen that the max error is about 0.05 %. The trend of increased accuracy with increased number of samples is observed in the plot of Fig. 32.

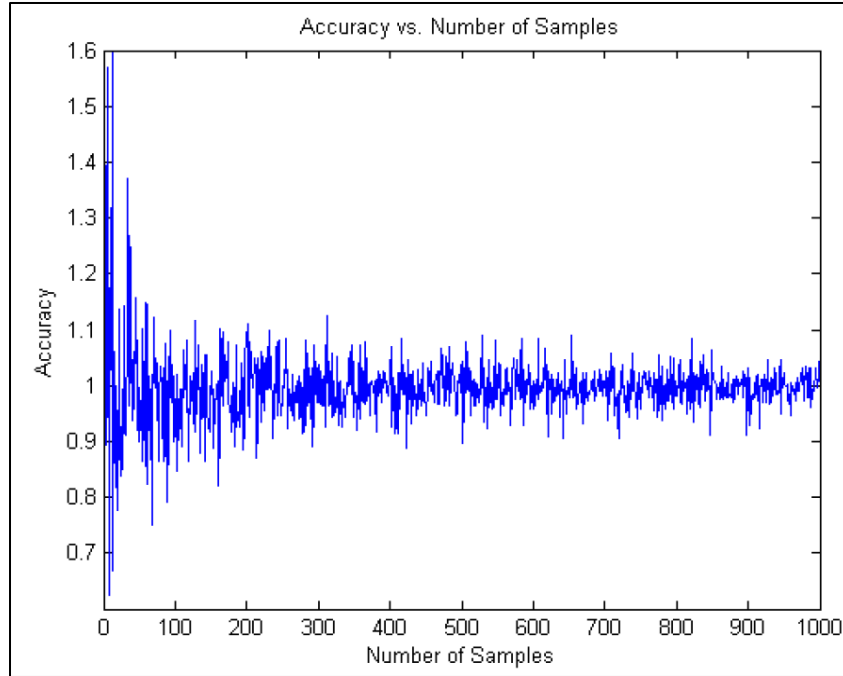


Fig. 32. Accuracy vs. number of samples for randomly generated systems.

In practice it is important to consider the situation where synchrophasor measurements are not available at every bus. The method for estimating the admittance matrix of a system with incomplete measurements can also be used to estimate a subset of the admittance matrix with missing bus values. For buses where a PMU is not available for i^{th} synchrophasor measurement corresponds to a Y_{bus} matrix estimate that is missing the corresponding i^{th} column and i^{th} row as illustrated Fig. 33. The Y_{bus} estimation is otherwise accurate for the other matrix elements even though an incomplete set of PMU measurements is used. The actual Matlab M-files used to obtain the presented results is provided in the appendix.

Y_{11}	Y_{12}	...	Y_{1k}	$Y_{1(k+1)}$
Y_{21}	Y_{22}	...	Y_{2k}	$Y_{2(k+1)}$
\vdots	\vdots	\ddots
Y_{i1}	Y_{i2}	\vdots	Y_{ik}	$Y_{i(k+1)}$
$Y_{(i+1)1}$	$Y_{(i+1)2}$	\vdots	$Y_{(i+1)k}$	$Y_{(i+1)(k+1)}$

Fig. 33. Effect of a missing measurement.

b. Validation using the 68-bus benchmark system

The proposed Y_{bus} estimation method was next evaluated based on a benchmark transmission system. The intent is to validate the proposed Y_{bus} estimation method for a realistic transmission network. The 68-bus IEEE stability model used in this evaluation is shown in Fig. 21. The method was used to estimate the Y_{bus} from simulated I_{bus} and V_{bus} . Then various analysis was done on the result. A Similar set of plots to those discussed in the previous section was developed for the 68-bus benchmark model.

Fig. 34 shows the worst case error of the method for each case for a normally distributed random bus injection current. Each case corresponds to a different number of samples used in estimating the Y_{bus} . Results indicate that a sufficiently accurate estimate was produced when enough samples were used. At 1000 samples, the estimated Y_{bus} error was within 5% of the actual Y_{bus} . 1000 samples corresponds to using 1000 synchrophasor frames. If frames are reported at a rate of 30 frames per second, then using 1000 samples corresponds to an acquisition duration of 33.33 seconds of recorded synchrophasor data.

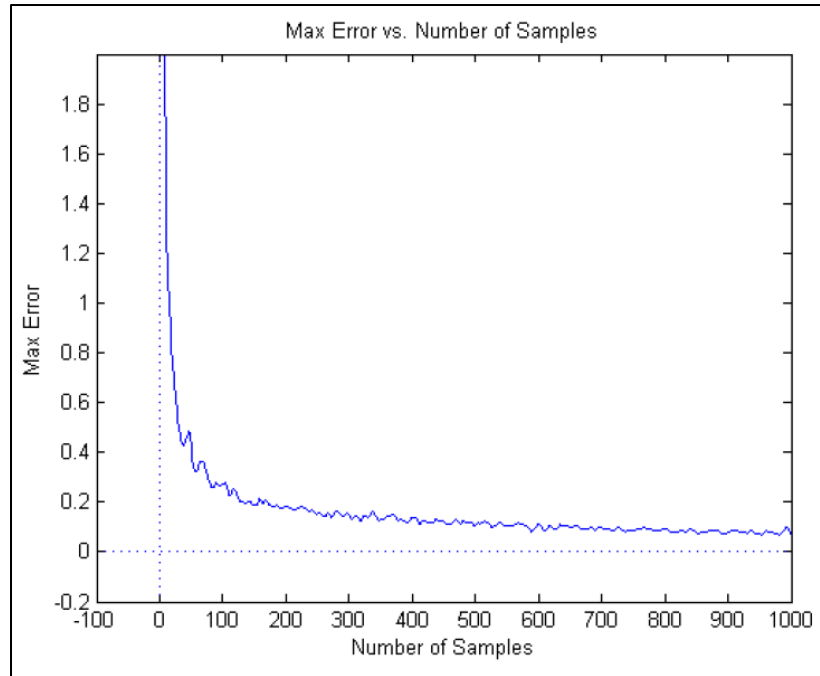


Fig. 34. Max error vs. number of samples for the IEEE 68-bus benchmark system.

Each case was repeated 100 times. The accuracy of the estimate was calculated each time. If the accuracy was plotted for each repeat for all cases, that yields a range of Y values for each X value. That is a range of accuracy for each case. Fig. 35 shows a plot of the accuracy range for each case. The y-axis shows the accuracy, while the x-axis shows the number of sample used.

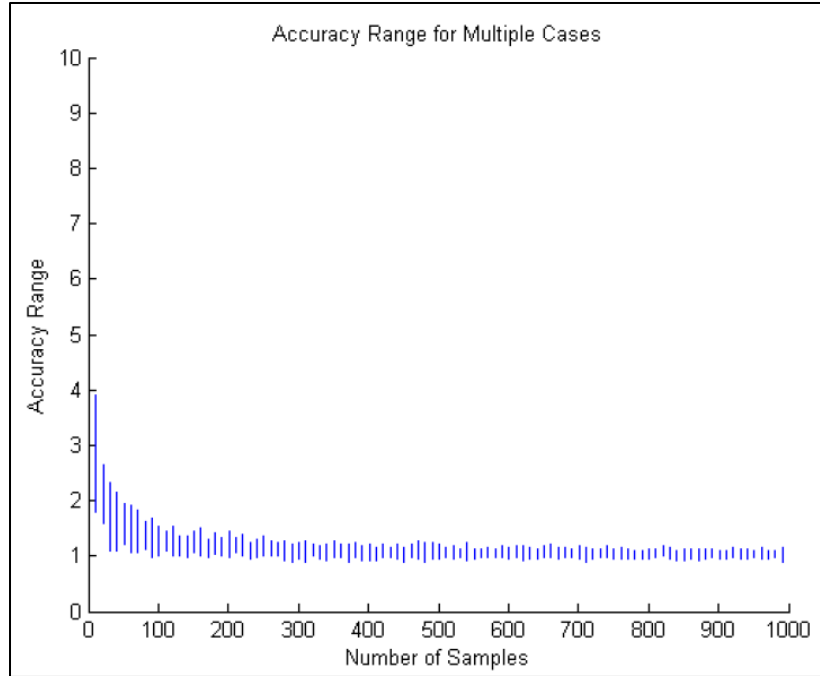


Fig. 35. Accuracy range for multiple cases for the IEEE 68-bus benchmark system.

The plot in Fig. 36 Also shows the accuracy range versus the number of samples. More cases are plotted, that is Fig. 36 has higher resolution. And the scale was zoomed in around one to demonstrate how accurate the method is. An accuracy of one corresponds to a Y_{bus} estimate that is exactly the same as the actual Y_{bus} in accordance with equation (29).

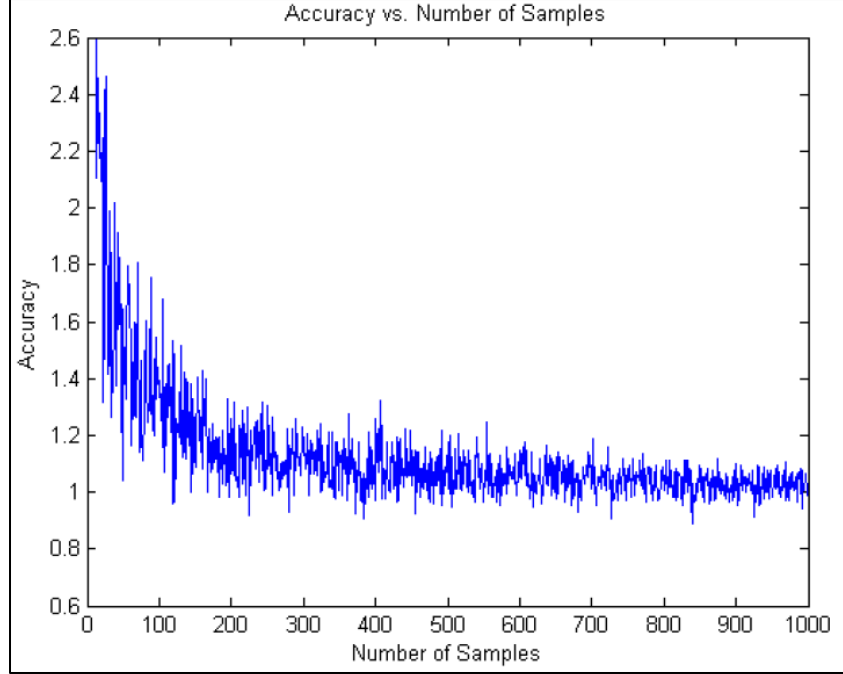


Fig. 36. Accuracy vs. number of samples for the IEEE 68-bus benchmark system.

It is worth noting that an entry in ith row and the kth column of Y_{bus} matrix represents an actual physical connection between the ith bus and kth bus. An empty entry means that there is no direct physical connection. Therefore, extracting the Y_{bus} inherently extracts the bus interconnection in the system. The actual Matlab files used to obtain the results presented validating the method using the IEEE 68-bus system are provided in the appendix. It is also noticed from Fig. 35 and Fig. 36 that the envelope of the accuracy gets narrower with using more samples. Meaning that the longer the duration of recorded synchrophasors used, the more accurate the estimated is.

The power spectral density describes the how the power of the signal is distributed over different frequencies as in (43).

$$PSD(x(t)) = \lim_{T \rightarrow \infty} \mathbf{E}[|\hat{x}_T(w)|^2] \quad (43)$$

White noise has a constant power spectral density. For a stationary random process, the power spectral density and the autocorrelation function are a Fourier transform pair. The constant power spectral density of white noise translates to no autocorrelation and high variation in white noise. The power spectral density of white noise is demonstrated in Fig. 37.

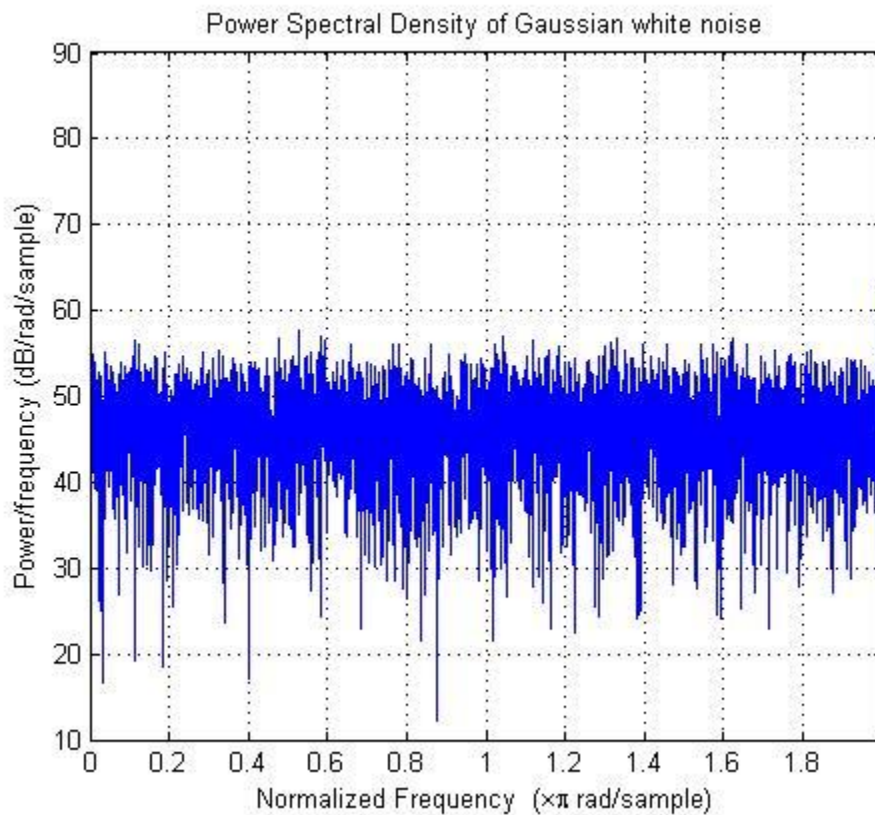


Fig. 37. Power spectral density of white noise.

Results obtained by assuming a white noise for current synchrophasors demonstrate the validity of the Y_{bus} estimation method, but are unrealistic in terms of the assessment of number of samples needed. The power spectral density of actual current synchrophasors was studied. Fig. 38 and Fig. 39 demonstrate power spectral density of actual current synchrophasor data.

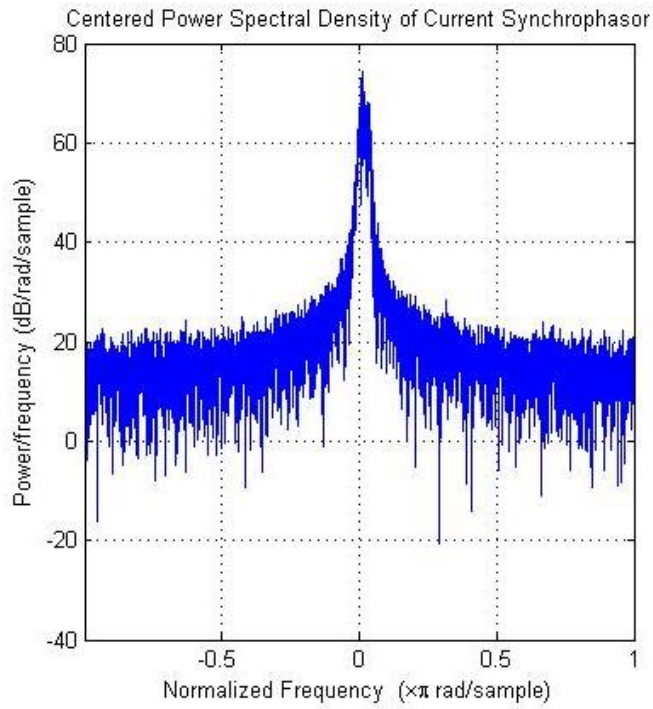


Fig. 38. Centered power spectral density of actual synchrophasors.

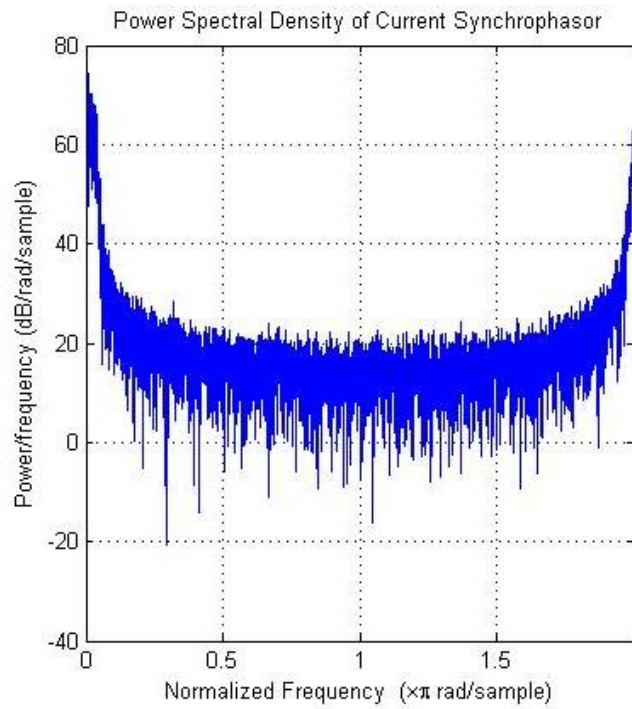


Fig. 39. Power spectral density of actual synchrophasors.

Actual current synchrophasor's power spectral density are centered on dc. That is, actual current synchrophasors contain less variation than white noise in the same duration of time. This leads to the need of more synchrophasor samples to obtain an accurate Y_{bus} estimate. More samples translate to a longer duration of recorded synchrophasor measurements.

Filtered white noise was used to obtain a more realistic measure of needed duration of synchrophasor measurements to accurately estimate Y_{bus} . A non-causal Gaussian filter was applied to match the power spectral density of actual synchrophasors as in Fig. 40.

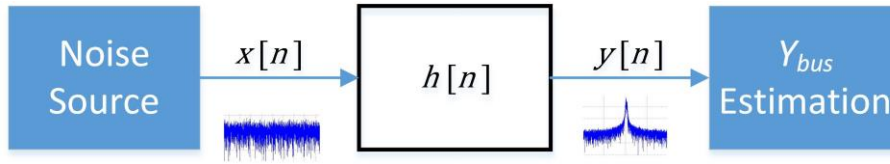


Fig. 40. White noise filtration.

An advantage of using a Gaussian filter is that its response is of the same form in the frequency domain and the time domain. Another advantage is that it is completely described by the mean and the variance. The response of the filter in the time domain is described in (44) and (45).

$$y[n] = \sum_{-M/2}^{M/2} x[n]h[n] \quad (44)$$

$$h[n] = \frac{\sqrt{\pi}}{a} e^{-\frac{\pi^2 n^2}{a^2}} \quad (45)$$

The response of the filter in the frequency domain follows (46).

$$H(e^{j\theta}) = e^{-ja^2\theta} \quad (46)$$

The output of the filter, $Y(n)$ is given in Fig. 41 and Fig. 42.

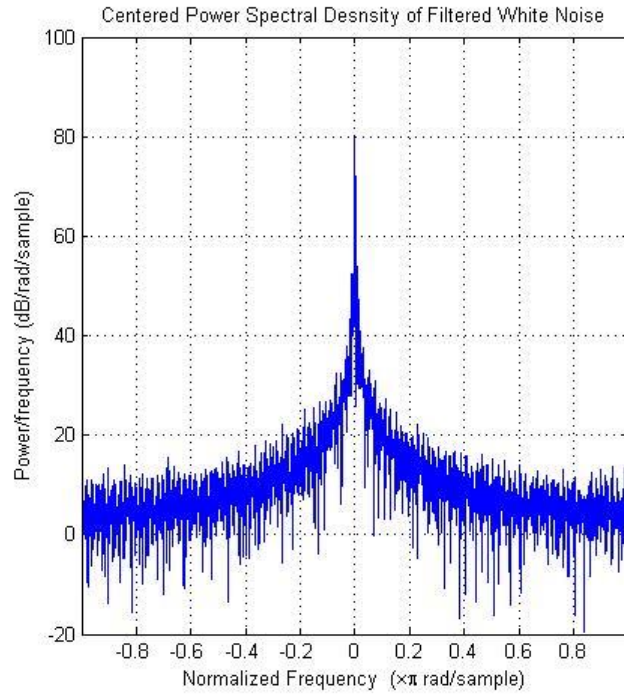


Fig. 41. Centered power spectral density of filter output.

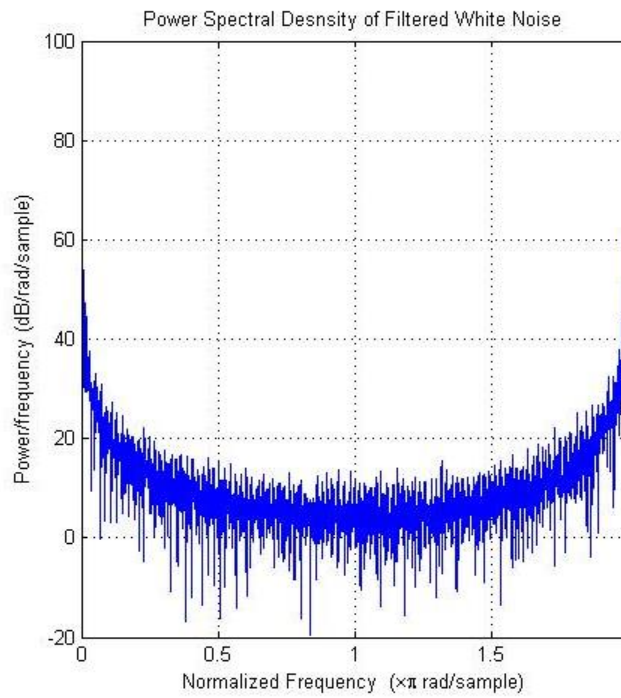


Fig. 42. Power spectral density of filter output.

$Y(t)$ was then used as the input to the Y_{bus} estimation technique. It was used to estimate the IEEE 68-bus benchmark system as in Fig. 43 Below.

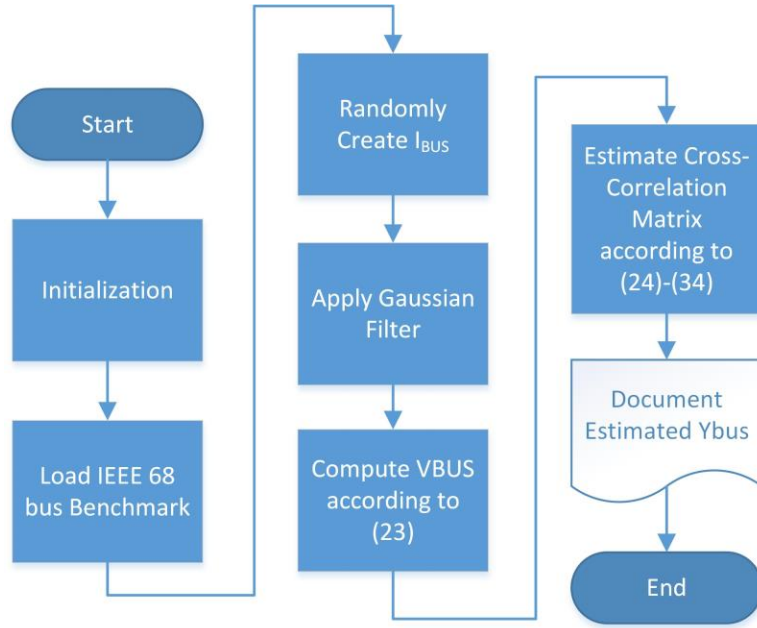


Fig. 43. Y_{bus} estimation process using filtered white noise.

Multiple cases were simulated using the Y_{bus} estimation method to assess the needed duration of recorded synchrophasor measurements. The IEEE 68-bus benchmark system was used for this purpose. The accuracy of the estimated Y_{bus} was assessed by comparing it to the known IEEE 68-bus benchmark Y_{bus} . Each case corresponds to an estimation of the IEEE 68-bus benchmark system using a certain number of synchrophasor samples. For each case, the number of samples was changed to compute the dependence of the accuracy of this method on the number of samples used. Each case was repeated one hundred times to statistically compute the expected accuracy of using this method. The error index used here is described in (42). The closer the error index is to zero, the more accurate the estimated Y_{bus} is. A detailed flow chart is presented in Fig. 29 to show the process that was followed.

Fig. 44 through Fig. 49 demonstrate the accuracy of the Y_{bus} estimation technique using realistic synchrophasor simulation. Fig. 44 demonstrates the dependence of error on the number of samples used for up to 5000 samples. Fig. 45 demonstrate the dependence of accuracy on the number of samples used for up to 5000 samples as well. It can be observed that the estimate is not accurate for this range of sample duration. Even though the estimate is not accurate with up to 5000 samples an improvement in accuracy can be observed with increasing number of samples. 5000 samples correspond to about 2.8 minutes of synchrophasor data collection.

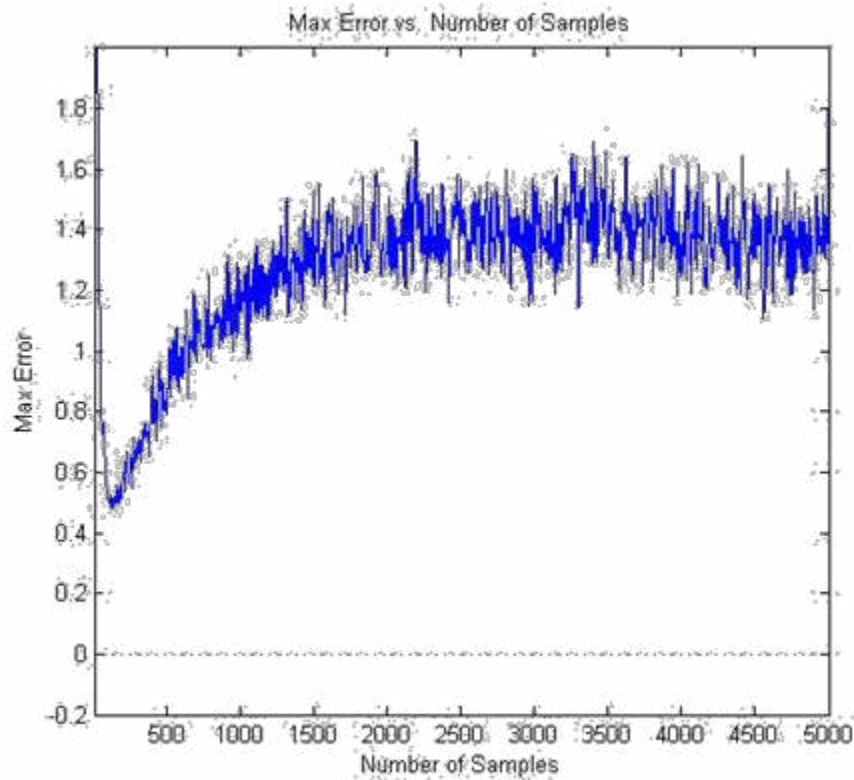


Fig. 44. Max error vs. number of samples for the IEEE 68-bus benchmark system using Gaussian filtered white noise.

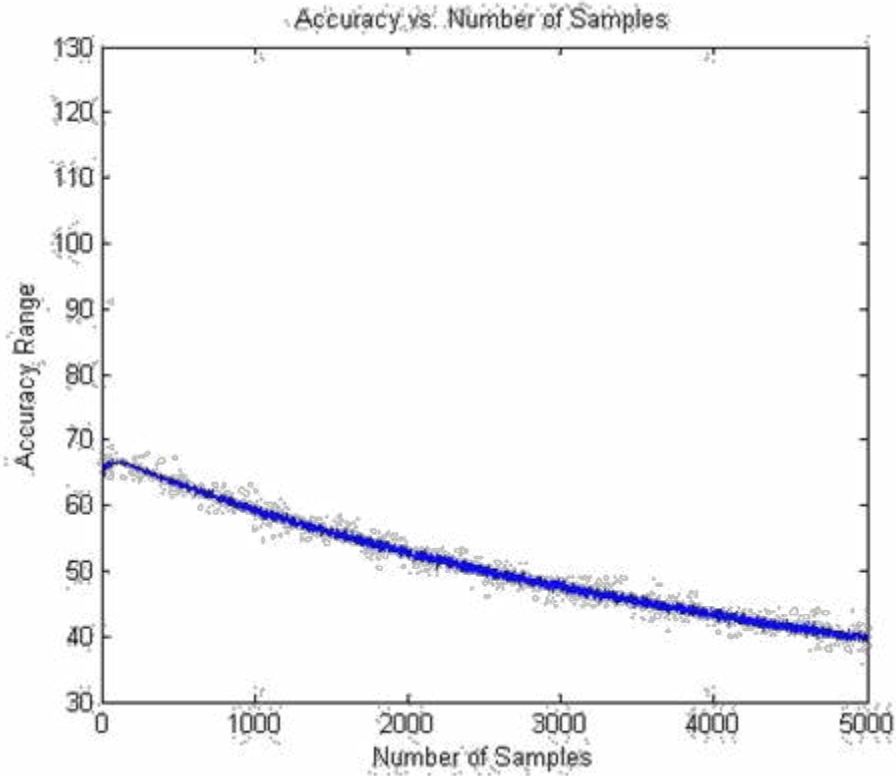


Fig. 45. Accuracy vs. number of samples for the IEEE 68-bus benchmark system using Gaussian filtered white noise.

Fig. 46 demonstrates the accuracy range of estimating the IEEE 68-bus system using Gaussian filtered white noise with a sample range of 100k to 100.1k. Fig. 47 demonstrates the accuracy range of the estimation technique for a sample range of 100k to 100.1k. 100k samples correspond to about an hour of synchrophasor data collection.

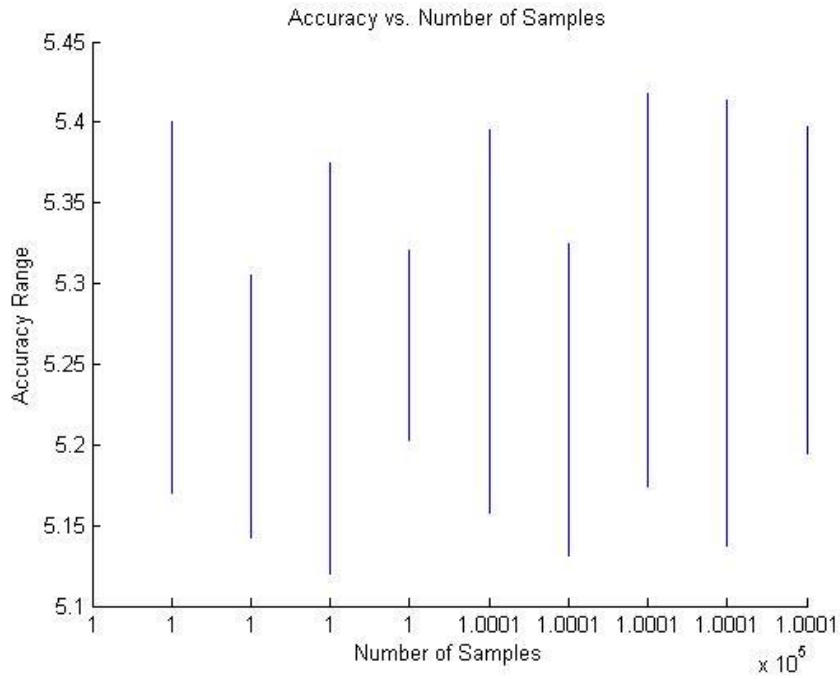


Fig. 46. Accuracy vs. number of samples for the IEEE 68-bus benchmark system using Gaussian filtered white noise.

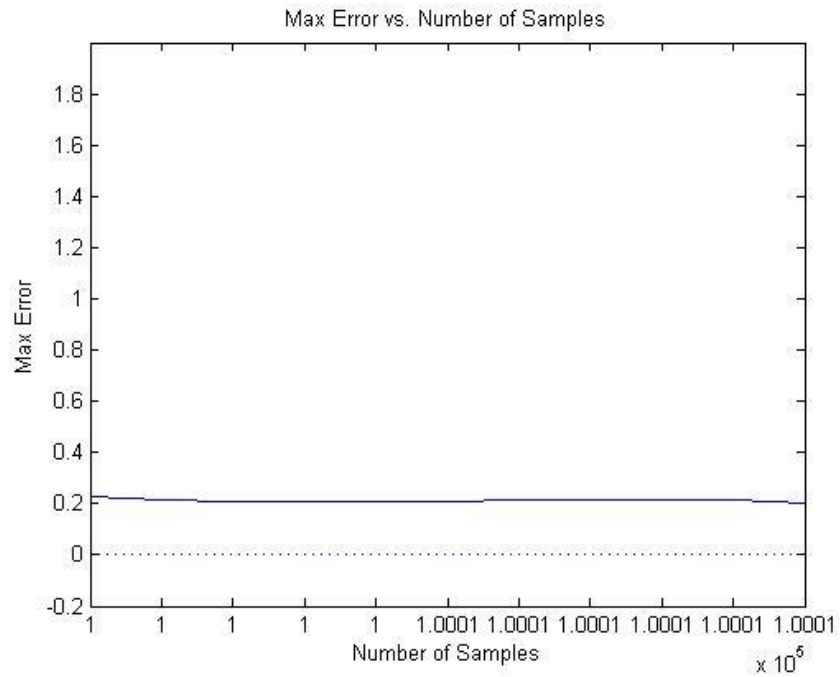


Fig. 47. Max error vs. number of samples for the IEEE 68-bus benchmark system using Gaussian filtered white noise.

Fig. 48 demonstrates the maximum error of the estimation technique when estimating the IEEE 68-bus system using Gaussian filtered white noise using up to 250k samples. Fig. 49 demonstrates the accuracy range vs the number of samples used for up to 250k samples used. The use of 250k samples correspond to 139 minutes of synchrophasor data collection. A significant improvement can be noticed in the maximum error and the accuracy range between 100k samples and 250k samples.

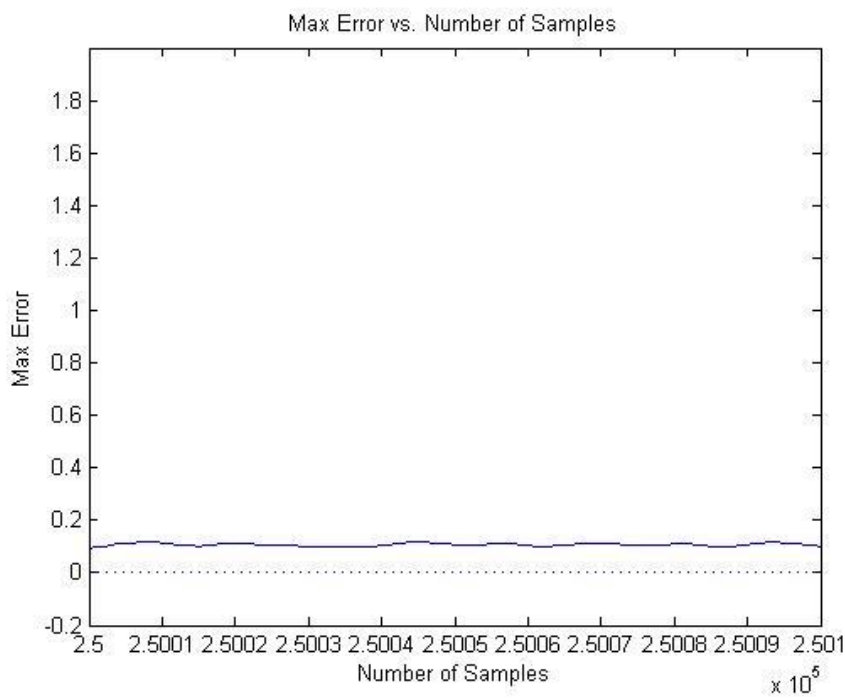


Fig. 48. Max error vs. number of samples for the IEEE 68-bus benchmark system using Gaussian filtered white noise.

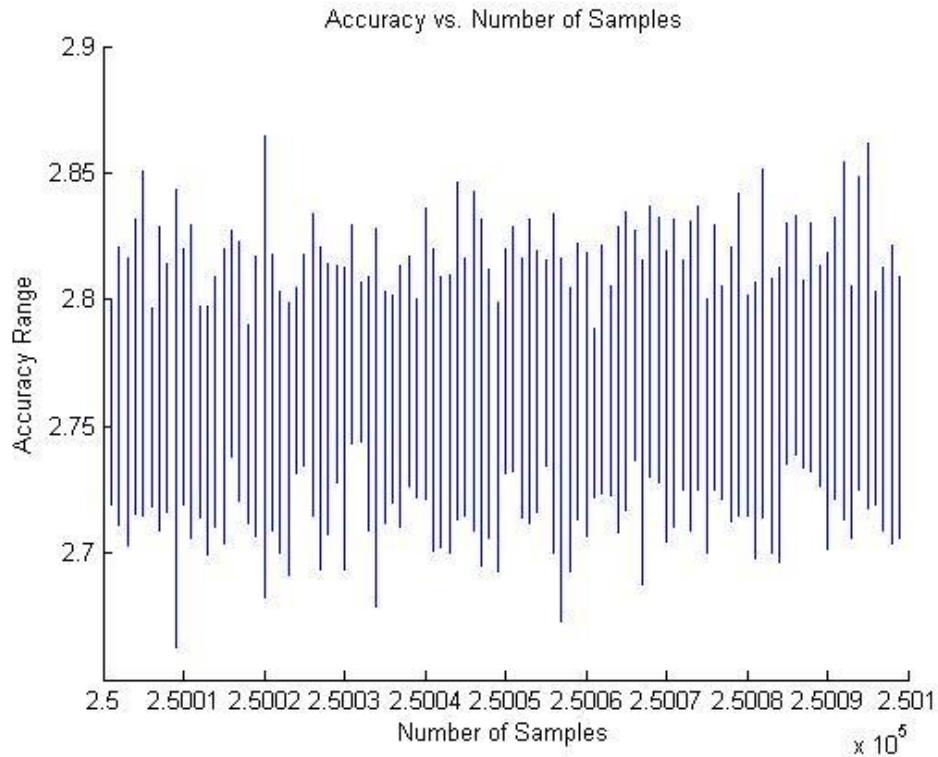


Fig. 49. Accuracy vs. number of samples for the IEEE 68-bus benchmark system using Gaussian filtered white noise.

Even though the change in the maximum error and the accuracy plateaus as the number of samples is increased, there is still considerable improvement. Each one of the simulation results presented in Fig. 44 through Fig. 49 took more than 9 hours to simulate. For that reason, the repetition was not done for subsequent simulations. Then the estimate was obtained using one million samples. The use of one million samples resulted in an estimate with an accuracy of 1.44. The use of one million samples correspond to about nine and a half hours of synchrophasor data collection. Finally the estimate was obtained using 2.5 million samples. An estimate with an accuracy of 1.18 was obtained when 2.5 million samples were used. The use of 2.5 million samples correspond to synchrophasor data collection of about one day. A synchrophasor data collection of one day corresponds to a complete cycle of daily load variation.

c. Implementation requirements

After the validation of the Y_{bus} estimation approach using randomly generated systems and the IEEE 68-bus benchmark system, it was applied it to the benchmark system. Lines 8, 2, 4, and 16 were identified to estimate a partial Y_{bus} . In order to perform Y_{bus} estimation, the current injection matrix I_{bus} and the voltage matrix V_{bus} were needed. To be able to determine current injection at each bus (substation), electrical interconnection information are needed similar to those presented in Fig. 22. Substation electrical interconnection information were not available for the benchmark system.

Terminal IDs measuring currents contributing to the current injection were identified as in Table 12 below based on the naming convention of the terminal IDs. Corresponding synchrophasor column vectors were processed in Matlab to produce complex phasors from magnitude and angle measurements. Then, current injection matrices were created by adding respective terminal ID currents. Resulting V_{bus} and I_{bus} were used to estimate the partial Y_{bus} using Y_{bus} estimation method. The code used in this estimation is provided in the Appendix.

Table 12. Terminal IDs corresponding to current injections.

Bus	Terminal IDs
1	46-53
2	0, 1, 211, 212, 216, 217, 227, & 228
3	112, 114, 115, 137, 138, 155, 246, 247, & 248
4	146-148
5	78-87 & 189
6	16-19

The Y_{bus} estimation result was not correct. After further investigation, some terminal IDs were not providing synchrophasor measurements. That is, there were PMU terminal IDs in place, but no measurements were provided. Without a complete set of synchrophasor measurements within a substation, current injections were not correct. Leading to an invalid Y_{bus} estimation. And in some cases there were no PMU terminal ID in place to begin with.

It is important here to distinguish between the effect of a missing current injection value and a missing branch current value (synchrophasor measurement). A missing current injection value leads to a missing i^{th} column and i^{th} row from the estimate as discussed previously and demonstrated in Fig. 33. A missing synchrophasor measurement within a substation invalidates the current injection value for that substation (bus in reduced system). So the effect of this is an “all or none” situation for each substation.

Another source of error identified is the ambiguity in direction of placement of the current transformers. Other than the electrical interconnection information of the substation, directional information of the current transformers in the substation is important to calculate the current injection appropriately.

To summarize, the following are needed to adequately implement the Y_{bus} estimation technique on actual systems:

- Electrical interconnection information for the substations of interest.
- Complete synchrophasor measurements for the substations of interest.
- Directional placement information for current transformers.

VIII. Conclusions & Future Work

A model development and validation process was structured and developed. The process was used to develop a proposed wind energy transmission benchmark model. Representative PMU synchrophasor measurements were provided by the GRAPES center and were analyzed for deriving power system models. Power angles were extracted from those synchrophasor measurements and used for validating the proposed benchmark model. Results show that power flows are within NERC recommendations, suggesting that the benchmark model is accurate. Therefore, the model development and validation process is also sound. The model development and validation process can be used with various criteria for various systems to develop reduced models for various simulation needs.

PMU synchrophasors were used for validation purposes. The resolution of available PMU synchrophasors is 33 milliseconds. The duration of events used is on the order of minutes. The benchmark model was derived based on guidance from the GRAPES center. Operational models were updated based on SCADA data that is updated every 10 or 15 minutes. Exact timing of the operational model conditions was not available. An averaging approach was used for comparison. Averaging was used to obtain PMU values of power angles, real power and reactive power. There are sources of error in the validation process. One source of error is the high variability in wind generation along with the low resolution of operational models. Another source of error is the averaging approach used in the validation. If more specific timing information is available for operational models, then a smaller averaging window can be used and aligned more precisely to the operation model conditions. Using a smaller averaging window results in reduced errors.

A new transmission system model/parameter estimation method was developed. This method not only extracts network parameters, but also the electrical interconnection between the buses. No prior knowledge of the transmission system is needed to apply this proposed estimation method. It was demonstrated that this method estimates the admittance matrix based on synchrophasor measurements with reasonable accuracy if a sufficient number of samples is used. This method performs well even if PMU measurements are not available at all buses throughout in the system.

IX. References

- [1] U.S. Department of Energy, “Wind Vision: A New Era for Wind Power in the United States,” DOE/GO-102015-4557, Mar. 2015.
- [2] T. Ackermann, *Wind Power in Power Systems*. John Wiley & Sons, 2012.
- [3] North American Electric Reliability Corporation, “Standard TPL-001-4 - Transmission System Planning Performance Requirements.” Feb-2013.
- [4] R. Majumder, C. Bartzsch, P. Kohnstam, E. Fullerton, A. Finn, and W. Galli, “Magic Bus: High-Voltage DC on the New Power Transmission Highway,” *IEEE Power Energy Mag.*, vol. 10, no. 6, pp. 39–49, Nov. 2012.
- [5] G. Rogers, *Power System Oscillations*. Springer Science & Business Media, 2012.
- [6] “PowerWorld Simulator 18 PowerWorld.” [Online]. Available: <http://www.powerworld.com/powerworld-simulator-18>. [Accessed: 10-Jun-2015].
- [7] “System disturbance stability studies for Western System Coordinating Council (WSCC),” Powertech Labs Inc., British Columbia, Canada, EPRI Report TR-108256, Apr. 1997.
- [8] NERC, “White Paper on Power System Model Validation.” Dec-2010.
- [9] K. E. Martin, “Synchrophasor Standards Development - IEEE C37.118 and IEC 61850,” in *2011 44th Hawaii International Conference on System Sciences (HICSS)*, 2011, pp. 1–8.
- [10] E. O. Schweitzer and D. E. Whitehead, “Real-world synchrophasor solutions,” in *Protective Relay Engineers, 2009 62nd Annual Conference for*, 2009, pp. 536–547.
- [11] NERC, “Real-Time Application of Synchrophasors for Improving Reliability.” Oct-2010.
- [12] J. D. Glover, M. Sarma, and T. Overbye, *Power Systems Analysis and Design*. Cengage Learning, 2007.
- [13] Grainger, *Power System Analysis*. McGraw-Hill Education (India) Pvt Limited, 2003.
- [14] P. W. Sauer and M. A. Pai, *Power System Dynamics and Stability*. Stipes Publishing L.L.C., 2006.
- [15] S. Djukic and A. Saric, “Dynamic model reduction: An overview of available techniques with application to power systems,” *Serbian J. Electr. Eng.*, vol. 9, no. 2, pp. 131–169, 2012.
- [16] WECC Modeling and Validation Work Group, “WECC Wind Plant Dynamic Modeling Guidelines,” Apr. 2014.

- [17] J. H. Chow, *Power System Coherency and Model Reduction*. Springer Science & Business Media, 2013.
- [18] D. Shi, “Power System Network Reduction for Engineering and Economic Analysis,” Ph.D., Arizona State University, United States -- Arizona, 2012.
- [19] J. B. Ward, “Equivalent circuits for power-flow studies,” *Electr. Eng.*, vol. 68, no. 9, pp. 794–794, Sep. 1949.
- [20] M. Adamiak, B. Kasztenny, and W. Premerlani, “Synchrophasors: definition, measurement, and application,” *Proc. 59th Annu. Ga. Tech Prot. Relaying Atlanta GA*, 2005.
- [21] B. Pal and B. Chaudhuri, *Robust Control in Power Systems*. Springer Science & Business Media, 2006.
- [22] “IEEE Standard for Synchrophasor Measurements for Power Systems,” IEEE Std C371181-2011 Revis. IEEE Std C37118-2005, pp. 1–61, Dec. 2011.
- [23] J. E. Dagle, “The North American SynchroPhasor Initiative (NASPI),” in *2010 IEEE Power and Energy Society General Meeting, 2010*, pp. 1–3.
- [24] NASPI, “Model Validation Using Synchrophasors NASPI Technical Workshop.” U.S. Department of Energy, Oct-2013.
- [25] A. Chakraborty, “Estimation, analysis and control methods for large-scale electric power systems using synchronized phasor measurements,” Ph.D., Rensselaer Polytechnic Institute, United States -- New York, 2008.
- [26] C. Dufour, J. Mahseredjian, and J. Belanger, “A Combined State-Space Nodal Method for the Simulation of Power System Transients,” *IEEE Trans. Power Deliv.*, vol. 26, no. 2, pp. 928–935, Apr. 2011.
- [27] J. Dagle, “North American SynchroPhasor Initiative - An Update of Progress,” in *42nd Hawaii International Conference on System Sciences*, 2009. HICSS '09, 2009, pp. 1–5.
- [28] A. Chakraborty and P. P. Khargonekar, “Introduction to wide-area control of power systems,” in *American Control Conference (ACC)*, 2013, 2013, pp. 6758–6770.
- [29] J. Zhang, G. Welch, G. Bishop, and Z. Huang, “Reduced Measurement-space Dynamic State Estimation (ReMeDySE) for power systems,” in *PowerTech*, 2011 IEEE Trondheim, 2011, pp. 1–7.
- [30] M. Dehghani and S. K. Y. Nikraves, “State-Space Model Parameter Identification in Large-Scale Power Systems,” *IEEE Trans. Power Syst.*, vol. 23, no. 3, pp. 1449–1457, Aug. 2008.
- [31] E. S. Q.-O. Peter Benner, “State-space truncation methods for parallel model reduction of large-scale systems,” *Parallel Comput.*, vol. 29, pp. 1701–1722, 2003.

- [32] E. Allen, D. N. Kosterev, and P. Pourbeik, "Validation of power system models," in 2010 *IEEE Power and Energy Society General Meeting*, 2010, pp. 1–7.
- [33] J. Xia and A. Dysko, "UK transmission system modelling and validation for dynamic studies," in *Innovative Smart Grid Technologies Europe (ISGT EUROPE)*, 2013 4th IEEE/PES, 2013, pp. 1–5.
- [34] G. Troullinos and J. Dorsey, "Coherency and model reduction: state space point of view," *IEEE Trans. Power Syst.*, vol. 4, no. 3, pp. 988–995, Aug. 1989.
- [35] Majid Oloomi Buygi, "Transmission Expansion Planning in Deregulated Power Systems," Darmstadt University of Technology, 2004.
- [36] R. Romero, A. Monticelli, A. Garcia, and S. Haffner, "Test systems and mathematical models for transmission network expansion planning," *Gener. Transm. Distrib. IEE Proc.*, vol. 149, no. 1, pp. 27–36, Jan. 2002.
- [37] M. M. Elmetwally, F. A. Aal, M. L. Awad, and S. Omran, "A Hopfield Neural Network approach for integrated transmission network expansion planning," in *Power Systems Conference, 2006. MEPCON 2006. Eleventh International Middle East*, 2006, vol. 1, pp. 371–376.
- [38] J. De La Ree, V. Centeno, J. S. Thorp, and A. G. Phadke, "Synchronized Phasor Measurement Applications in Power Systems," *IEEE Trans. Smart Grid*, vol. 1, no. 1, pp. 20–27, Jun. 2010.
- [39] J. Beau, C. Blalock, E. Frye, F. Harley, C. Odom, H. Lu, and J. Zhao, "An Introduction to Synchrophasors."
- [40] Y. Xu, Z. Y. Dong, Z. Xu, R. Zhang, and K. P. Wong, "Power system transient stability-constrained optimal power flow: A comprehensive review," in 2012 *IEEE Power and Energy Society General Meeting*, 2012, pp. 1–7.
- [41] L. Vanfretti, "Phasor measurement-based state estimation of electric power systems and linearized analysis of power system network oscillations," Ph.D., Rensselaer Polytechnic Institute, United States -- New York, 2009.
- [42] S. G. Ghiocel, "Applications of synchronized phasor measurements for state estimation, voltage stability, and damping control," Ph.D., Rensselaer Polytechnic Institute, United States - New York, 2013.
- [43] A. Chakraborty, J. H. Chow, and A. Salazar, "A measurement-based framework for dynamic equivalencing of large power systems using WAMS," in *Innovative Smart Grid Technologies (ISGT)*, 2010, pp. 1–8.
- [44] A. Chakraborty and J. H. Chow, "Interarea model estimation for radial power system transfer paths with voltage support using synchronized phasor measurements," in 2008

IEEE Power and Energy Society General Meeting - Conversion and Delivery of Electrical Energy in the 21st Century, 2008, pp. 1–7.

- [45] J. H. Chow, A. Chakraborty, L. Vanfretti, and M. Arcak, “Estimation of Radial Power System Transfer Path Dynamic Parameters Using Synchronized Phasor Data,” *IEEE Trans. Power Syst.*, vol. 23, no. 2, pp. 564–571, May 2008.
- [46] A. Chakraborty, J. H. Chow, and A. Salazar, “A Measurement-Based Framework for Dynamic Equivalencing of Large Power Systems Using Wide-Area Phasor Measurements,” *IEEE Trans. Smart Grid*, vol. 2, no. 1, pp. 68–81, Mar. 2011.
- [47] J. R. Hockenberry, “Evaluation of uncertainty in dynamic, reduced-order power system models,” Ph.D., Massachusetts Institute of Technology, United States - Massachusetts, 2000.
- [48] D. N. Kosterev, C. W. Taylor, and W. A. Mittelstadt, “Model validation for the August 10, 1996 WSCC system outage,” *IEEE Trans. Power Syst.*, vol. 14, no. 3, pp. 967–979, Aug. 1999.
- [49] J. P. Yang, G. H. Cheng, and Z. Xu, “Dynamic Reduction of Large Power System in PSS/E,” in *Transmission and Distribution Conference and Exhibition: Asia and Pacific*, 2005 IEEE/PES, 2005, pp. 1–4.
- [50] N. Zhou, S. Lu, R. Singh, and M. A. Elizondo, “Calibration of reduced dynamic models of power systems using phasor measurement unit (PMU) Data,” in *North American Power Symposium (NAPS)*, 2011, 2011, pp. 1–7.
- [51] S. D. Đukić and A. T. Sarić, “A new approach to physics-based reduction of power system dynamic models,” *Electr. Power Syst. Res.*, vol. 101, pp. 17–24, Aug. 2013.
- [52] NERC, “Reliability Assessment Guidebook.” Aug. 2012.
- [53] H.-D. Chiang, *Direct Methods for Stability Analysis of Electric Power Systems: Theoretical Foundation, BCU Methodologies, and Applications*. John Wiley & Sons, 2011.
- [54] C. Bila, “Power system dynamic state estimation and load modeling,” *Electr. Comput. Eng. Masters Theses*, Jan. 2014.
- [56] J. Mahseredjian, C. Dufour, U. Karaagac, and J. Bélanger, “Simulation of power system transients using state-space grouping through nodal analysis,” *Proc. Int. Conf. Power Systems Transients*, Netherlands, 2011.
- [57] P. Kundur, N. J. Balu, and M. G. Lauby, *Power system stability and control*. McGraw-Hill, 1994.

X. Appendix

A. Representative Matlab m-file script

Below is a sample Matlab m-file script provided as an example of estimating an impedance matrix from normally distributed random current injection and bus voltage measurements.

```
% Estimation of a randomly generated Z-bus matrix  
  
% from normally distributed random bus injections  
  
clear  
  
M=300; % Select number of buses  
  
missing=45; % Number of buses without PMU measurements  
  
P=random('unid',M,1,missing); % random missing %bus index array  
  
Y1=random('Normal',0,1,M,M);  
  
Y2=j*random('Normal',0,1,M,M);  
  
Y12=Y1+Y2;  
  
Y=Y12+conj(Y12'); % Create random Y-bus matrix  
  
Z=inv(Y); % Compute impedance matrix  
  
N=1e5; % Number of PMU sample measurements  
  
% Creat random array of bus current injections.
```

```

% Polar form: Random magnitudes and angles

% Per-unit values

Ibase=3.0; % Nominal current in the network

Imag=random('Normal',Ibase,2.5,M,N);

Iphase=random('Normal',-0.5,0.125,M,N);

I=zeros(M,N);

for n=1:N

    for m=1:M

        I(m,n)=Imag(m,n)*exp(j*Iphase(m,n));

    end

end

% Create placeholder for node voltages.

V=zeros(M,N);

% Compute node voltages from current injections

for k=1:N;

    V(:,k)=Z*I(:,k);

end

Imean=mean(I'); % Compute mean of column data

```



```

Imean=Imean';

Vmean=mean(V);

Vmean=Vmean';

% Use mean of PMU for missing PMU measurements

for m=1:missing

    I(P(m,:),:)=Imean(P(m));

end

for m=1:missing

    V(P(m,:),:)=Vmean(P(m));

end

Istd=std(I);

Istd=Istd';

Ivar=zeros(M,N);

% Subtract the mean current value and normalize

for k=1:N;

    Ivar(:,k)=(I(:,k)-Imean)./(Istd.^2);

end

Vmean=mean(V);

```

```

Vmean=Vmean';

Vstd=std(V');

Vstd=Vstd';

for k=1:N;

    Vvar(:,k)=V(:,k)-Vmean;

end

Zvar=zeros(M,M);

for n=1:N;

    Zvar=Zvar+Vvar(:,n)*Ivar(:,n)';

end

Zhat=(Zvar)/N;

% Modify Z for missing rows & columns

% For error analysis set 'actual' Z

% row and column elements to zero for

% missing PMU buses.

for n=1:missing

    for m=1:M

        Z(P(n),m)=0;

```

```

    Zhat(P(n),m)=0;

end

end

for n=1:missing

    for m=1:M

        Z(m,P(n))=0;

        Zhat(m,P(n))=0;

    end

end

Zmag=norm(Z);

Zhatmag=norm(Zhat-Z);

delta=Zhatmag/Zmag

```

B. Randomly generated Ybus systems M-files

The two codes below produced Fig. 30 through Fig. 32

a. **Ybus estimation error calculation**

This code below corresponds to the flow chart in Fig. 29.

```

clear

clc

close all

```

```

x=2.5; % this is the variance for the current magnitude

f=0; % this is a counter

h=0; % another counter initialization

max_m=400; % maximum number of samples

max_i=20; % number of times each number of samples is being repeated.

z3=zeros(1,max_m);

zznorep=zeros(max_m,max_i);

 yynorep=zeros(max_m,max_i);

%%

for m=1:max_m;

    y=m;

    for i=1:max_i;

        Z = estimationerror(x, y); %Ybus estimation as a function

            %it takes current magnitude Variance

            %and number of samples as inputs.

            %it returns the "accuracy" as

            %output

        f=f+1; %counter

        zznorep (m,i)=Z; %records input and output

        yynorep (m,i)=y;

    end

```

```

        clc

        disp('Running... ');fprintf('\b');fprintf('%0.2f',f/(max_m*max_i)*100);disp('%'); %display
        progressend

    end

    %% pre recorded data

    load('prerec_1000_50.mat')

    maxmprerec=length(zzprerec);

    for g=1:maxmprerec

        zvarprerec(g)=max(zzprerec(g,:))-min(zzprerec(g,:));

    end

    figure (12)

    plot(yyprerec(:,1),smooth(smooth(smooth((zvarprerec))))))

    ylim([-0.2 2])

    xlim([-100 1000])

    hline=refline([0,0]);

    set(hline,'LineStyle',':');

    hline= line([0,0],[-0.2,10]);

```

```
set(hline,'LineStyle',':');
```

```
figure (11)
```

```
plot(yyprerec(:,1),zvarprerec)
```

```
title('Max-min');
```

```
figure (10)
```

```
for b=1:maxmprerec
```

```
if b==1
```

```
    hold
```

```
end
```

```
plot(yyprerec(b,:),zzprerec(b,:))
```

```
title('parallel vertical lines "range of accuracy"');
```

```
end
```

```
figure (9)
```

```
hold
```

```
for ww=1:10:maxmprerec
```

```
plot (yyprerec(ww,:),zzprerec(ww,:))
```

```
end
```

```
%figure (8)
```

```
%plot (yyprerec(maxmprerec/2,:),zzprerec(maxmprerec/2,:))
```

figure (7)

w=9;

plot(yyprerec(:,w),zzprerec(:,w))

%% this section plots the variance in the "accuracy" for each specific #of samples

for g=1:max_m

z3(g)=max(zznorep(g,:))-min(zznorep(g,:));

end

figure (6)

plot(yynorep(:,1),smooth(smooth(smooth(z3))))

ylim([-0.2 2])

*xlim([-0.1*max_m max_m])*

hline=refline([0,0]);

set(hline,'LineStyle',':');

hline= line([0,0],[-0.2,10]);

set(hline,'LineStyle',':');

figure (5)

```
plot(yynorep(:,1),z3)
```

```
title('Max-min');
```

```
%% this section plots the maximum "accuracy" for each #of samples
```

figure (4)

```
for b=1:max_m
```

```
if b==1
```

```
    hold
```

```
end
```

```
plot(yynorep(b,:),z3norep(b,:))
```

```
title('parallel vertical lines "range of accuracy"');
```

```
end
```

```
%scatter(yy,zz)
```

```
%plot(yy,zz)
```

```
%%
```

figure (3)

```
hold
```

```
for ww=1:10:max_m
```

```
plot (yynorep(ww,:),z3norep(ww,:))
```


end

figure (2)

```
plot (yynorep(max_m/2,:),zznorep(max_m/2,:))
```

figure (1)

```
w=9;
```

```
plot(yynorep(:,w),zznorep(:,w))
```

b. Ybus error estimation.

The code below corresponds to Fig. 28.

```
% Estimate Y-bus from measurements of V and I
```

```
% Assume gaussian noise distribution in current injection
```

```
% Use Admittance matrix formulation as in Glover-Sarma Page 326-327
```

```
% (Chap 6 Power Flow in terms of bus injection current)
```

```
function [error]=estimationerror(Var, Iterations)
```

```
% Creat large scale complex-valued symmetric matrix
```

```
M=2; % Number of buses
```

```
P=1*M; % Number of buses with PMU measurements
```

```
Y1=random('Normal',10,10,M,M);
```

```
Y2=j*random('Normal',5,1,M,M);
```

```
Y12=Y1+Y2;
```

Y=Y12+conj(Y12');

Z=inv(Y);

N=Iterations; % Number of data samples

%%%%%%%%%%

+++++

%%%%%%%%%% Same before this line

%%%%%%%%%%

+++++

% Creat random array of bus current injections. Each column is a set of

% three current sources [i1 i2 i3]' at a particular time.

% Columns denote time sequence of currents.

% Current injections are random - changed each time program is run

% Z=eye(M);Y=eye(M);

Imag=random('Normal',3.671,Var,M,N);

Iphase=random('Normal',-0.5,0.125,M,N);

I=zeros(M,N);

for n=1:N

for m=1:M

I(m,n)=Imag(m,n)*exp(j*Iphase(m,n));

end

end

```

% Creat placeholder for node voltages. Same format as bus injection

% currents I.

V=zeros(M,N);

% Compute node voltages from current injections

for k=1:N;

V(:,k)=Z*I(:,k);

end

%%
%%%%%%%%%%%%%%%%%%%%%%%%%%%%%%%%%%%%%%%%%%%%%%%%%%%%%%%%%%%%%%%%%%%%%%%%
%%                               Same after this line
%%%%%%%%%%%%%%%%%%%%%%%%%%%%%%%%%%%%%%%%%%%%%%%%%%%%%%%%%%%%%%%%%%%%%%%%
%%

Imean=mean(I); % The "mean" command compute mean as column data

Imean=Imean'; % note complex transpose is reversed.

Istd=std(I);

Istd=Istd';

Ivar=zeros(M,N);

% Subtract the mean current value and normalize variance

```

```

for k=1:N;

    Ivar(:,k)=I(:,k)-Imean;

    Ivar(:,k)=(I(:,k)-Imean)./(Istd.^2); % This correct results with no normalization to Vvar
end

Vmean=mean(V');

Vmean=Vmean';

Vstd=std(V');

Vstd=Vstd';

% Subtract mean voltage and normalize variance

for k=1:N;

    Vvar(:,k)=V(:,k)-Vmean;

end

Zvar=zeros(M,M);

% Using Therrien book (statistical signal processing)

% Compute using estimated correlation matrix from data Page 41 applied
% to the covariance matrix

for k=1:N;

    Zvar=Zvar+Vvar(:,k)*Ivar(:,k)'; % equivalent to I*V but yields conjugate

    % Zvar=Zvar+Ivar(:,k)*Vvar(:,k)'; % This gives the conjugate of Zbus
end

% Compute impedance data Z-matrix

```

```

% Zmean=Vmean*Imean';

%%% Corrected scaling

Zhat=(Zvar)/N;

%%%% Corrected conjugate

Yhat=inv(Zhat);    % Note conjugate transpose in matrix inverse needed

    % if use the alternate Zvar=Zvar+Ivar(:,k)*Vvar(:,k)';

    % Could also Yhat=inv(Zhat) then Yhat=Yhat'

% Compare known (admittance) Y-matrix to estimated Y-matrix

error=norm(Zhat)/norm(Z);

% Zhat=(norm(Z)/norm(Zhat))*Zhat

% abs(Y);

% abs(Yhat);

% Yerr=norm(Y-Yhat)/norm(Y)  % Compute percent error in estimated Y-matrix

    % typically 1% for 500,000 samples if sufficient

    % variance in current source injections. If variance

    % is low then will have large errors. If zero

    % variance, e.g. I=random('Normal',10,0,3,N); then

    % system may not be able to solve.

```

C. IEEE 68-bus benchmark system M-files

The two codes below produced Fig. 34 through Fig. 36.

a. Ybus estimation error calculation

clear

clc

close all

x=2.5; % this is the variance for the current magnitude

f=0; % this is a counter

h=0; % another counter initialization

max_m=1000; % maximum number of samples

max_i=20; % number of times each number of samples is being repeated.

z3=zeros(1,max_m);

zxnorep=zeros(max_m,max_i);

yynorep=zeros(max_m,max_i);

%%

for m=1:max_m;

y=m;

for i=1:max_i;

Z = estimationerror(x, y); %Ybus estimation as a function

%it takes current magnitude Variance

%and number of samples as inputs.

%it returns the "accuracy" as

%output

f=f+1; %counter

zxnorep (m,i)=Z; %records input and output

```

    yynorep (m,i)=y;

end

clc

disp('Running... ');fprintf('\b');fprintf('%0.2f',f/(max_m*max_i)*100);disp('% '); %display
progressend

end

%%% this section plots the variance in the "accuracy" for each specific #of samples

for g=1:max_m

    z3(g)=max(zznorep(g,:))-min(zznorep(g,:));

end

figure (6)

plot(yynorep(:,1),smooth(smooth(smooth(z3))))

ylim([-0.2 2])

xlim([-0.1*max_m max_m])

hline=refline([0,0]);

set(hline,'LineStyle',':');

```

```
hline= line([0,0],[-0.2,10]);
```

```
set(hline,'LineStyle',':');
```

```
figure (5)
```

```
plot(yynorep(:,1),z3)
```

```
title('Max-min');
```

```
%% this section plots the maximum "accuracy" for each #of samples
```

```
figure (4)
```

```
for b=1:max_m
```

```
if b==1
```

```
    hold
```

```
end
```

```
plot(yynorep(b,:),z3norep(b,:))
```

```
title('parallel vertical lines "range of accuracy"');
```

```
end
```

```
%scatter(yy,zz)
```

```
%plot(yy,zz)
```

```
%%
```

```
figure (3)
```

```
hold
```

```
for ww=1:10:max_m
```

```
plot (yynorep(ww,:),z3norep(ww,:))
```


end

figure (2)

plot (yynorep(max_m/2,:),zznorep(max_m/2,:))

figure (1)

w=9;

plot(yynorep(:,w),zznorep(:,w))

b. Ybus error estimation.

% Estimate Y-bus from measurements of V and I

% Assume gaussian noise distribution in current injection

% Use Admittance matrix formulation as in Glover-Sarma Page 326-327

% (Chap 6 Power Flow in terms of bus injection current)

function [error]=estimationerror(Var, Iterations)

load('Ybus.mat')

M=length(YI);

*P=I*M;*

Y=full(YI);

%{

% Creat large scale complex-valued symmetric matrix

M=2; % Number of buses

*P=I*M; % Number of buses with PMU measurements*

```

Y1=random('Normal',10,10,M,M);
Y2=j*random('Normal',5,1,M,M);
Y12=Y1+Y2;
Y=Y12+conj(Y12');

%}

Z=inv(Y);

N=Iterations; % Number of data samples

%%

%%%%%%%%

+++++

%%%%%%%% Same before this line

%%%%%%%%

+++++

% Creat random array of bus current injections. Each column is a set of
% three current sources [i1 i2 i3]' at a particular time.

% Columns denote time sequence of currents.

% Current injections are random - changed each time program is run

% Z=eye(M);Y=eye(M);

Imag=random('Normal',3.671,Var,M,N);
Iphase=random('Normal',-0.5,0.125,M,N);
I=zeros(M,N);

```

```

for n=1:N
    for m=1:M
        I(m,n)=Imag(m,n)*exp(j*Iphase(m,n));
    end
end

% Creat placeholder for node voltages. Same format as bus injection
% currents I.
V=zeros(M,N);

% Compute node voltages from current injections

for k=1:N;
    V(:,k)=Z*I(:,k);
end

%%
%%%%%%%%%%%%%%%%%%%%%%%%%%%%%%%%%%%%%%%%%%%%%%%%%%%%%%%%%%%%%%%%%%%%%%%%
%%                               Same after this line
%%%%%%%%%%%%%%%%%%%%%%%%%%%%%%%%%%%%%%%%%%%%%%%%%%%%%%%%%%%%%%%%%%%%%%%%
%%

Imean=mean(I); % The "mean" command compute mean as column data
Imean=Imean'; % note complex transpose is reversed.

```

```

Istd=std(I');
Istd=Istd';
Ivar=zeros(M,N);

% Subtract the mean current value and normalize variance
for k=1:N;
    Ivar(:,k)=I(:,k)-Imean;
    Ivar(:,k)=(I(:,k)-Imean)./(Istd.^2); % This correct results with no normalization to Vvar
end

Vmean=mean(V');
Vmean=Vmean';
Vstd=std(V');
Vstd=Vstd';

% Subtract mean voltage and normalize variance
for k=1:N;
    Vvar(:,k)=V(:,k)-Vmean;
end

Zvar=zeros(M,M);

% Using Therrien book (statistical signal processing)
% Compute using estimated correlation matrix from data Page 41 applied
% to the covariance matrix
for k=1:N;

```

```

Zvar=Zvar+Vvar(:,k)*Ivar(:,k)'; % equivalent to I*V but yields conjugate
% Zvar=Zvar+Ivar(:,k)*Vvar(:,k)'; % This gives the conjugate of Zbus
end

% Compute impedance data Z-matrix

% Zmean=Vmean*Imean';

%% Corrected scaling

Zhat=(Zvar)/N;

%% Corrected conjugate

Yhat=inv(Zhat); % Note conjugate transpose in matrix inverse needed

% if use the alternate Zvar=Zvar+Ivar(:,k)*Vvar(:,k)';

% Could also Yhat=inv(Zhat) then Yhat=Yhat'

% Compare known (admittance) Y-matrix to estimated Y-matrix

error=norm(Zhat)/norm(Z);

% Zhat=(norm(Z)/norm(Zhat))*Zhat

% abs(Y);

% abs(Yhat);

% Yerr=norm(Y-Yhat)/norm(Y) % Compute percent error in estimated Y-matrix

% typically 1% for 500,000 samples if sufficient

% variance in current source injections. If variance

% is low then will have large errors. If zero

% variance, e.g. I=random('Normal',10,0,3,N); then

% system may not be able to solve.

```

D. Benchmark system Ybus estimation

clear

clc

load BusVoltage;

load BusCurrent;

I=BusCurrent;

V=BusVoltage;

[M,N]=size(BusCurrent); % Number of PMU sample measurements

% Select number of buses

Imean=mean(I'); % Compute mean of column data

Imean=Imean';

Vmean=mean(V');

Vmean=Vmean';

Istd=std(I');

Istd=Istd';

Ivar=zeros(M,N);

% Subtract the mean current value and normalize

for k=1:N;

Ivar(:,k)=(I(:,k)-Imean)./(Istd.^2);

end

Vmean=mean(V');

Vmean=Vmean';

Vstd=std(V');

```
Vstd=Vstd';  
for k=1:N;  
    Vvar(:,k)=V(:,k)-Vmean;  
end  
Zvar=zeros(M,M);  
for n=1:N;  
    Zvar=Zvar+Vvar(:,n)*Ivar(:,n)';  
end  
Zhat=(Zvar)/N
```